The Pennsylvania State University
The Graduate School

DATA-DRIVEN SERVICE OPTIMIZATION AND QUALITY MANAGEMENT IN CYBER-PHYSICAL MANUFACTURING SYSTEMS

A Dissertation in
Industrial Engineering
by
Ruimin Chen

Submitted in Partial Fulfillment
of the Requirements
for the Degree of

Doctor of Philosophy

August 2021

The dissertation of Ruimin Chen was reviewed and approved by the following:

Hui Yang
Harold and Inge Marcus Career Professor of Industrial and Manufacturing Engineering
Dissertation Advisor, Chair of Committee

Soundar Kumara
Allen E. Pearce and Allen M. Pearce Professor of Industrial Engineering

Timothy W. Simpson
Paul Morrow Professor in Engineering Design and Manufacturing

Edward W. Reutzel
Director of Center for Innovative Materials Processing through Direct Digital Deposition (CIMP-3D)

Yan Lu
Special Member
National Institute of standard and technology, System Integration Division

Steven J. Landry
Department Head and Professor of Industrial and Manufacturing Engineering

Abstract

Recent advancements in sensing and communication technology provide unprecedented opportunities to synchronize the additive manufacturing (AM) machine world and facilities to the cyber computational space. The new paradigm of AM cyber-physical system is a convergence of interconnectivity and intelligence to form adaptable and resilient processes in the factory of future.

The potential for AM cyber-physical systems to improve productivity leads to the new wave of technological changes and triggers paradigm shifts to service optimization and quality management. Sensing technology leads to a data-rich environment and provides a unique opportunity for different learning algorithms to accelerate the development of the AM cyber-physical systems. However, realizing the full potentials of data and transforming them into useful information and knowledge depends to a great extent on the development of novel analytical methods and tools. Specifically, the transition from the conventional manufacturing systems to the novel AM cyber-physical systems brings the following challenges:

1. The emergence of sharing economy enabled by sensing data provides opportunities in acquiring, providing, and sharing access to goods and services. Novel analytical approaches are urgently needed for optimal service management.

2. Advanced sensing brings a large amount of data with nonlinear and nonhomogeneous patterns, which calls for effective analytical methods to exploit acquired knowledge and extract sensitive features for process monitoring and control.

3. The presence of extraneous noises and complex interactions in modern systems prevent the extraction of hidden patterns and reveal of root cause in causal inferences from a large amount of data.

The goal of this dissertation is to improve the service quality of AM cyber-physical systems. The service management in AM cyber-physical systems includes not only the service optimization between resources (i.e., between service providers and seekers), but also the quality of the service that each provider can offer. Therefore,

this dissertation is aimed at developing new machine learning methodologies to enhance understanding of design-quality interactions, facilitate causality discovery, to eventually improve service management in AM cyber-physical systems. My research accomplishments include:

1. Chapter 2 developed a bipartite matching framework to model and optimize resource allocation among customers and service providers through a stable matching algorithm in AM cyber-physical systems. The framework is implemented in the customer-manufacturing allocation in cyber-physical platforms. Experimental results show that the proposed framework shows strong potentials to optimize resource allocation in the AM sharing economy.

2. Chapter 3 focused on conducting a design of experiment to investigate how design parameters (e.g., build orientation, thin-wall width, thin-wall height, and hatching spacing) interact with edge roughness in thin-wall builds. This work sheds insights on the optimization of engineering design to improve the quality of AM builds.

3. Chapter 4 targeted leveraging data to characterize and detect irregular and nonlinear patterns of signals, 2D images, and 3D voxels. We proposed heterogeneous recurrence analysis and generalized recurrence network analysis to not only capture recurrence dynamics in complex systems but also take the computational complexity into account. A tailored design of experiment study was developed to reveal the relationship between network quantifiers and design parameters (i.e., orientation, width, height, hatching pattern). The designed methodology is implemented to characterize the AM in-process layerwise data. This work enables the on-the-fly assessment of AM builds and real-time defect mitigation.

4. Chapter 5 focused on developing a knowledge-driven Bayesian network for manufacturing complex systems to identify the root cause of quality outcomes and offer a comprehensive solution. This research is aimed at aggregating machine parameters, material information, design parameters, process parameters into a Bayesian network. With the network representation, the causal relationships among variables can be identified and then be used to facilitate prediction, diagnosis, and support decision-making in manufacturing production.

Table of Contents

List of Figures

List of Tables

Acknowledgments

I would like to express my gratitude to Dr. Hui Yang for his guidance and support during my study. Throughout the past five years, I have been extremely inspired and tremendously benefited from his critical way of thinking about research problems. The experience of working with him will be a precious treasure in my future life.

I also would like to thank my other committee members: Dr. Kumara for his guidance and help in my research projects; Dr. Timothy Simpson for his suggestions for improving my research; Dr. Edward W. Reutzel for his generous helps in providing important process insights; and Dr. Yan Lu for the helpful discussion and constructive suggestions on my research. Furthermore, I want to express my sincere appreciation to my mentors, Dr. Paul Witherell, Dr. Albert W. Jones, Dr. Prahalada Rao and Dr. Changqing Cheng.

In addition, I would like to extend my deepest appreciation to all my labmates in Complex Systems Monitoring, Modeling, and Control Laboratory and Laboratory for Intelligent Systems and Analytics. My special thank to Dr. Farhad Imani whose unconditional support allowed my study to go the extra mile and friendship made my pursuit of Ph.D. easier. I would also like to thank the Harold and Inge Marcus Department of Industrial and Manufacturing Engineering at Penn State for their generous help during my study. I appreciate the Center For Innovative Materials Processing Through Direct Digital Deposition (CIMP-3D) at Penn State, NSF I/UCRC Center for Healthcare Organization Transformation (CHOT) (NSF I/UCRC award #1624727) and the National Institute of Standards and Technology (NIST) for continuous support and provide data of this research. Any opinions, findings, or conclusions found in this dissertation are those of the author and do not necessarily reflect the views of the sponsors.

Finally, my gratitude goes to my family. I wish to thank my beloved parents for their endless love and enduring support.

Chapter 1 Introduction

1.1 Motivation

Although the prior manufacturing paradigm enabled shifting from manual to mass production, the introduction of additive manufacturing (AM) provides a unique opportunity to further shifting from mass production to mass customization. AM is a process to construct customized builds layer-by-layer directly from a digital design. This expanding technology enables the creation of complex and freeform geometries and reduces tooling and intermediate steps that are difficult to realize using conventional manufacturing techniques [1]. Recent advances in sensing technologies and information systems open an exciting possibility to further boost the development of AM [2]. The combination of digital information with AM machines creates an AM cyber-physical system, where sensing data is analyzed in the cyber world and the production is then taken place in the physical world. In addition, advanced functional materials along with innovative design techniques remarkably extend the degrees of freedom in AM design and manufacturing. The design and manufacturing flexibility offered by AM is valuable in a variety of strategic applications ranging from aerospace to biomedical with a predicted market size of $50 billion by 2031 (See Figure 1.1) [3–6]. For instance, using AM to make builds for the Cessna Denali aircraft engine mitigated the number of components from 855 to 12 and improved the fuel efficiency of the engine, along with the power by over 10% [4, 5].

The market is expanding, however, the lack of service management and inefficiency in quality assurance are among key obstacles preventing AM from further proliferation in the manufacturing market.

Figure 1.1. Examples of AM printed parts in variety of domains such as aerospace and biomedical. Resources: 3dhubs.com (up left), redusers.com (up right), cgtrader.com (down left), todaysmedicaldevelopments.com (down right).

- **Service management:** AM brings the opportunities of mass customization, however, the current production speed of AM is not remarkable. In the AM cyber-physical system, due to the mass customization, there are no large inventories for the build. Consequently, current AM systems may not be able to scale up production in case of sudden increases in demand. To realize the capability of AM, new frameworks are required to leverage the spare time of available AM machines to improve productivity in the AM cyber-physical systems.

- **Quality assurance and causal discovery:** The significant challenge of metal AM is the occurrence of various defects such as cracks [7], delamination, distortion [8], lack of fusion [9], porosity [10], foreign inclusions [11] that deteriorate the build strength, hardness, and fatigue life [12, 13]. This inconsistency originated from complex physical and metallurgical processes, including heating, melting, Marangoni convection, evaporation, solidification. In fact, more than 50 different process input variables (e.g., design and job preparation, feedstock material, equipment, and process condition) affect the characteristics of finished builds [12].

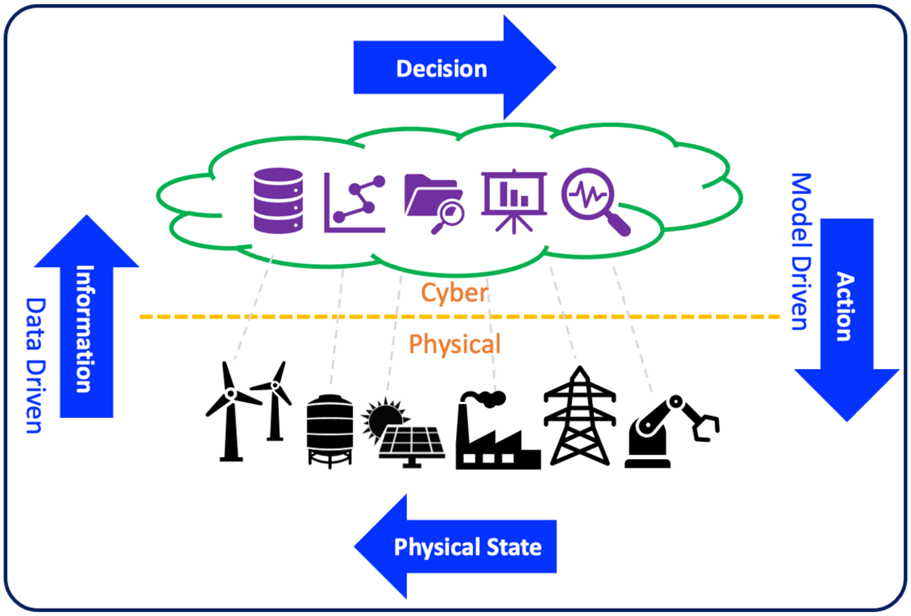

Figure 1.2. An illustration of a cyber-physical AM system.

Recent advancement in the internet of things (IoT) technology provides the opportunity of producing personalized products at low cost. Besides, over the past few years, the sharing economy has been changing the way that people share and conduct transactions in cyberspaces. New cyber-physical-based platforms enable owners to "share" their assets and services to non-owners [14]. As illustrated in Figure 1.2, the physical world is integrated, monitored, and controlled by the cyber system. Today, sharing economy firms are disrupting traditional industries across the world [15]. For example, the valuation of Airbnb is \$35 billion, while Hilton is at \$25 billion. However, the concept of sharing is still relatively new to the field of AM. As the price of 3D printers decreases, the medium-and-small-sized manufacturers are able to own machines and "share" their idle machines with others who do not own 3D printers, further compete with traditional enterprises. Such decentralization in the market results in the emergence of cyber-physical-based AM platforms, which help customers who do not have resources to print their designs at manufacturers who provide service and shorten the AM supply chain. Few, if any, previous works have been done to study characteristics and needs in such a market. There is an urgent need to study the sharing economy in AM. As the sharing economy generates its value by matching the customers and manufacturers, the creation of an appropriate framework to efficiently solve the resource allocation is one of the critical problems in market design. Our focus is to design a matching framework to model the resource allocation between customers and manufacturers.

It is not sufficient to only understand the interaction, we also need to separately understand the physical components and the computational components [15]. To optimize complex AM processes, different performance indicators such as mechanical properties, surface texture, part density total build time have been introduced as optimization criteria [16–19]. These key performance indicators (KPIs) are conducive to quantify operational efficiency and outputs in AM processes. The common practice is to utilize physical testing to calculate KPIs. However, experimentation costs of raw materials, time, and human resources are prohibitively expensive in AM. On the other hand, the development of reliable process models enables accurate prediction of the performance of the manufacturing process with the least experimentation effort and waste of resources [20]. The recent breakthrough in sensing provides a unique opportunity for more efficient quality management in AM. Various sensors such as X-ray computed tomography (XCT), optical imaging, and acoustic emission are integrated with AM machines to characterize the quality and improve understanding of complex AM processes [19,21]. Although the sensing techniques have shown promising capability in efficient quality management, their performance relies on appropriate data-driven models that work with high-dimensional and noisy manufacturing data.

In summary, to move AM from the prototype-demonstrator role into the industrial-scale production realm, there is a dire need to tackle the quality assurance problem also to develop a new matching and pricing framework. As shown in Figure 1.3, product design, manufacturing, quality management, and service optimization are the most important key factors that impacting the future status of AM in manufacturing markets. As a result, this dissertation focuses on addressing the following critical challenges in AM service optimization and quality management are as follows:

1. The emergence of sharing economy enabled by sensing data provides opportunities in acquiring, providing, and sharing access to goods and services. Novel analytical approaches are urgently needed for optimal service management.

2. Advanced sensing brings a large amount of data with nonlinear and nonhomogeneous patterns, which calls for effective analytical methods to exploit

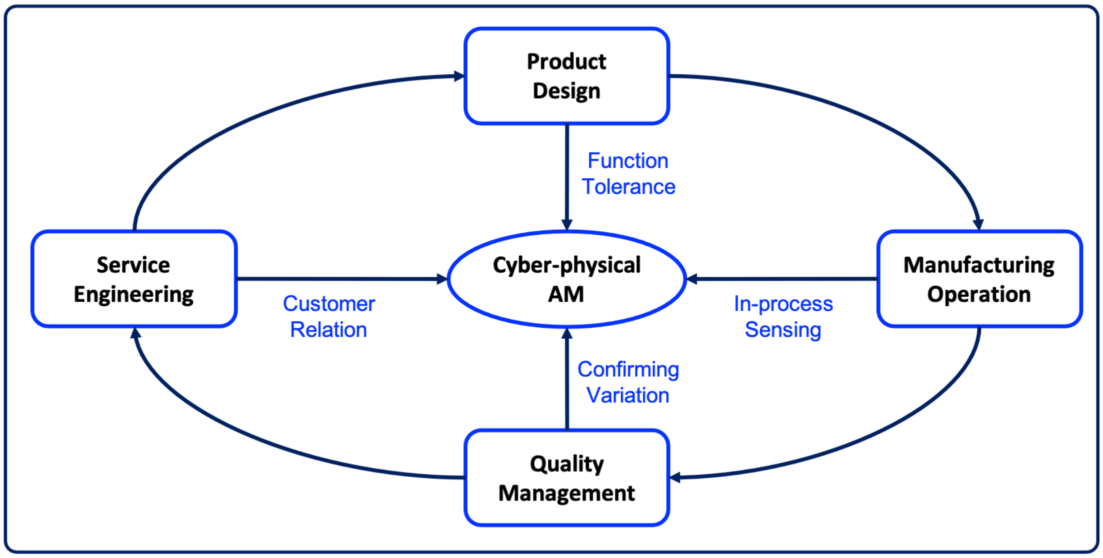

Figure 1.3. Important factors influencing the prospects of AM.

acquired knowledge and extract sensitive features for process monitoring and control.

3. The presence of extraneous noises and complex interactions in modern AM processes prevent the extraction of hidden patterns and reveal of root cause in causal inferences from a large amount of data.

1.2 Research Background

1.2.1 Sharing Economy and Additive Manufacturing

Sharing economy can be viewed as a set of peer-to-peer (P2P) driven activities that share access to goods and services through cyber-physical systems or platforms [22,23]. As such, physical assets can be shared as services. In the market of AM, a similar concept can be obtained through manufacturing networks. In the distributed AM network, manufacturers can cut down their delivery time and shipping costs when shipping their products to customers that are based in their region. At the same time, AM is shifting business models towards mass customization and responsible production paradigms [24]. According to the literature, AM has experienced a double-digit growth for 20 of the past 30 years, taking it from a promising set of uncommercialized technologies in the early 1980s to a market that was worth over \$4 billion in 2014 [25]. The AM market is expected to grow to more than $335 billion by 2025 [26].

As mentioned, cyber-physical AM platforms connect manufacturers and customers and create a new shape of two-sided market. Therefore, new models need to be proposed to handle the resource allocation of the supply chain in the new form. The decentralized market introduced the shortened supply chain. And the creation of a new matching framework between manufacturers and customers will efficiently solve the resource allocation is one of the critical problems in the market design.

1.2.2 Design in Additive Manufacturing

Rather than removing materials or introducing another manufacturing technique, AM produces physical objects by adding materials layer by layer directly through CAD models and create complex structures that cannot be easily produced using conventional subtractive manufacturing processes. Although AM techniques increase productivity while enabling a reduction in the cost, however, the physical phenomena that occurs during AM processes have a strong impact on the quality of the final builds. Therefore, it is essential to consider the effect of design on the quality of AM products.

The term "design for AM" has been discussed used in the literature [27–31]. By considering constraints of production and the manufacturing goal at the same time, design of AM is defined as the practice of designing and optimizing a product together with its production system to reduce development time and cost and increase performance, quality, and profitability [32]. Usually, the design for AM contains three levels. In the first level, the design of AM is usually process-specific, feature-specific, and activity-specific [33]. In the second level, the design of AM is aimed at understanding and quantifying the effect of the design process on manufacturing [34]. In the third level, the design of AM explores the relationship between design and manufacturing and its impact on the designer, the design process, and design practice [35].

The development of AM design, including the knowledge, methodologies, and standards, all challenge the advancement of AM. Insufficient understanding of AM processes still limits the widespread of AM to the industry, thereby preventing the mass production of AM builds. Therefore, there is a dire need to understand the relationship between the design of AM and the quality of AM output.

1.2.3 Causal Analysis and Additive Manufacturing

To encode the domain manufacturing knowledge, traditional machine learning representations, such as ontologies [36, 37], first-order logic rules [38], or probabilistic reasoning systems [39], have been utilized to achieve plausible interpretation (e.g., causal reasoning). Modeling efforts to capture the stochastic dynamics underlying AM mechanisms have been made. However, linear models, such as ARIMA, ARMAX [40], or multi-dimension time series models [41, 42] show limitations in capturing nonstationary and stochastic features. Multi-variate models introduce the curse of computational dimensionality [43, 44]. Black-box models, such as deep learning models, parametric maps, or manifold learnings, are notoriously difficult to interpret [45].

A Bayesian network (BN) contains a graphical structure that represents causal relationships among a large number of variables and allows for probabilistic causal inferences using the observed variables. The graph structure is widely utilized in expert system development and represent the causal relationship [46–52]. It moves one step forward to support the inference of causality from observational data and improve interpretability at the same time. The conditional probabilities are used to represent complex relationships by the BNs [53]. BNs can be utilized for a wide range of tasks including diagnostics, prediction, anomaly detection, decision making under uncertainty, and reasoning. Traditionally, causal networks are generated by expert's knowledge. For example, one can specify the causal relationship between nodes through their experiences and knowledge. Recently, multiple automated learning algorithms have been proposed to obtain the BN structure from data [54–61]. However, automated learning methodologies are based on probabilistic information and can also be affected by the property of collected data. In the domain of AM, ontology has been widely studied to provide formal and structured guidelines for designers [37, 62]. Combing the domain ontology and the novel automated BN learning algorithms will enable the detection of critical information and performing effective quality monitoring and control for AM.

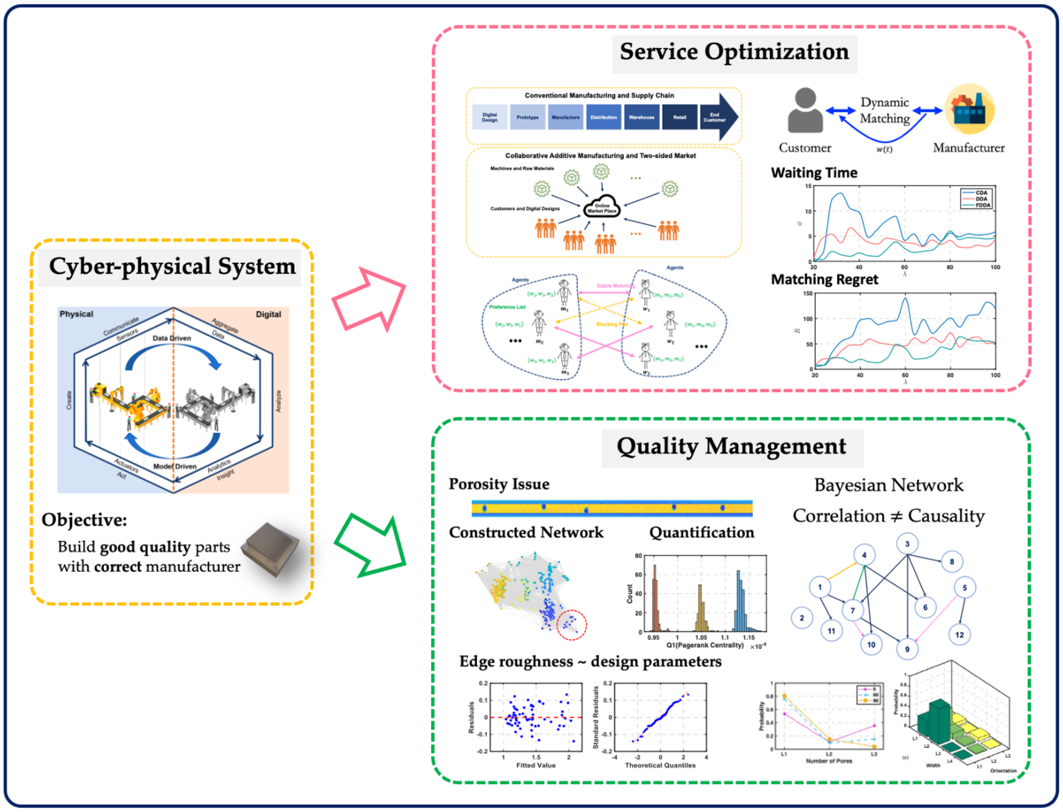

Figure 1.4. Roadmap of the dissertation. The objective of the research to build AM parts with good quality with the correct service provider in the AM cyber-physical systems.

1.3 Objectives

My research goal is to develop new machine learning methodologies for quality management and service optimization of large-scale complex systems. Specifically, my research objective is to develop data-driven models and create enabling methodologies for process monitoring, system diagnostics and prognostics, root cause analysis, and service optimization, with disparate applications in advanced manufacturing. My research will enable and assist in:

1. handling of massive and complex data generated from advanced sensing systems in manufacturing settings
2. designing novel models for interpretation of uncertain relations and extraction of pertinent information about system dynamics

3. exploitation of acquired knowledge for data-driven decision-making and service optimization

1.4 Organization

This dissertation is organized from multiple journals and conference manuscripts. We organize this dissertation in a top-down manner. First, we discuss the emergence of sharing economy and service optimization in the new cyber-physical AM system. Then, we explore the quality management for the individual in the system. The remainder of the dissertation is organized as follows:

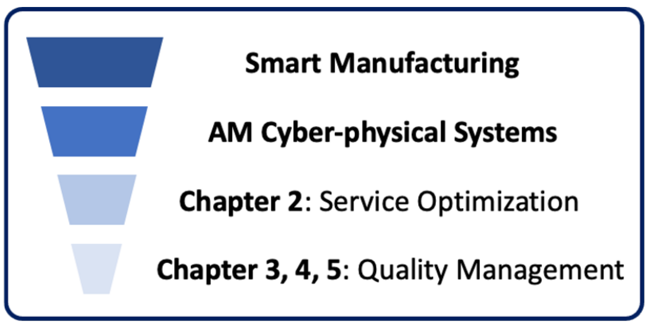

Figure 1.5. The overall top-down structure of proposed research methodologies in this dissertation.

In Chapter 2, we develop a bipartite matching framework to model and optimize resource allocation among customers and service providers through a stable matching algorithm in cyber-physical systems. The framework is implemented in customer-manufacturing allocation in cyber-physical platforms. The proposed sharing economy framework shows strong potential to realize a smart and decentralized AM sharing economy.

In Chapter 3, we present a design of AM experiments to investigate how design parameters (e.g., build orientation, thin-wall width, thin-wall height, and hatching spacing) interact with quality characteristics (i.e., edge roughness) in thin-wall builds. This research sheds insights on the optimization of engineering design to improve the quality of AM builds.

In Chapter 4, we utilize a generalized recurrence network analysis to not only capture recurrence dynamics in complex systems but also take the computational complexity into account. Here, as an extension of Chapter 2, we present another design of AM experiments to investigate how design parameters (e.g., build orientation, thin-wall width, thin-wall height, and hatching spacing) interact with different quality characteristics in thin-wall builds. The proposed design-quality analysis shows great potential to optimize engineering design and enhance the quality of PBF-AM builds.

In Chapter 5, we develop an ontology-based Bayesian network (BN) model to represent causal relationships between AM parameters (i.e., design parameters and process parameters) and QA/QC requirements (e.g., structure properties and mechanical properties). With the network representation, the causal relationships among variables can be identified and then be used to facilitate prediction, diagnosis, and support decision making in manufacturing production.

In the end, Chapter 6 concludes the dissertation and summarizes the contributions. Future research directions are also discussed in this chapter.

Chapter 2
Stable Matching of Customers and Providers for the Sharing Economy of Additive Manufacturing

Recently, sharing economy becomes a new way for people to "share" assets and services with others that disrupts traditional business models across the world. In particular, rapid growth of additive manufacturing (AM) enables individuals and small manufacturers to own machines and share under-utilized resources with others. Such a decentralized market calls upon the development of new analytical methods and tools to help customers and manufacturers find each other and further shorten the AM supply chain. This paper presents a bipartite matching framework to model the resource allocation among customers and manufacturers and leverage the stable matching algorithm to optimize matches between customers and AM providers. We perform a comparison study with Mix Integer Linear Programming (MILP) optimization as well as the first-come-first-serve (FCFS) allocation strategy for different scenarios of demand-supply configurations (i.e., from 50% to 500%) and system complexities (i.e., uniform parts and manufacturers, heterogeneous parts and uniform manufacturers, heterogeneous parts and manufacturers). Experimental results show that the proposed framework shows strong potentials to optimize resource allocation in the AM sharing economy.

2.1 Introduction

Assets (e.g., cars and houses) often require significant investments but may be underused. When the usage is low and as time passes, asset values are depreciated. Sharing economy turns underutilized assets owned by individuals into productive resources, which is a new way to supply goods and services, and enable individuals and small companies to compete with traditional large industries [63]. The emergence of sharing economy introduces new players in many fields, where some of them (e.g., Uber and Airbnb) have topped traditional companies and gained competitive advantage [64]. The size of sharing economy will increase to 335 billion by 2025 compared to the market size of 15 billion in 2015 [26]. Sharing economy not only provides highly compatible services, but also leads to significant social impacts such as reduction of ecological footprint [65], attitude change towards product ownership [66], and value re-distribution in the supply chain [67].

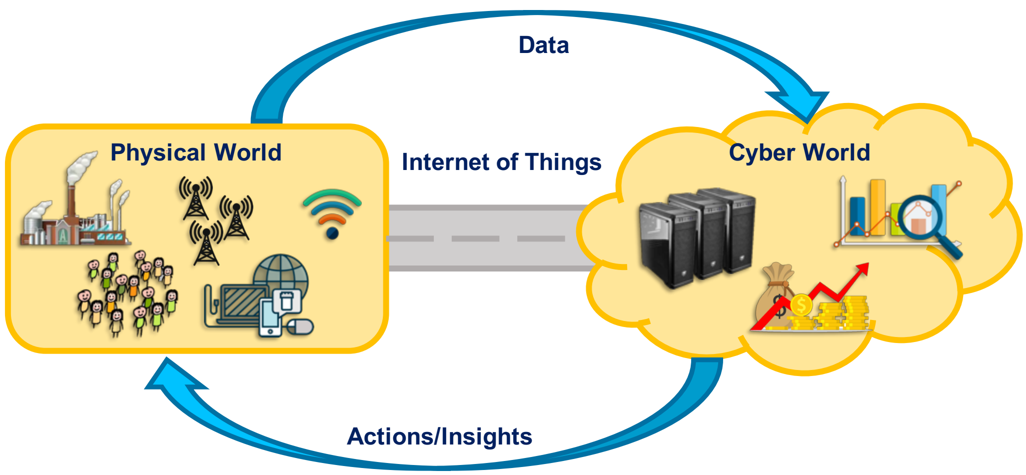

Figure 2.1. An illustration of cyber-physical interaction in the sharing economy. The organization is reflected in the cyber space through data, and analytics run in the cyber space feed the actions back to the physical world.

Sharing economy involves short-term transactions to share idle assets and services through an online cyber-physical platform. As shown in Figure 2.1, the physical world is reflected in the cyberspace through data-driven information processing, modeling, and simulation. For example, Uber collects data pertinent to the locations of passengers and available cars in the mobile application; and then runs scheduling algorithms to match a customer with the driver to provide rides. Similarly, Airbnb provides rooms as well as attribute information (e.g., price, reviews) of real estate properties to match with a customer. Cyber-physical integration provides the marketplace for peer-to-peer asset sharing and "on-demand" services for customers. However, the idea of "sharing economy" is relatively new to the field of Additive Manufacturing (AM).

AM prints parts directly from computer-aided designs (CAD) layer by layer without the need for expensive part-specific tooling. The AM market is projected to reach \$35.6 billion by 2024, a significant increase from the market size of \$11.8 billion in 2019 [68]. The growth of AM customers and manufacturers brings increasing complexity in the market. As the entry cost (e.g., asset and production costs) decreases, individuals and small manufacturers are now able to enter the market and compete with traditional large companies [69]. Conventionally, manufacturing companies acquire raw materials from suppliers, then processed and assembled parts, and finally shipped the products to end customers through distribution centers, warehouses, and retailers. On the contrary, AM bypasses the traditional supply chain. As shown in Figure 2.2, AM enables customers to submit their digital designs through the internet, and then providers manufacture and ship the product directly to customers.

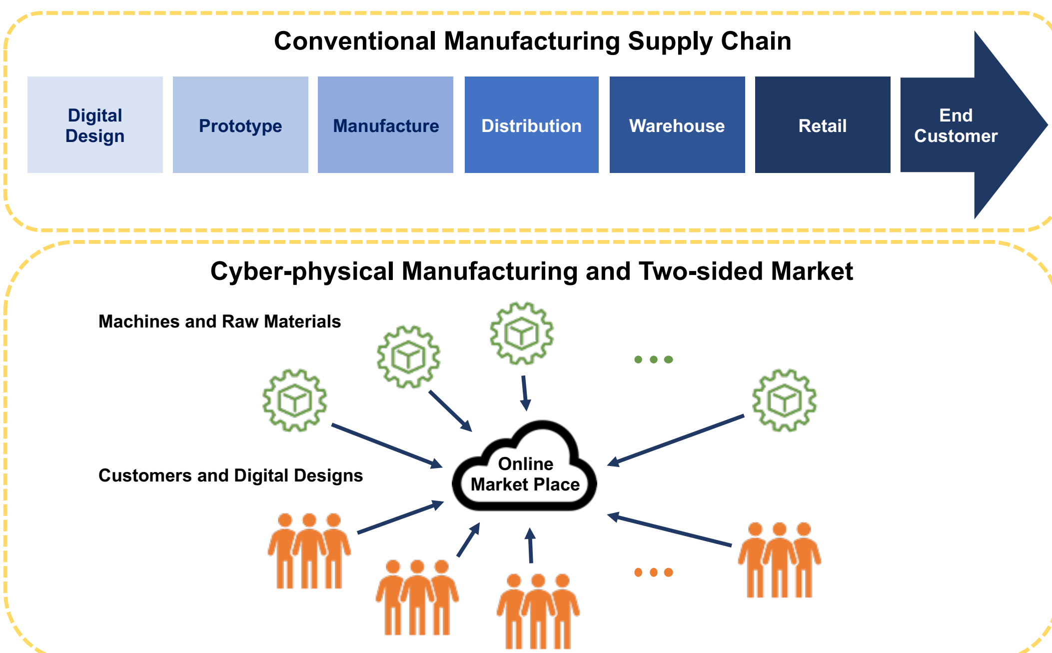

Figure 2.2. The illustration of traditional manufacturing supply chains and two-sided market.

As a result, the market becomes more and more decentralized. There is an urgent need to study the characteristics of the decentralized market and design a new framework to match customers with manufacturers. This paper presents a bipartite matching framework to model the resource allocation between customers and manufacturers and leverage the stable matching algorithm to optimizes matches between customers and AM providers. We perform a comparative study with Mix Integer Linear Programming (MILP) optimization as well as the first-come-first-serve (FCFS) allocation strategy for different demand-supply configurations, i.e., from 50% to 500%, which represent different scenarios. Experimental results show that the proposed framework effectively improves the performance of resource allocation in terms of the following metrics: namely customer's waiting time, manufacturer's lead time, customer's satisfaction, manufacturer's satisfaction, and matching regret. In comparison with the commonly used FCFS priority rule, experimental results show the stable matching algorithm decreases the matching regret by 35.52% when the demand is greater than supply; 36.75% when the demand equals supply; and 19.34% when the demand is less than supply.

The rest of this paper is organized as follows: Section 2.2 introduces an overview of the sharing economy and the cyber-physical AM. Section 2.3 shows the novel framework for AM sharing economy. Section 2.4 presents the experimental design and performance evaluation. Experimental results are provided in section 2.6. Finally, section 2.7 concludes this research as well as the challenges and opportunities of AM.

2.2 Research Background

The terms of "sharing economy", peer-to-peer market, or collaborative consumption, have become popular words in public media since Bostman and Rogers published their book in 2010 [70]. The sharing economy refers to the peer-to-peer sharing and access to underutilized goods and services, which prioritizes utilization and accessibility over ownership [65]. It allows individuals and small companies to compete with traditional large providers of goods or services. New business opportunities emerge by rethinking the design of business models, day-to-day decision making, and the challenges on the gain of profits [64].

The emergence of sharing economy can be traced back to ancient times when sharing was among family and friends [67]. The practice of sharing economy is sprinted from non-profit organizations such as Freecycle and couchsurfing, and further shifted into a bigger profitable business model by taking a small fraction of sharing fees such as Airbnb and Uber. Many peer-to-peer rental firms were founded after the global financial crisis between 2008 and 2010 [71], when people were seeking opportunities to purchase services they need instead of owning the assets. Then, the concept of sharing economy gained widespread attentions between 2011 and 2012 with the successes of two startup companies, Uber and Airbnb, in Silicon Valley.

Internet and mobile computing are two main driving forces of the sharing economy, which lead to a new generation of cyber-physical platforms. The physical world is reflected in the cyberspace through data-driven information processing, modeling, and simulation. Analytics in the cyberspace exploits the knowledge and useful information acquired from data to feed optimal actions (or control schemes) back to the physical world [23]. For example, the Uber app shows cars around a rider and provides a price based on the trip-related information. Algorithms in the cyberspace consider real-time factors such as traffic, driver's rating, and the distance to optimize the match between driver and rider. The automated systems establish ride-share matches with little effort from participants, enables people to share rides and increase the efficiency of urban transportation by connecting riders with drivers in real time [72]. Indeed, matching the supply and demand in a efficient and effective manner is critical to optimize the resource allocation in sharing economy platforms.

Current matching practices are summarized into two categories, namely optimization-based procedures and list-based solutions [73]. Conventional optimization-based procedures often consider the preference from one side. However, customers and providers have different objectives that often conflict with each other. As such, there is an urgent need to optimize resource allocation by taking the preference of both customers and service providers into account. It is insufficient for a decentralized market if only the objective of one group is considered and satisfied, either providers or customers. On the other hand, list-based solutions allow customers to self-select options in the list of options as displayed in the website or mobile applications. Here, customers need to scroll through the list to make their final selection. The transaction is completed only when a customer and a service provider reach an agreement, where the customer is willing to pay the price and the provider has the availability of assets or services which the customer is seeking. The FCFS is the most common approach in this structure where a customer who arrives the earliest will get treated or served before customers who enter later. Despite its simplicity, the FCFS approach is insufficient and limited in the ability to provide the optimal solution for customers and providers. To address the limitations of traditional practices, we propose a stable matching framework to optimize the customer-manufacturer pairing in a cyber-physical AM platform, and the proposed framework is benchmarked with both optimization-based procedures and as well as the FCFS priority rule.

The concept of stable matching is first introduced by Gale and Shapley in 1962 [74]. Abraham et al. [75] introduced two algorithms for a generalization of the student-project problem where students are assigned to projects based on their preferences. Results show that the matching produced by their algorithm is simultaneously best-possible for all students. Knuth proposed the three-dimensional extension of stable matching theory [76], where there are three sets of agents in the system. Gu et al. [77] proposed the use of matching theory for resource management in wireless networks, including one-to-one matching for device-to-device (D2D) communication, and a three-layer cache model (many-to-one) matching for online content caching. However, peer effects (i.e., device-to-device communication) are abundant in the wireless environment. In the AM cyber-physical platforms, each customer is treated as an individual and they rarely share information in real time as wireless devices.

The application of matching algorithms for subtractive manufacturing is mainly focused on service composition or capacity sharing. For example, Li et. al [78] optimized the service composition between two different sets of service candidates in cloud manufacturing. They compared service candidates in pairs to generate a multiple service composition solution. Here, the composition is based on a fixed set of services and their corresponding capacities. Similarly, resources can be only exchanged and shared among a limited number of manufacturers in [79]. In addition, Argoneto and Renna [80, 81] analyzed a model of capacity sharing for a set of geographically distributed and independent firms, they also discussed the implementation to realize such sharing framework [82]. Note that the work assignment among over-loaded and under-loaded machines is within a single manufacturer. As a result, service composition is a collaborative environment where a number of partner services are collectively used to achieve a business objective. However, the market of sharing economy is often characterized by a high degree of heterogeneity, where customers and providers may be interested in specific products or services [69]. The sharing economy market not only allows individuals and small manufacturers to compete with

Table 2.1. Summary of Notation

Notation	Definition
$\mathcal{X}$	binary allocation matrix
I	The number of manufacturers
$\mathcal{M}$	The set of manufacturers
J	The number of orders
$\mathcal{O}$	The set of orders
Q_i	The capacity of manufacturer i
r_i	Rating to the service provided by manufacture i
$\mathcal{C}_i$	The set of previous customers of manufacturer i
$PL_O(i,j)$	The preference of order i over manufacturer j
$PL_M(j,i)$	The preference of manufacturer j over order i
P	Market selling part of the part
C	Cost of the part
$\succeq$	Strictly prefer
$\succ$	Prefer
w	Order waiting time, a quantifier for evaluating the model performance.
LT_j	Order lead time at manufacturer j, a quantifier for evaluating the model performance.
$satis_c$	Customer's satisfaction, a quantifier for evaluating the model performance.
$satis_m$	Manufacturer's satisfaction, a quantifier for evaluating the model performance.
R	Matching regret, a quantifier for evaluating the model performance.

traditional large providers of goods or services but also provides an online marketplace for buyers and sellers to find each other. The value is generated by matching assets with customers who are willing to pay for the services [63]. The resource allocation for service composition in traditional manufacturing is different from the matching in AM sharing economy. Sharing economy shows strong potentials to revolutionize the AM market. Optimal match between customers and AM providers offers a higher degree of satisfaction among both sides, thereby leading to the development of AM market. There is an urgent need to investigate the stable matching framework for cyber-physical AM.

2.3 The Supply Chain Matching Problem for AM Market

In this section, we present a framework to model the resource allocation between customers and manufacturers and leverage the stable matching algorithm to optimize matches between customers and AM providers. We also benchmark the stable matching with Mixed Integer Linear Programming (MILP) and FCFS priority rule. Our model considers factors such as part's geometrical property (i.e., width, length, and height), manufacturer's capacity, cost of the raw material and so on. Moreover, we investigate the proposed framework for different system complexities and benchmark with other algorithms. Table 2.1 summarizes the math notations used in this paper.

2.3.1 System Model and Problem Formulation

The model is aimed at matching customer orders with the manufacturers in a two-sided market. We assume that there are I manufacturers $\mathcal{M} = \{m_1, m_2, \ldots, m_i, \ldots, m_I\}$ each with the capacity of Q_i, and J orders $\mathcal{O} = \{o_1, o_2, \ldots, o_j, \ldots, o_J\}$. Suppose orders are shipped right after they are manufactured. The shipping time is only proportional to the distance between the customer and the manufacturer. Both the processing time and shipping time are considered in the experiments. To formulate such an allocation problem, we first define two matrices, namely, the satisfaction matrix and the allocation matrix.

Definition 1 *The satisfaction matrix consists of element $\mathcal{S}_{ij}$ that describes the satisfactory level of a customer when order j is matched with manufacturer i, which is a composite index of building time T_b, transportation time T_t, service rating SR_i of manufacturer m_i, and market selling price P_j:*

$$\mathcal{S}_{ij} = \frac{SR_i}{P_j} * \frac{1}{(T_{bj} + T_{tj})} \quad \forall\ i = 1, ..., I, j = 1, ...J \tag{2.1}$$

$$SR_i = \sum_{l=l_1}^{l_{L_i}} r_{il} \quad \forall\ i = 1, ..., I \tag{2.2}$$

where r_{il} is the rating that customer l gives to the service provided by manufacturer i, and $\mathcal{L}_i = l_1, l_2, \ldots l_{L_i}$ is the set of previous customers of manufacturer i.

Definition 2 *The allocation matrix $\mathcal{X}$ consists of the binary element $x_{ij} \in 0, 1$, where $\forall\ i = 1, ..., I,\ j = 1, ..., J$, describes the allocation of the order o_j to manufacturer m_i.*

Because the allocation matrix $\mathcal{X}$ is with binary values, we formulate the matching between orders and manufacturers as a MILP allocation problem. The objective function is to maximize the satisfaction of customers in a decentralized market. The MILP formulation is as follows:

$$\max_{\mathcal{X}} \sum \mathcal{S} \circ \mathcal{X} \tag{2.3}$$

$$\sum_{i \in I} x_{ij} = 1 \quad \forall\ o_j \in \mathcal{O} \tag{2.4}$$

$$\sum_{j \in J} x_{ij} < Q_i \quad \forall\ m_i \in \mathcal{M} \tag{2.5}$$

$$x_{ij} \in 0, 1 \quad \forall\ m_i \in \mathcal{M}, o_j \in \mathcal{O} \tag{2.6}$$

where $\circ$ in equation (2.3) is the Hadamard product. Equation (2.4) guarantees that each order is only assigned to one manufacturer. Equation (2.5) poses a constraint on capacity of each manufacturer. Equation (2.6) defines the $\mathcal{X}$ as a binary matrix. The formulated MILP problem is solved by MATLAB, and it is utilized as the benchmark to the proposed matching framework.

2.3.2 Stable Matching

As the market size increases, the computational complexity of MILP problem increases exponentially. Therefore, we propose a bipartite matching framework to achieve an efficient solution for recourse allocation in the cyber-physical AM platform. The classical stable marriage considers a set of man and another set of women (both sets are with size n), and each person has his or her preference list over all other people in the opposite set. The goal is to match each man with one woman in a stable manner. When the matching is stable, no blocking pair exists. Note that a block pair is defined as a pair of man and woman have a better partner from other pairs based on their preference lists. This is one-to-one matching because we are only matching one man with one woman, and the stable condition could be reached through the Gale-Shapley Algorithm. During the matching process, one accepts the match if the new match has a better ranking in his or her preference list, and rejects otherwise. No one knows others' preferences during the process, and the algorithm terminates when no more matching request is needed.

For one-to-one matching problems, each entity of one set can be only matched to at most one entity from the other set. The other two types are many-to-one matching and many-to-many matching problems. For many-to-one matching problems, the entities from one set can be matched to entities from the other set without any quota limitation. However, entities from the other set could only be matched to at most one entity from the set. Examples such as the hospital resident allocation while one resident can only go for one hospital, and one hospital could handle a limited number of residents. For many-to-many matching problems, entities from both sets are able to match to as many as entities from the other set up to their capacities. Examples include the kidney exchange problem and the partnership formation problem.

Definition 3 *(Stable Pair) A pair* (m_i, o_j) *is defined as a stable pair when for all other possible pairs* $(m_i, o_{j'})$ *and* $(m_{i'}, o_j)$ *(where* $o_{j'} \in \mathcal{O} \backslash o_j$ *and* $m_{i'} \in \mathcal{M} \backslash m_i$*), at least one of the following is true:*

1. $m_i \succeq_{o_j} m_{i'}$
2. $o_j \succeq_{m_i} o_{j'}$

Note that $m_i \succeq_{o_j} m_{i'}$ indicates the statement "order o_j prefers manufacturer m_i over manufacturer $m_{i'}$". The operator $\succeq_{o_j}$ denotes the preference list of o_j to $m_i \in \mathcal{M}$.

Definition 4 *(Stable Matching) A joint matching* $\langle \mathcal{M}, \mathcal{O} \rangle$ *returns stable matching if all pairs in the set* $\{(m_i, o_j) | m_i \in \mathcal{M}, o_j \in \mathcal{O}\}$ *are stable pairs.*

As discussed in Section 4.1, the key of stable matching algorithm is to generate the preference list. In the two-sided AM market, the customer prefers high-quality products at a lower price, as well as less waiting time, while the manufacturer prefers more profits. Therefore, each set has its property. We propose the preference list of orders (i.e., customers) and the preference list of manufacturers as follows.

Definition 5 *For a order* o_j*,* $\forall o_j \in \mathcal{O}$*, the preference list over the manufacturer* m_i*,* $\forall m_i \in \mathcal{M}$*, is formulated as*

$$PL_o(i,j) = \frac{SR_i}{P_j} * \frac{1}{(T_{bj} + T_{tj})} \quad \forall\ i = 1, ..., I, j = 1, ...J \tag{2.7}$$

Note that the PL_{order} is a $I \times J$ matrix. The larger the number is in the preference matrix, the order is more preferred to be built at the corresponding manufacturer.

Definition 6 *For a manufacturer* m_i*,* $\forall\ m_i \in \mathcal{M}$*, the preference list over the order* o_j*,* $\forall\ o_j \in \mathcal{O}$*, is formulated as*

$$PL_M(j,i) = P_{ji} - C_{ji} \quad \forall\ i = 1...,I, j = 1,...J \tag{2.8}$$

With the input of preference lists, the capacity, and the time matrix, we develop the stable marriage algorithm to identify many-to-one matching between orders and manufacturers, as shown in Algorithm 2.

The proposed algorithm begins with the initialization of preference lists and auxiliary matrices $\mathcal{M}_{OrderSingle}$ and $\mathcal{M}_{Proposed}$. It is worth mentioning that the $\mathcal{M}_{OrderSingle}$ is a $J \times 1$ binary matrix checking if the order is matched to a manufacturer or not, and the $\mathcal{M}_{Proposed}$ is a $I \times J$ binary matrix indicating the proposal status of the orders. After initialization, the matching algorithm first pairs orders and manufacturers by prioritizing the capacity of manufacturers. Then, the next order will be matched to the first available manufacturer according to its preference list. In other words, the model begins with order-oriented matching. After all manufacturers reached their capacity, the model shifts to manufacturer-oriented stable matching. In addition, the algorithm swaps between a matched order k with an unmatched order i if i is more preferred than k by manufacturer j (see line 15-21). Finally, the algorithm terminates when all stable pairs are identified.

Algorithm 1 The Proposed Stable Marriage Algorithm for Order-Manufacturer Matching

Input:
$Capacity \leftarrow$ the capacity of each manufacturer
$ProcessTime \leftarrow$ the process time of each order
$ShippingTime \leftarrow$ the shipping time of each order
Initialization:
PL_{mfg} : the preference list of manufacturers to orders
PL_{order} : the preference list of orders to manufacturers
$\mathcal{M}_{OrderSingle}$: a binary matrix, indicating whether an order is matched or not
$\mathcal{M}_{Proposed}$: a binary matrix, indicating whether an order has proposed to a manufacturer or not
$\mathcal{X}$: the binary allocation matrix

While $\mathcal{M}_{OrderSingle} \neq \phi$
  If all manufacturers have reached to their maximum capacities
    match the first available mfg j to its favorite unmatched order i according to $PL_{mfg}(j,:)$
    $\mathcal{M}_{Proposed}(i,j) = 1$
    $\mathcal{M}_{OrderSingle}(i) = 0$
    $\mathcal{X}(i,j) = 1$
  Else
    select a random order i, find the best unproposed manufacturer j according to $PL_{order}(i,:)$
    $\mathcal{M}_{Proposed}(i,j) = 1$
    If manufacturer j has not reached to its capacity
      \\match i and j
      $\mathcal{M}_{OrderSingle}(i) = 0$
      $\mathcal{X}(i,j) = 1$
    Else \\if j has already reached to its capacity
      If order i is more preferred than a matched order k according to $PL_{mfg}(j,:)$
        \\match i and j and unmatch k and j
        $\mathcal{M}_{OrderSingle}(i) = 0$
        $\mathcal{X}(i,j) = 1$
        $\mathcal{M}_{OrderSingle}(k) = 1$
        $\mathcal{X}(k,j) = 0$
      End
    End
  End
End While
Output: $\mathcal{X}$

2.4 Experimental Design and Performance Evaluation

Figure 2.3 shows the design of simulation experiments to evaluate and validate the proposed matching framework. The system complexity consists of three scenarios, namely (1) uniform parts and manufacturers; (2) heterogeneous parts and uniform manufactures; (3) and heterogeneous parts and manufacturers. In the first scenario, parts with the same design and manufacturers with same capacities are generated. We vary the distance between manufacturers and customers as well as the number of orders with respect to the demand-supply configuration. Then, we add variation to the design of parts. Therefore, the building time and the cost will be different among parts. Finally, we add variations to manufacturers. For example, we set the cost of restocking and the rating of manufacturers different. As shown in Figure 2.3, the factor of demand-supply configuration also varies from 50% to 500%.

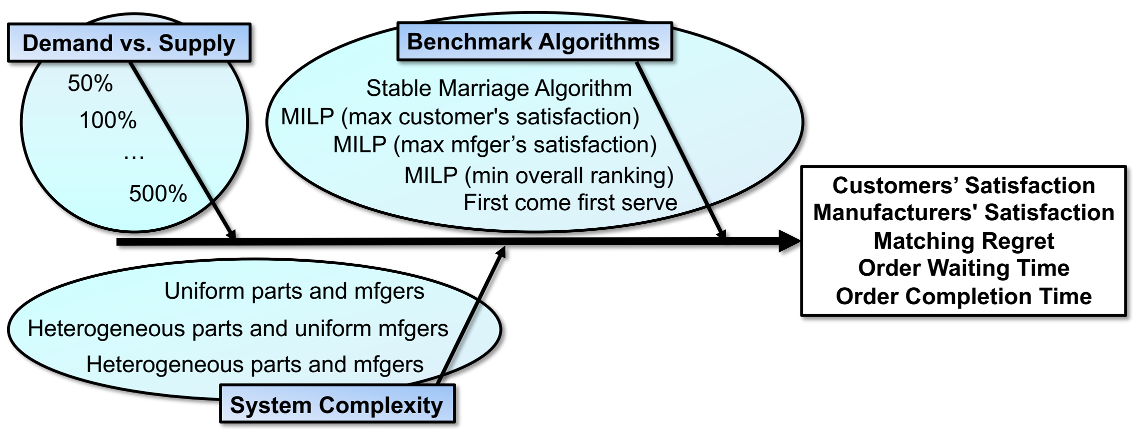

Figure 2.3. The cause-and-effect diagram for experimental design.

Further, we benchmark the stable-marriage algorithm with the FCFS model as well as three MILP models, i.e., MILPcustomer, MILPmfg, and MILPordinal, respectively. The first model, MILPcustomer, maximizes the satisfaction of customers. The second model, MILPmfg, maximized the satisfaction of manufacturers. The third model, namely the MILPordinal, aims at minimizing the overall manufacturer rankings, which introduces the ranked preference list from stable matching to the objective function and solves the problem using the centralized optimization model. The objective functions of three benchmark models are summarized in Table 2.3.

Table 2.2. Summary of Benchmark Models

Model	Objective Function	Description
MILPcustomer	$max\ PL_O \circ \mathcal{X}$	maximize the satisfaction of customers
MILPmfg	$max\ PL_M \circ \mathcal{X}$	maximize the satisfaction of manufacturers
MILPordinal	$min\ \text{ordinal}(PL_O) \circ \mathcal{X}$	minimizing the overall manufacturer rankings

2.4.1 Performance Evaluation of matching models

Five quantifiers are used to evaluate allocation results and compare the performance of different matching models.

- **Customer waiting time (w)**

  The customer waiting time is the time from an order is submitted until it is being received by the customer.

- **Manufacturer lead time (LT)**

  The manufacturer's lead time is the time that a manufacturer needs in total to finish all assigned orders.

- **Customer's satisfaction ($satis_c$)**

  The customer's satisfaction is calculated by equation. 2.7, which is the rating over price and time. This indicates that the customers want to pay less but get a high quality product, as well as less waiting time. Note that in the next section, we output the normalized customer's satisfaction for easier comparison.

- **Manufacturer's satisfaction ($satis_m$)**

  The manufacturer's satisfaction is calculated by

$$satis_m = \frac{P_{ji} - C_{ji}}{LT_j} \quad \forall\ i = 1..., I, j = 1, ...J \tag{2.9}$$

  where LT_j is the total manufacturer lead time of all orders assigned to manufacturer j. Similar as the previous quantifier, we output the normalized manufacturer's satisfaction for a better visualization.

- **Matching regret (R)**

The matching regret is calculated as:

$$R = \sum_{i \in I} \sum_{j \in J} PL_O(i,j) + PL_M(j,i) \tag{2.10}$$

which quantifies the regret that each order obtains when it is not assigned to its most preferred manufacturer, as well as when each manufacturer is not matched to its most preferred order. Smaller regret indicates a better matching result.

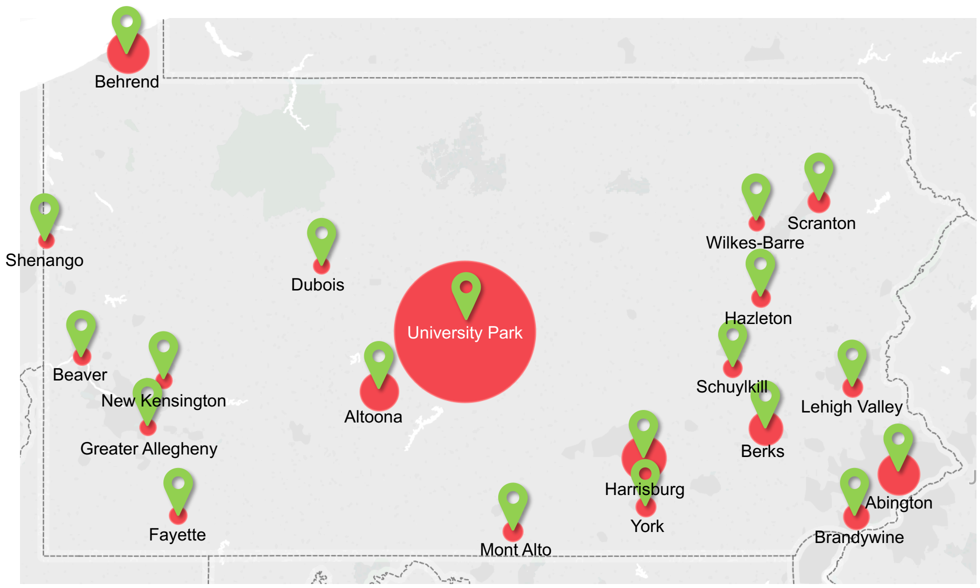

Figure 2.4. Penn State DIGI-Net. Green pins show the location of Penn State campuses across Pennsylvania, and the size of red dots are associated with the number of students studying on the campus.

As a large research institution, Penn State has invested in many different types of digital fabrication resources, which are spread among a number of different academic colleges and departments. The Digital Inquiry and Group Innovation Network, also known as DIGI-Net, seeks to enhance design processes for the Penn State community. The goal of DIGI-Net is to democratize digital fabrication and make it easier for people to access, learn about, and use Penn State's resources [83]. Our simulation aims at providing a better matching model for the Penn State DIGI-Net. In the case study, the digital fabrication network of AM manufacturers (e.g., small, medium, and large providers) are assumed to spread over a geographic region. The digital AM network democratizes the low-volume-high-mix manufacturing with an aim to make it easier for manufacturers and customers to find each other. The simulation studies are conducted on a 3.30 GHz Intel Xeon CPU with 16 GB RAM, 64-bit operating system.

2.5 Experimental Results

2.5.1 Case I: Uniform parts and manufacturers

In the first case study, we assume uniform parts and manufacturers. Parts have the same design, and manufacturers have the same capacity. However, the manufacturers are geographically distributed in the spatial region, and therefore the distances to customers vary. Also, the number of orders (or parts) varies with respect to the demand-supply ratio.

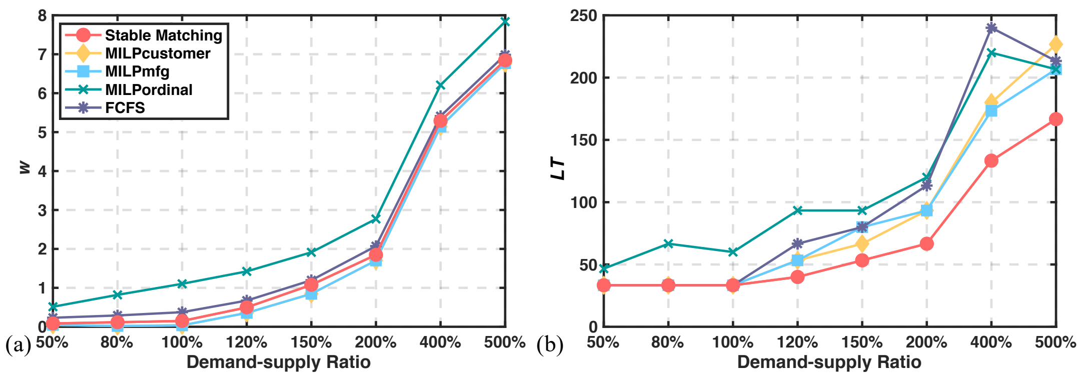

Figure 2.5. (a) The average waiting time of orders and (b) the average order lead time of manufacturers for different matching models when there are uniform parts and manufacturers.

As shown in Figure 2.5 (a), the waiting time of orders increases as the number of order increases. Among five matching models, the stable marriage, the MILPmfg, and the MILPcustomer (overlapping with MILPmfg) have a shorter waiting time, and the MILPordinal has the longest waiting time compared to other methods. There is almost no waiting time for stable matching, MILPmfg, and MILPcustomer when the demand-supply ratio is low. However, MILPordinal (i.e., the green line) has a longer waiting time, customers need to stay in the queue and wait to be matched. This is because of the proposed algorithm allocates the orders evenly - it not only considers the preference of customers, but also the desire of manufacturers. MILPmfg and

MILPcustomer assign the order based on one-side satisfaction value. It is also worth mentioning that the MILPordinal does not give a good matching result regarding the order waiting time. The minimization of the overall ordinal ranking causes queue in manufacturers no matter how the demand-supply configuration changes. This indicates that the MILPordinal does not work well in this case. The FCFS priority rule gives the matching result slightly worse than stable matching, MILPcustomer, and MILmfg because it does not generate optimal matches.

Figure 2.5 (b) evaluates the average order lead time of manufactures. Note that the manufacturer lead times of the stable matching, MILPcustomer, MIMPmfg, and FCFS are same with each other when the demand-supply configuration is less than or equal to 100%. This is because that there are uniform parts and manufacturers. Again, the stable matching provides the lowest completion time and the MILPordinal gives the worst. Among three other models, manufacturers need more time to complete work requests under the FCFS model.

We further output the customer's satisfaction, the manufacturer's satisfaction, and the matching regret. Note that we normalize $satis_c$ and $satis_m$ for a better illustration. According to Figure 2.6 (a), MILPcustomer yields the best result regarding the customer's satisfaction, and stable matching performs slightly worse than it. This is because that MILPcustomer only focuses on one-side (i.e., customer), and stable matching focuses on both sides.

As shown in Figure 2.6 (b), the performance of stable matching starts to outperform other algorithms as the number of customer increases (i.e., the demand-supply configuration increases). Comparing MILPmfg and MILPordinal, it is observed that the MILPmfg produces less customer satisfaction but higher manufacturers satisfaction. The criteria that customers and manufacturers target are different as the preference list indicates, thus there exists a trade-off between the satisfaction of the customer and the satisfaction of the manufacturer. The MILPcustomer and MILPordinal, since they only consider the preference of customers, present a better output of $satis_c$. Similarly, the MILPmfg brings a better satisfactory level for the manufacturer but opposite for the customer. The stable matching, which considering both sides of the market, gives a "balanced" matching result in between. The MILPordinal performs the worst no matter how the configuration of demand and supply changes.

Figure 2.6 (c) shows the matching regret calculated from different matching

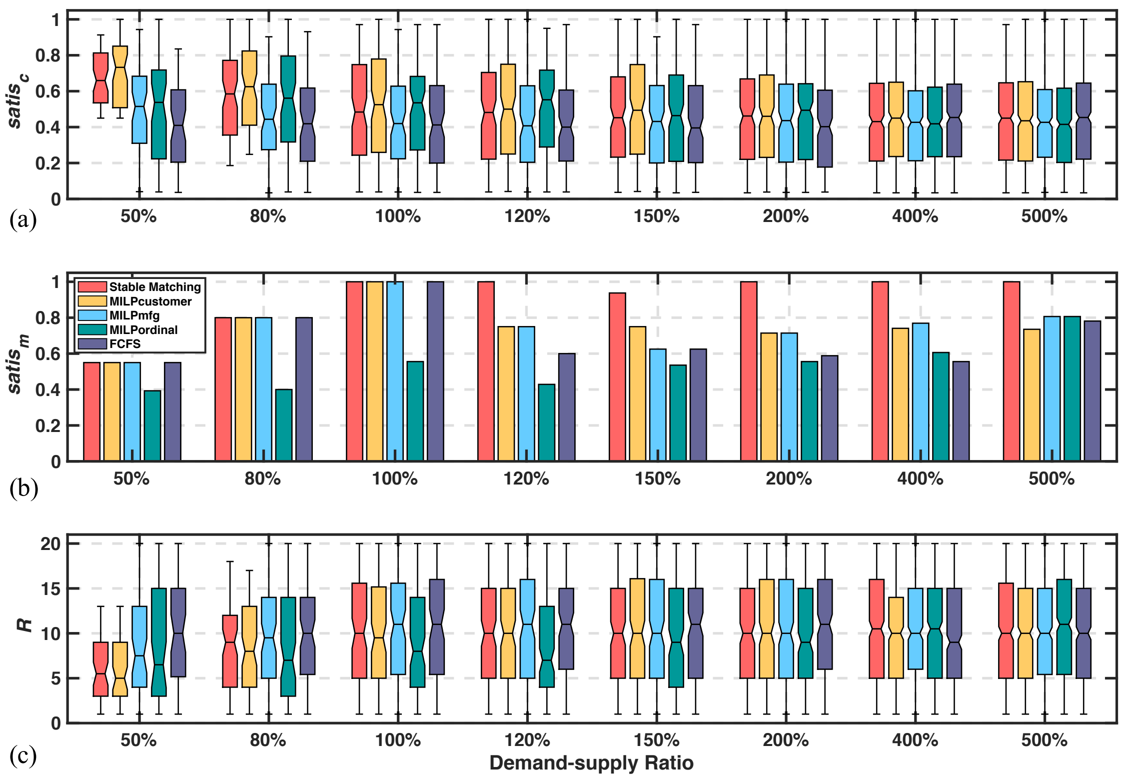

Figure 2.6. (a) Normalized customer's satisfaction, (b) normalized manufacturer's satisfaction, and (c) matching regret for different matching models when there are uniform parts and manufacturers.

models. MILPordinal outperforms other models due to the fact that the objective of the matching algorithm is to minimize the overall ordinal ranking. It may also be noted that as the demand-supply increases, the result of all models gives very close results. For example, in Figure 2.6 (a) and (c), models result in very similar $satis_c$ and $satis_m$. This is because when there exists a long queue, the system begins to be "saturated". However, the stable matching will help manufacturers to gain more benefits. Overall, the stable matching algorithm performances the best. It is better to use the actual satisfaction instead of the ranking in the objective.

2.5.2 Case II: Heterogeneous parts and uniform manufactures

We then add some variations to the parts but keep all manufactures the same capacity. The added variation to the part includes different distribution for layer thickness and the dimension of the part. Then the building time (T_b) and the cost (C) will be different among parts.

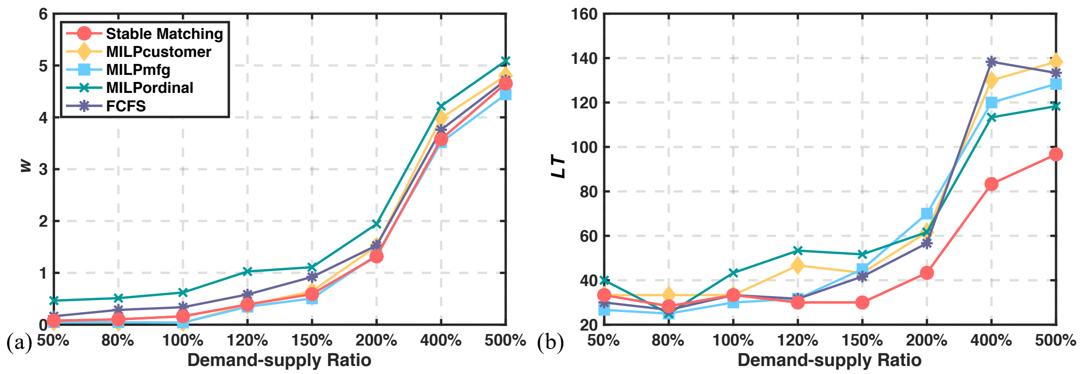

Figure 2.7. (a) The average waiting time of orders and (b) the average order lead time of manufacturers for different matching models when there are heterogeneous parts and uniform manufacturers.

As shown in Figure 2.7 (a), the stable matching, MILPmfg, and MILPcustomer return very close waiting times when the demand-supply configuration is relatively low, but the MILPcustomer brings more waiting time as the configuration keeps increasing. When there exists a queue in the system, the MILPmfg will first select the part with more benefit. Since we have uniform manufacturers, which means that the price of raw material is the same. The bigger the volume that a part has, the more the manufacturer is willing to take the order. Therefore, the MILPmfg will first select the order with longer processing time, so the waiting time will be less for the rest of those in the queue. This is the reason why the average waiting time of part is lower when using the MILPmfg than MILPcustomer when the demand-supply ratio gets larger. Figure 2.7 (b) illustrates the average order lead time of manufacturers. When the scale of the system is small, the is not much difference between stable matching, MILPcustomer, MILPmfg, and FCFS. However, as more customer enters, stable matching gives relatively shorter lead time.

As shown in Figure 2.8 (a), MILPcustomer still results in a better $satis_c$ compared to other methods. The variation of parts explains outliers and lower value of $satis_c$

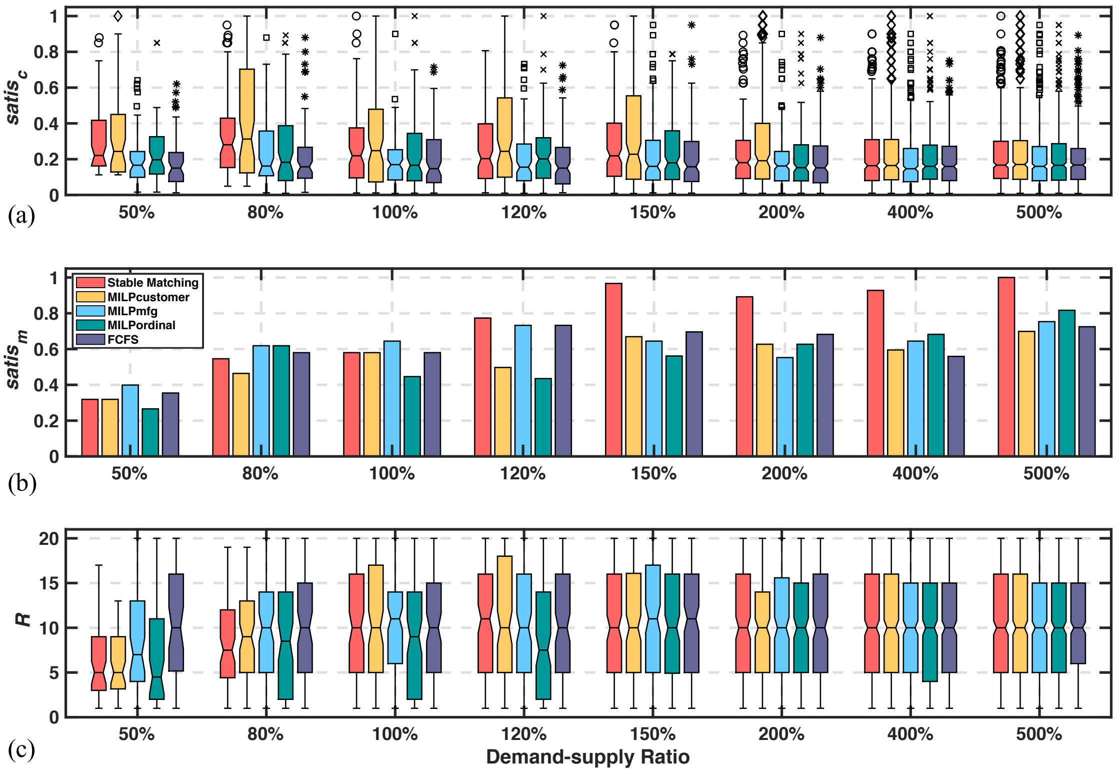

Figure 2.8. (a) Normalized customer's satisfaction, (b) normalized manufacturer's satisfaction, and (c) matching regret for different matching models when there are heterogeneous parts and uniform manufacturers.

compared to Figure 2.6 (a). If we only looking at MILPcustomer and MILPmfg, it is not hard to find that the MILPcustomer outperforms MILPmfg in Figure 2.8 (a), but MILPmfg outperforms MILPcustomer in 2.8 (b). In Figure 2.8 (b), MILPmfg yields better satisfaction for manufacturers when the demand-supply configuration is less than 100%. However, always selecting the part with more profit might lead to the shrinkage of total profit as the total number of orders produced is decreased at a single manufacturer. The more customer in the system, the stable matching will outperform other models. The matching regret is shown in Figure 2.8 (c). Here, the MILPordinal demonstrates a smaller matching regret than other algorithms. The result is as expected since the MILPtwosides takes the ordinal preference into account and aims at minimizing regret.

2.5.3 Case III: Heterogeneous parts and manufacturers

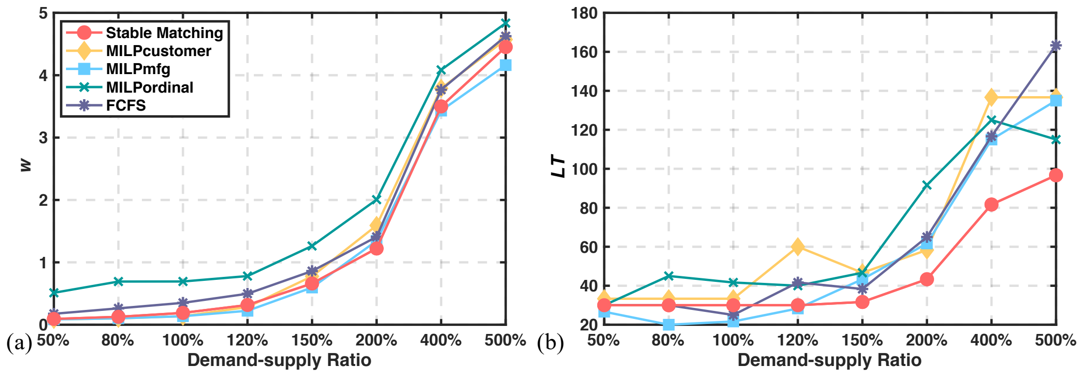

Figure 2.9. (a) The average waiting time of orders and (b) the average order lead time of manufacturers for different matching models when there are heterogeneous parts and manufacturers.

In the last case study, variations are added to both parts and manufacturers. Here, we vary the part geometry based on a normal distribution with the mean of the part geometry in Section 2.5.1. For the manufacturers, we vary the cost of raw materials, the number of previous customers, and the average rating, and the capacity. As mentioned before, the new form of AM markets allows the individuals and small manufacturers to enter and compete with larger enterprises. These bigger manufacturers might have discounts when purchasing a great number of metal powders because they have the capability to handle more orders as well as return customers. They might also produce products with better quality (this will result in a higher customer's rating) since they are more "professional" in the sense that they have more experience in manufacturing. Therefore, the order waiting time and the order lead time in Figure 2.9 are smaller than values in Figure 2.5.

As shown in Figure 2.10 (a), there are more outliers compared to Figure 2.6 (a) and Figure 2.8 (a). The trade-off between manufacturer's preference and customer's preference can still be seen by comparing yellow boxes and blue boxes in Figure 2.8 (b). Furthermore, in Figure 2.10 (c), the average of matching regret indicates that the average ranking that the matching model can achieve. For example, when the demand-supply configuration is 50%, the average matching regret of stable matching (i.e., in red) and MILPordinal (i.e., in green) are around 5 and 4.5, respectively. This means that when utilizing stable matching, the orders are mostly matched to the ranked 5 manufacturers and vice versa. The MILPordinal can achieve a better

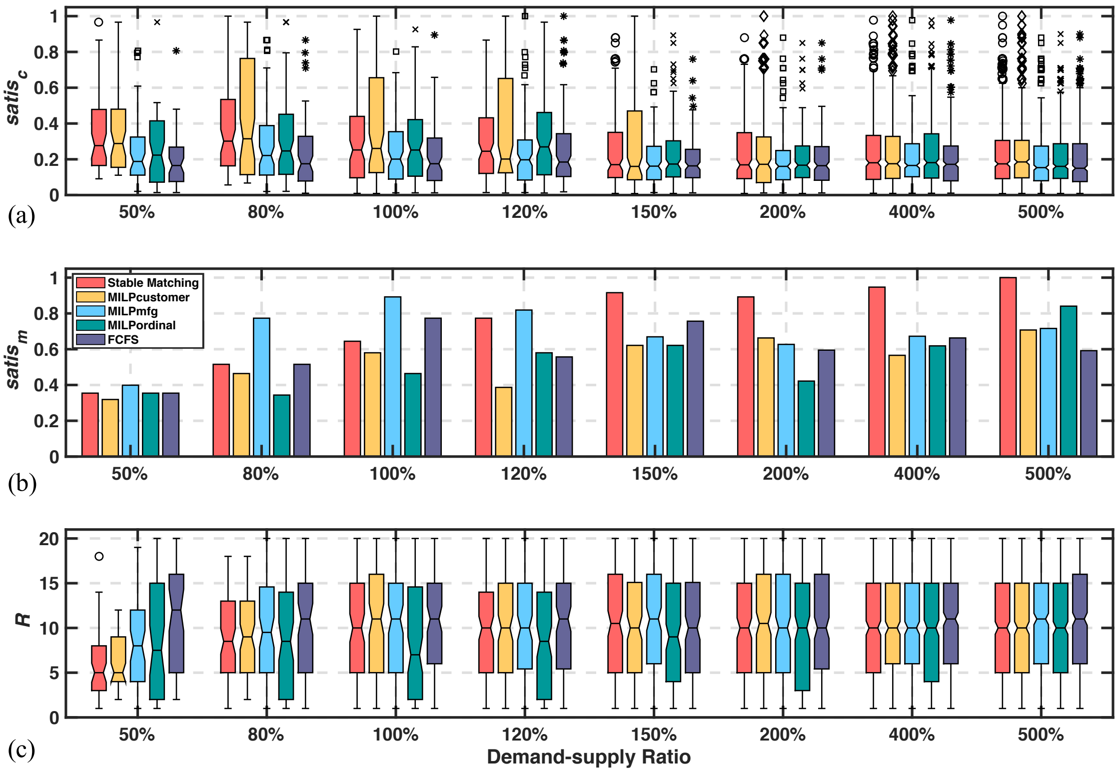

Figure 2.10. (a) Normalized customer's satisfaction, (b) normalized manufacturer's satisfaction, and (c) matching regret for different matching models when there are heterogeneous parts and manufacturers.

allocation result with respect to R. When the demand-supply configuration increases, the matching regrets of four matching models start converging to 10. Matching regret will not be a good criterion to consider if the number of customers is way more than capacity of system.

In addition, we summarized the improvement of the proposed stable matching algorithm in comparison with other proposed algorithms (i.e., MILPcustomer, MILP-manufacturer, MILPordinal, and FCFS) in Table 2.3. Results ($mean \pm std$) are based on 100 replications. As shown in Table 2.3, we compared the performance of different algorithms for case I, II, and III and eight demand-supply configurations. When demand is less than supply, stable matching decreases LT but does not improve w. However, the proposed stable matching algorithm starts to reduce customers waiting time and manufacturer lead time simultaneously when the demand increases. For example, when the demand-supply configuration is 50%, stable matching algorithm improves LT by 31.39% from MILPcustomer, but MILPcustomer provides a 17.06% better w than stable matching. However, when the demand-supply configuration reaches to 150%, stable matching algorithm outperforms MILPcustomer regarding both w and LT. In most of the cases, stable matching algorithm yields better $satis_s$ and $satis_m$ because of balanced considerations of preferences of both manufacturers and customers. Overall, the stable matching algorithm yields better matching pairs when the demand-supply ratio is high.

Table 2.3. Performance comparison of stable marriage and other algorithms.

Case	Algorithm	Quantifier	Demand-supply Configuration							
			50%	80%	100%	120%	150%	200%	400%	500%
Case I	stable matching vs. MILPcustomer	w	−30.01 ± 2.13%	−56.23 ± 4.25%	−74.46 ± 3.65%	−24.88 ± 0.26%	−11.35 ± 0.08%	−6.86 ± 0.03%	−3.31 ± 0.01%	−2.65 ± 0.01%
		LT	0.00 ± 0.00%	0.00 ± 0.00%	0.00 ± 0.00%	25.98 ± 0.35%	25.46 ± 0.50%	30.03 ± 0.39%	26.99 ± 0.31%	26.05 ± 0.32%
		$satis_c$	−1.81 ± 0.25%	−7.94 ± 0.35%	0.07 ± 0.06%	0.26 ± 0.33%	−0.64 ± 0.41%	−0.60 ± 0.34%	−0.72 ± 0.43%	−0.81 ± 0.40%
		$satis_m$	−10.39 ± 0.14%	−3.66 ± 0.15%	−5.24 ± 0.32%	−2.64 ± 1.62%	−4.71 ± 1.43%	−5.43 ± 0.82%	−6.35 ± 0.80%	−6.06 ± 0.63%
		R	0.00 ± 0.00%	0.00 ± 0.00%	0.00 ± 0.00%	36.00 ± 1.33%	35.38 ± 1.74%	44.10 ± 1.82%	37.80 ± 1.22%	36.04 ± 1.20%
	stable matching vs. MILPmfg	w	−30.01 ± 2.13%	−56.23 ± 4.25%	−74.46 ± 3.65%	−24.88 ± 0.26%	−11.35 ± 0.08%	−6.86 ± 0.03%	−3.31 ± 0.01%	−2.65 ± 0.01%
		LT	0.00 ± 0.00%	0.00 ± 0.00%	0.00 ± 0.00%	27.19 ± 0.41%	26.02 ± 0.48%	30.45 ± 0.37%	27.26 ± 0.32%	25.69 ± 0.31%
		$satis_c$	47.35 ± 0.12%	10.41 ± 0.17%	0.60 ± 0.16%	0.87 ± 0.27%	0.01 ± 0.39%	1.04 ± 0.33%	0.93 ± 0.33%	1.40 ± 0.37%
		$satis_m$	43.17 ± 0.58%	25.93 ± 0.41%	6.38 ± 0.54%	4.78 ± 0.62%	2.37 ± 1.21%	1.87 ± 0.69%	−0.28 ± 0.55%	0.29 ± 0.55%
		R	−0.01 ± 0.00%	−0.02 ± 0.00%	0.00 ± 0.00%	38.50 ± 1.78%	36.38 ± 1.74%	44.90 ± 1.73%	38.35 ± 1.28%	35.36 ± 1.12%
	stable matching vs. MILPordinal	w	51.69 ± 0.45%	41.31 ± 0.43%	36.54 ± 0.35%	18.29 ± 0.11%	11.59 ± 0.05%	6.71 ± 0.03%	2.61 ± 0.01%	2.08 ± 0.01%
		LT	33.81 ± 0.84%	47.42 ± 0.60%	54.35 ± %0.39	50.27 ± 0.39%	42.70 ± 0.51%	42.25 ± 0.53%	32.32 ± 0.41%	29.50 ± 0.30%
		$satis_c$	−15.35 ± 3.63%	−25.34 ± 6.15%	−32.40 ± 2.28%	−22.32 ± 2.27%	−15.64 ± 1.10%	−10.51 ± 1.07%	−4.37 ± 0.73%	−2.26 ± 0.45%
		$satis_m$	3.17 ± 0.28%	2.15 ± 0.85%	−17.89 ± 0.47%	−14.88 ± 0.89%	−13.95 ± 0.74%	−12.70 ± 0.92%	−7.35 ± 0.77%	−6.33 ± 0.59%
		R	53.80 ± 4.10%	94.40 ± 8.73%	123.20 ± 10.00%	104.50 ± 7.74%	77.25 ± 5.03%	75.90 ± 4.95%	49.10 ± 2.13%	42.72 ± 1.31%
	stable matching vs. FCFS	w	83.61 ± 0.02%	83.41 ± 0.01%	82.81 ± 0.01%	64.36 ± 0.01%	48.66 ± 0.01%	33.97 ± 0.01%	14.92 ± 0.01%	11.59 ± 0.01%
		LT	−0.50 ± 0.12%	0.00 ± 0.00%	0.00 ± 0.00%	26.41 ± 0.30%	26.21 ± 0.42%	30.90 ± 0.34%	26.23 ± 0.25%	25.85 ± 0.26%
		$satis_c$	49.81 ± 0.50%	12.53 ± 0.69%	0.15 ± 0.13%	0.79 ± 0.31%	1.02 ± 0.42%	0.11 ± 0.44%	0.54 ± 0.36%	1.54 ± 0.36%
		$satis_m$	58.35 ± 7.61%	31.62 ± 2.18%	6.64 ± 0.52%	4.35 ± 0.97%	3.10 ± 1.16%	0.17 ± 0.79%	−1.10 ± 0.57%	0.47 ± 0.56%
		R	−0.40 ± 0.08%	−0.02 ± 0.01%	0.00 ± 0.00%	36.67 ± 1.12%	36.63 ± 1.62%	45.80 ± 1.70%	36.20 ± 0.93%	35.52 ± 0.96%
Case II	stable matching vs. MILPcustomer	w	−15.77 ± 0.65%	−28.32 ± 1.66%	−38.18 ± 1.58%	−0.26 ± 3.24%	16.92 ± 0.83%	14.11 ± 0.35%	8.63 ± 0.09%	6.14 ± 0.05%
		LT	13.06 ± 0.84%	11.45 ± 0.55%	6.00 ± 0.42%	32.03 ± 0.80%	36.35 ± 0.69%	33.51 ± 0.48%	29.41 ± 0.39%	27.97 ± 0.43%
		$satis_c$	0.00 ± 0.00%	5.12 ± 0.68%	−1.08 ± 0.35%	2.39 ± 0.57%	2.20 ± 0.64%	2.03 ± 0.44%	1.57 ± 0.31%	−0.03 ± 0.40%
		$satis_m$	−4.48 ± 0.98%	−11.19 ± 0.47%	−6.19 ± 2.28%	10.21 ± 1.44%	9.68 ± 0.94%	−1.07 ± 0.95%	0.67 ± 0.27%	0.15 ± 0.22%
		R	16.34 ± 1.64%	13.72 ± 0.92%	6.91 ± 0.61%	49.78 ± 4.24%	59.87 ± 4.62%	52.16 ± 2.99%	42.82 ± 1.75%	40.07 ± 1.95%
	stable matching vs. MILPmfg	w	−15.77 ± 0.65%	−28.32 ± 1.66%	−38.18 ± 1.58%	−13.66 ± 5.40%	−4.62 ± 1.75%	−5.04 ± 0.67%	−2.26 ± 0.13%	−2.44 ± 0.07%
		LT	−31.02 ± 4.24%	−12.25 ± 1.94%	−10.48 ± 1.47%	13.59 ± 0.99%	27.29 ± 0.65%	29.85 ± 0.50%	27.52 ± 0.32%	26.08 ± 0.26%
		$satis_c$	47.34 ± 0.09%	18.57 ± 0.31%	3.11 ± 0.31%	4.84 ± 0.53%	5.97 ± 0.45%	5.42 ± 0.35%	3.07 ± 0.34%	1.63 ± 0.39%
		$satis_m$	91.08 ± 6.17%	38.29 ± 0.93%	24.52 ± 1.29%	22.63 ± 1.54%	21.07 ± 1.51%	15.14 ± 0.94%	6.52 ± 0.33%	4.52 ± 0.25%
		R	−21.77 ± 1.56%	−9.57 ± 1.22%	−8.41 ± 1.00%	17.29 ± 1.93%	39.35 ± 2.77%	43.99 ± 2.11%	38.86 ± 1.34%	35.95 ± 0.95%
	stable matching vs. MILPordinal	w	56.57 ± 0.52%	47.75 ± 0.30%	43.15 ± 0.32%	32.55 ± 0.45%	22.82 ± 0.24%	13.56 ± 0.15%	4.87 ± 0.05%	3.39 ± 0.04%
		LT	5.79 ± 4.01%	23.50 ± 1.85%	28.22 ± 1.55%	37.31 ± 0.93%	41.20 ± 0.60%	38.75 ± 0.47%	30.34 ± 0.39%	28.49 ± 0.38%
		$satis_c$	−32.44 ± 13.65%	−13.41 ± 4.50%	−30.21 ± 4.23%	−21.05 ± 2.78%	−12.89 ± 1.73%	−5.62 ± 0.86%	−1.65 ± 0.39%	−0.55 ± 0.48%
		$satis_m$	42.35 ± 3.34%	15.58 ± 1.73%	3.39 ± 1.58%	2.61 ± 1.78%	5.75 ± 1.56%	6.88 ± 1.14%	3.05 ± 0.16%	2.25 ± 0.23%
		R	11.09 ± 5.94%	35.26 ± 7.33%	43.73 ± 6.99%	63.52 ± 7.29%	73.08 ± 5.40%	65.28 ± 3.38%	44.77 ± 1.93%	40.94 ± 1.72%
	stable matching vs. FCFS	w	76.71 ± 0.38%	77.46 ± 0.12%	76.58 ± 0.09%	63.00 ± 0.19%	48.40 ± 0.16%	32.92 ± 0.15%	14.56 ± 0.07%	10.97 ± 0.04%
		LT	−27.23 ± 3.89%	−12.58 ± 1.60%	−12.10 ± 1.30%	14.33 ± 0.73%	29.25 ± 0.75%	31.43 ± 0.61%	28.39 ± 0.36%	26.41 ± 0.33%
		$satis_c$	51.82 ± 0.46%	23.60 ± 0.56%	2.90 ± 0.36%	3.73 ± 0.42%	4.42 ± 0.48%	5.04 ± 0.50%	3.58 ± 0.29%	2.29 ± 0.45%
		$satis_m$	117.33 ± 14.81%	47.33 ± 2.20%	26.07 ± 1.51%	22.41 ± 1.80%	20.52 ± 1.48%	14.66 ± 1.02%	6.58 ± 0.31%	4.81 ± 0.23%
		R	−19.47 ± 1.69%	−10.02 ± 1.11%	−9.85 ± 0.89%	17.93 ± 1.50%	43.57 ± 3.44%	47.87 ± 3.29%	40.68 ± 1.56%	36.75 ± 1.24%
Case III	Stable Matching vs. MILPcustomer	w	−17.06 ± 1.56%	−31.91 ± 0.70%	−56.74 ± 1.43%	−5.44 ± 2.85%	16.20 ± 2.82%	10.41 ± 0.42%	7.61 ± 0.08%	7.71 ± 0.06%
		LT	31.39 ± 1.30%	25.14 ± 0.90%	27.10 ± 1.22%	36.26 ± 0.79%	19.61 ± 0.56%	29.35 ± 1.50%	28.76 ± 0.35%	26.75 ± 0.34%
		$satis_c$	−7.26 ± 0.29%	−1.23 ± 0.85%	1.50 ± 0.33%	4.68 ± 0.24%	2.88 ± 0.52%	2.38 ± 0.37%	2.42 ± 0.25%	3.20 ± 0.22%
		$satis_m$	−5.98 ± 0.91%	−4.36 ± 0.26%	1.00 ± 1.69%	0.43 ± 0.57%	2.46 ± 0.27%	7.09 ± 0.52%	6.06 ± 0.41%	8.80 ± 0.29%
		R	49.98 ± 5.62%	36.80 ± 4.63%	39.24 ± 4.31%	48.85 ± 3.03%	8.79 ± 2.55%	18.59 ± 2.89%	22.91 ± 1.35%	16.76 ± 1.40%
	Stable Matching vs. MILPmfg	w	−17.06 ± 1.56%	−31.91 ± 0.70%	−56.74 ± 1.43%	−21.70 ± 2.85%	−8.13 ± 5.36%	−4.02 ± 1.19%	−3.82 ± 0.14%	−3.97 ± 0.08%
		LT	12.23 ± 1.03%	15.11 ± 1.92%	5.26 ± 2.53%	−2.62 ± 2.53%	14.22 ± 2.16%	29.98 ± 1.98%	28.13 ± 0.36%	28.62 ± 0.31%
		$satis_c$	42.30 ± 0.03%	28.88 ± 0.28%	16.55 ± 0.10%	12.83 ± 0.20%	11.29 ± 0.26%	7.44 ± 0.28%	6.22 ± 0.21%	4.55 ± 0.24%
		$satis_m$	85.34 ± 8.36%	79.98 ± 5.12%	37.42 ± 3.13%	29.49 ± 1.73%	26.27 ± 1.09%	14.55 ± 0.90%	12.20 ± 0.43%	13.37 ± 0.30%
		R	−61.40 ± 0.21%	−53.54 ± 0.40%	−16.91 ± 0.77%	−7.71 ± 1.82%	2.48 ± 1.51%	19.45 ± 2.54%	21.44 ± 1.43%	20.14 ± 1.30%
	Stable Matching vs. MILPordinal	w	50.59 ± 0.48%	47.67 ± 0.34%	44.43 ± 0.37%	32.05 ± 0.19%	17.63 ± 0.21%	5.19 ± 0.16%	3.88 ± 0.05%	3.41 ± 0.03%
		LT	−9.88 ± 4.56%	3.40 ± 4.87%	−0.41 ± 3.50%	−3.83 ± 3.45%	15.67 ± 3.02%	31.68 ± 2.06%	29.07 ± 0.39%	25.51 ± 0.40%
		$satis_c$	−8.13 ± 7.92%	−13.20 ± 4.41%	−18.90 ± 2.50%	−13.16 ± 1.51%	−5.64 ± 1.31%	−0.79 ± 0.80%	0.53 ± 0.28%	−1.31 ± 0.34%
		$satis_m$	24.30 ± 2.56%	14.10 ± 2.00%	−3.04 ± 2.35%	1.25 ± 1.00%	6.74 ± 0.92%	4.45 ± 0.76%	4.35 ± 0.29%	5.13 ± 0.29%
		R	−21.73 ± 4.48%	−19.52 ± 3.91%	33.29 ± 3.98%	39.15 ± 10.89%	39.12 ± 12.46%	45.25 ± 7.41%	41.48 ± 4.33%	33.84 ± 3.26%
	Stable Matching vs. FCFS	w	78.42 ± 0.36%	77.87 ± 0.11%	77.45 ± %0.07	63.69 ± 0.08%	44.36 ± 0.12%	18.50 ± 0.10%	13.96 ± 0.05%	13.94 ± 0.04%
		LT	−48.07 ± 8.78%	−21.42 ± 5.95%	−7.63 ± 6.55%	−4.34 ± 3.37%	15.40 ± 2.78%	30.57 ± 2.03%	28.03 ± 0.35%	26.56 ± 0.42%
		$satis_c$	29.19 ± 0.40%	16.36 ± 0.80%	12.67 ± 0.38%	12.69 ± 0.31%	20.65 ± 0.28%	7.30 ± 0.32%	6.11 ± 0.24%	8.18 ± 0.23%
		$satis_m$	64.21 ± 10.63%	47.17 ± 3.12%	28.50 ± 2.46%	29.87 ± 1.74%	25.55 ± 0.87%	14.88 ± 1.05%	11.83 ± 0.43%	12.48 ± 0.27%
		R	−52.37 ± 2.05%	−49.14 ± 1.34%	−16.57 ± 1.52%	−8.16 ± 1.92%	3.32 ± 2.02%	20.84 ± 2.78%	20.68 ± 0.09%	19.34 ± 1.23%

2.6 Discussion

Sharing economy enables individuals and small manufacturers to share their assets and services to non-owners. AM directly delivers printed products to customers and shortens the traditional supply chain, which typically includes suppliers, manufacturers, distributors, retailers, and customers. Cyber-physical AM platforms connect manufacturers and customers and create a new shape of two-sided market. In this paper, we consider a problem of matching manufacturers to customers for AM sharing economy.

2.6.1 Privacy in sharing economy

Privacy is one of the major concerns for participating in sharing economy which requires agents on both sides of the transaction to share private information. The cyber-physical platform supports the exchange of sensitive data such as addresses and credit card information from the customer's side, as well as machine information and manufacturing capability from companies. In the context of sharing economy, information, data, and other resources (i.e., space or object) are shared through the cyber-physical platform. As shown in Figure 2.11, service providers share their data with the platform, and retrieve data from customers for production and profit. Similarly, customers send data to the platform to gain access to service, then pay through the platform.

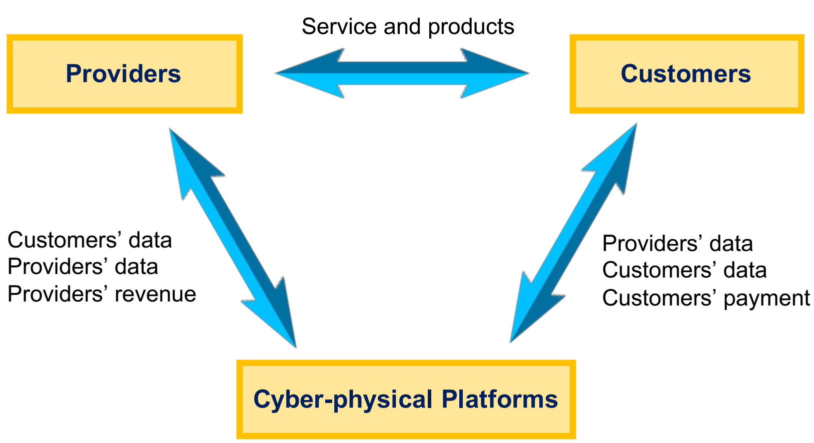

Figure 2.11. The data exchange between providers, customers, and the cyber-physical platform in the sharing economy.

The privacy challenges for providers, customers, and platforms are described as follows:

- **Providers privacy:** Providers often need to share information about who they are and what services they can deliver, which are advertised on the platform to attract customers. The privacy concerns arise when service providers interact with competitors and customers through the platform. In such cases, the providers are concerned about what information should be available to the platform, what information should be disclosed to customers, and what information should be open to the public to increase the participation in the economy.

- **Customers privacy:** Trust from customers to the platform is imperative because customers disclose sensitive information (e.g., credit card information, address) to receive service from providers. The information is then used to construct profiles and improve matching algorithm. Concerns of customers about privacy not only consist of the use of their personal information, but also include their social status and relations. These privacy concerns in different categories need further discussion.

- **Platform privacy:** The privacy-related concerns vary among organizations based on the scope of platforms (i.e., profit-oriented or community-oriented). In cyber-physical AM, the platform stores information from manufacturing resources (e.g., production capability), services (e.g., logistic capability), and customers (e.g., demand). The use of private data can improve the matching algorithm and benefit the manufacturer's economic survival. However, the leakage of private data might trigger a loss of trust from both providers and customers to the platforms. Therefore, platforms need to balance the trade-off between exploit of user data and their own benefits.

2.6.2 Opportunities

The opportunities of the AM sharing economy are as follows: (1) **Regulation:** The sharing economy has raised several regulation issues and attracted much attention from government regulators and traditional businesses. By gaining regulatory advantages, companies in the peer-to-peer market skirt many requirements and further earn profit. For example, most cities tax the taxi companies, cap the number of taxis, and regulate the price the taxi charges customers. Also, taxi companies are subject to specific licensing requirements for health and safety issues. Uber, however, allows anyone with a driver's license and a car to provide taxi services with a very limited background checking. The company also has a different pricing model which is sensitive to real-time demand. (2) **Collaborative manufacturing:** Traditionally, big companies may get large batch orders with thousands of parts. Instead of a single plant for order fulfillment, splitting the order into small batches and further leverage various providers will dramatically reduce the lead time. However, little has been done to study collaborative manufacturing and order splitting in the context of sharing economy. There is an urgent need to (i) develop a matching framework with collaborative manufacturing; (ii) introduce an integrated supply chain support that utilizes the data from different collaborative centers to improve the efficiency of the system; and (iii) design a distributed environment for fast computing. (3) **Order timelines:** Not only a manufacturer can get a large order, but also some time-sensitive orders. As some customers have time requirements in production and are willing to pay more, if delivering the order on time, there are also customers not in a rush and would like to keep the services as cheap as possible. A resource allocation paradigm with the time-precedence structure will help assign the priority of orders and satisfy both customers and manufacturers. (4) **Privacy:** Privacy is one of the major concerns for participating in sharing economy which requires agents on both sides of the transaction to share private information. The cyber-physical platform supports the exchange of sensitive data such as addresses and credit card information from the customer's side, as well as machine information and manufacturing capability from companies. Develop a framework to enable a privacy preserving environment is critical to the development of AM sharing economy. (5) **Blockchain-enabled sharing economy:** Blockchain is a novel technology to secure data transport with cryptography. Blockchain is first introduced to build e-cash systems [84], and further applied in other domains when there is a lack of trust between distributed parties. In the sharing economy, many distributed agents communicate with each other across the cyber-physical platforms through the internet. As aforementioned, data security and information privacy are rising problems for the design, development, and deployment of cyber-physical platforms. Therefore, it is worth investigating further the blockchain technology for a new and effective way to share data under secure control in a decentralized system.

For future research, one should consider the stable matching framework in a dynamic system. The dynamic optimization can be tackled by discretizing time epochs, then formulating a classic stable matching problem and solving them independently over time [85]. Also, this paper assumes preference lists calculated from two sets of agents are based on true information. In reality, the agent may provide counterfeit information to get a better matching pair. It is worth further investigating robust matching under uncertainty.

The future work or possible applications of the proposed framework may focus on the following aspects: (1) **Dynamic matching framework**: The proposed stable matching framework can be further extended to a dynamic model. The dynamic optimization can be tackled by discretizing time epochs, then formulating a classic stable matching problem and solving them independently over time [85]. (2) **Matching with uncertainty:** This paper assumes preference lists calculated from two sets of agents are based on true information. In reality, the agent may provide counterfeit information to get a better match between customers and providers. It is worth further investigating robust matching under uncertainty. (3) **Privacy preserving stable matching:** Privacy is one of the major concerns for participating in sharing economy which requires agents on both sides of the transaction to share private information [86]. The cyber-physical platform supports the exchange of sensitive data such as addresses and credit card information from the customer's side, as well as machine information and manufacturing capability from companies. Future work may consider a privacy preserving framework for stable matching.

2.7 Conclusions

Over the past few years, the sharing economy has changed the way people conduct business in daily lives. New cyber-physical platforms enable owners to "share" their assets and services to non-owners. Today, sharing economy disrupts traditional industries across the world. However, the concept of sharing economy is still relatively new in the field of AM. As the price of 3D printers decreases, small manufacturers enter the market and "share" their idle machines with potential customers, further compete with traditional large companies. Such decentralization in the market results in the emergence of cyber-physical AM platforms, which shorten the AM supply chain and help customers find service providers to print their designs through the internet. Nonetheless, little has been done to study market characteristics and needs in the AM sharing economy.

In this paper, we investigate a bipartite matching framework to solve supply chain matching problem in the AM sharing economy. The proposed algorithms are evaluated and validated with different experimental scenarios. We compared the proposed stable matching with MILP optimization as well as the FCFS allocation strategy for different scenarios of demand-supply configurations (i.e., from 50% to 500%) and system complexities (i.e., uniform parts and manufacturers, heterogeneous parts and uniform manufacturers, heterogeneous parts and manufacturers). Experimental results show that the proposed framework effectively improves the performance of resource allocation in the AM sharing economy, especially when the demand-supply ratio is relatively high and the system is complex. The proposed sharing economy framework shows strong potential to realize a smart and decentralized AM sharing economy.

For future research, one should consider the stable matching framework in a dynamic system. The dynamic optimization can be tackled by discretizing time epochs, then formulating a classic stable matching problem and solving them independently over time. In addition, information privacy is a rising concern for the design, development, and deployment of AM sharing economy. The cyber-physical platform supports the exchange of sensitive data such as engineering designs from the customer's side, as well as machine capability and production costs from companies. Privacy-preserving analytics is urgently needed for the development of AM sharing economy and smart manufacturing.

Chapter 3

From Design Complexity to Build Quality in Additive Manufacturing - A Sensor-based Perspective

Additive manufacturing (AM) provides a greater level of flexibility to build parts with complex structures than traditional subtractive manufacturing. It not only offers customizability while maintaining potential profitability but also provides freedom in design complexity. In Chapter 2, we introduced a bi-pipette matching framework for the AM cyber-physical systems regarding the growing demand in the AM sharing economy market. However, quality consistency is still one of the main challenges, especially in producing metal parts, for each manufacturer in the AM cyber-physical system. The more complex the engineering design is, the greater challenge is posed on the AM machine. From this chapter, we focus on the design-quality interactions in the metal AM processes.

Nowadays, advanced imaging is increasingly invested to increase the information visibility to cope with the complexity in AM processes. To understand the process better, there is an urgent need to leverage the available imaging data to investigate the interrelationships between design complexity and quality characteristics of AM builds. This chapter presents a design of experiments on the laser powder bed fusion (LPBF) machine to investigate how design parameters (i.e., recoating orientation, contour spacing, width, height) influence edge roughness in thin wall structures of the final builds. First, we perform the post-build inspection of final builds and collect large amounts of X-ray computed tomography (XCT) images. Second, we integrate the computer-aided designs (CAD) with XCT images for image registration and then characterize the edge roughness of each layer in a thin wall of the AM build. Finally, we perform an analysis of variance with respect to design parameters and develop a regression model to predict how build design impacts the edge roughness in each layer of the thin wall structures. Experimental results show that edge roughness are sensitive to recoating orientations, width and contour spacing. This research sheds insights on the optimization of engineering design to improve the quality of AM builds.

3.1 Introduction

Additive manufacturing (AM) provides a greater level of flexibility to build parts with complex structures than the traditional subtractive manufacturing [87]. This revolutionary technology also results in the shorter lead time, lower life-cycle cost, and the ability to produce parts directly from computer-aided designs (CAD) without the need for expensive part-specific tooling [88]. However, AM nowadays is still limited in the ability to achieve the high-level of quality and repeatability, thereby hampering the widespread application of the technology in the manufacturing industry. In the AM process, there are a number of factors impacting the quality of final builds such as powder materials, chamber environment, machine and process settings, and design complexity [89]. Our prior studies focused on the effects of machine and process settings (e.g., laser power, scanning velocity, and hatch spacing) on the quality of final builds [12, 90]. Deep learning models are also proposed to study the variant geometry in layerwise imaging profiles for additive manufacturing quality control [91, 92]. In addition, we characterized the multifractal patterns of in-situ layerwise images for the estimation of defect states in each layer [93, 94], and then developed a Markov decision process model to sequentially optimize the quality in complex systems [95, 96]. As a further step, we focus on the interrelationships between design complexity and quality characteristics of AM builds in the present paper.

It is well known that design complexity poses significant challenges on traditional subtractive manufacturing. AM provides more design freedom, and complex structures can now be fabricated layer by layer with the new AM technology. However, a

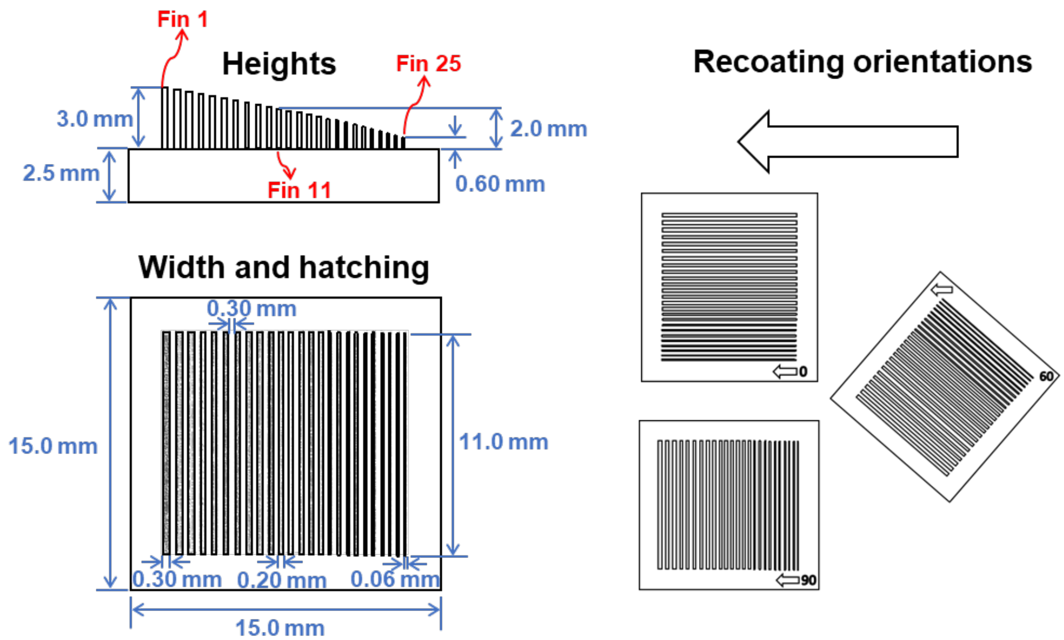

Figure 3.1. Front and top view of CAD model and recoating orientations.

higher level of design complexity can greatly degrade the quality of final AM builds. Advanced imaging is increasingly utilized to increase the visibility of post-build quality information in the face of increasing design complexity. Realizing the full potential of readily available imaging data calls upon the investigation of the interrelationships between design complexity and quality characteristics of AM builds. Therefore, this paper presents our experimental studies on the laser powder bed fusion (LPBF) machine to investigate how design parameters (i.e., recoating orientation, contour spacing, width and height) influence edge roughness in thin wall structures of the final builds.

As shown in Fig. 3.1, our experiments feature a thin-wall structure with different recoating orientations, widths, heights, and contour spacing (see Section 3.2. A). Thin wall structures are widely used in heat exchanger designs. A total of three thin-wall parts (also called Fin parts) were built, each differing in the manner of rotation upon the build plate, i.e., their planar inclination in the X-Y plane with respect to the recoater blade travel within the machine . After fabrication, we performed post-build inspection with X-ray computed tomography (XCT). Next, XCT images were registered layer-by-layer with the original CAD files to extract the quality features of edge roughness in each thin wall. Here, the edge roughness refers to the geometric deviation of build in registered XCT scan and CAD file. However, the average of absolute values of the profile height deviations from the mean line is generally used for edge characterization. These features were tracked across layers to detect impending collapse of thin-wall failures. Finally, we performed an analysis of variance with respect to design parameters and further developed a regression model to predict how design complexity impacts the edge roughness in each layer of the thin wall structures.

3.2 Research Methodology

This section introduces the detailed research methodology. As shown in Fig. 3.2, the present investigation focuses on metal printing with the EOS M280 laser powder bed fusion (LPBF) machine. The data utilized in this study consist of the CAD design files (i.e., the expected quality) and the XCT images of each layer in the thin wall (i.e., the delivered quality). We leverage the layerwise CAD to perform a shape-to-image registration for the XCT images, which provides the measure of edge roughness for each layer of each thin wall. Finally, we analyze the impacts of experimental factors on the edge quality and then develop a regression model to predict how design complexity impacts the edge roughness in each layer of the thin wall structures.

3.2.1 Experimental Setup and Factors

In this experiment, raw materials are Spherical ASTM B348 Grade 23 Ti-6Al-4V powder, available from the LPW technology, with a size distribution of 14 μm - 45 μm. Each fin part comprises a 15 mm $\times$ 15 mm $\times$ 55 mm platform upon which are built a total of 25 fin walls. The experimental factors such as orientation, width, height and contour spacing are detailed as follows:

1. **Orientation**: Fin parts were built vertically upwards with layer thickness of 60 μm in 3 orientations with respect to the recoater blade travel direction. The arrow shows the recoating direction.

2. **Width**: The width of fin walls varies from 0.06 mm to 0.3 mm with the step size of 0.01 mm, and the distance between two fins is 0.3mm.

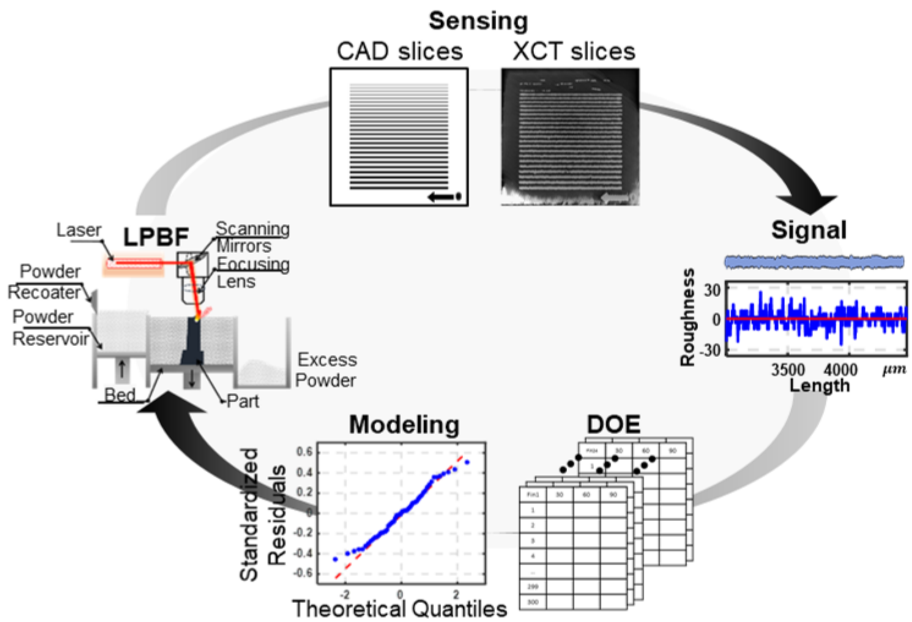

Figure 3.2. Flow diagram of the proposed research methodology.

3. **Height**: The designed height of fin walls differs from 0.6 mm to 3.0 mm with the step size of 0.1 mm. Note that the height is proportional to the width in each thin wall with an aspect ratio of 0.1.

4. **Contour**: Thin-walls 1-24 includes one outer contour on the blue line, one inner contour with hatches at the same angle inside. Thin-wall 25 does not have the inner contour as others. The designed contour spacing of fin walls, which employ the standard EOS processing path, are significantly different as the width increases. Note that there is a 67-degree rotation for the hatching paths on each layer by the default setting of the EOS 280 machine. Fig. 3.3 shows 4 contour spacing.

3.2.2 Image Registration and Edge Characterization

This experiment uses post-build X-ray CT images to quantify the geometric variations of each fin. Although metrology methods such as 3D scanning or coordinate measuring machines are widely used to measure the geometric dimensionality, they are limited in the resolution to comprehensively measure the 3D geometry of Fin builds. High-end X-Ray CT, albeit expensive, offers an advantage to examine the internal structure of the builds, as well as quantify the 3D geometric variations of the build.

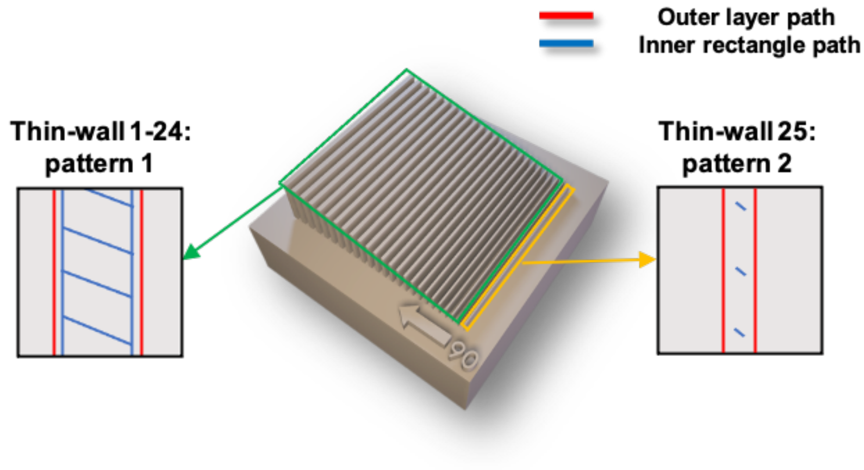

Figure 3.3. contour spacing of the fin walls.

For each fin part, we have a CAD file and the corresponding post-build XCT data. Note that we slice the 3-dimensional CAD model and XCT volumetric scans into 300 layers (i.e., with a thickness of 10 μm per layer). To transform the two sources of data (i.e., CAD model and XCT scan) into a single coordinate system, we leverage the layerwise CAD file and XCT scan to perform a shape-to-image intensity-based registration and to extract the region of interests. Intensity-based methods consider correlation metrics to compare the intensity patterns in the target image (i.e., XCT) and the source image (i.e., CAD). The registration process aims to transform (i.e., affine transformation) the target image into the source image. After registration, we removed noise (i.e., connected objects that are less than 20 pixels) and extract fin walls for each layer.

As illustrated in Fig. 3.4 (a), by defining the edge from the CAD file as the referencing horizontal axis, we first measure the distance between the edge of the registered XCT scan and the CAD file, then concatenate the upper and lower edge signals to generate the edge roughness signal (see top right of Fig. 3.4 (b)). Fig. 3.4 (b) shows the signal is approximately represented by a normal distribution for the fin 2 of layer 11. It is worth mentioning that the characteristics of edge roughness of Fin wall 2 are different under the changing recoating directions (see bottom right of Fig. 3.4). After approximating the edge signals with a normal distribution, we obtained standard deviation (STD) of each edge in each layer of a thin wall for further analysis.

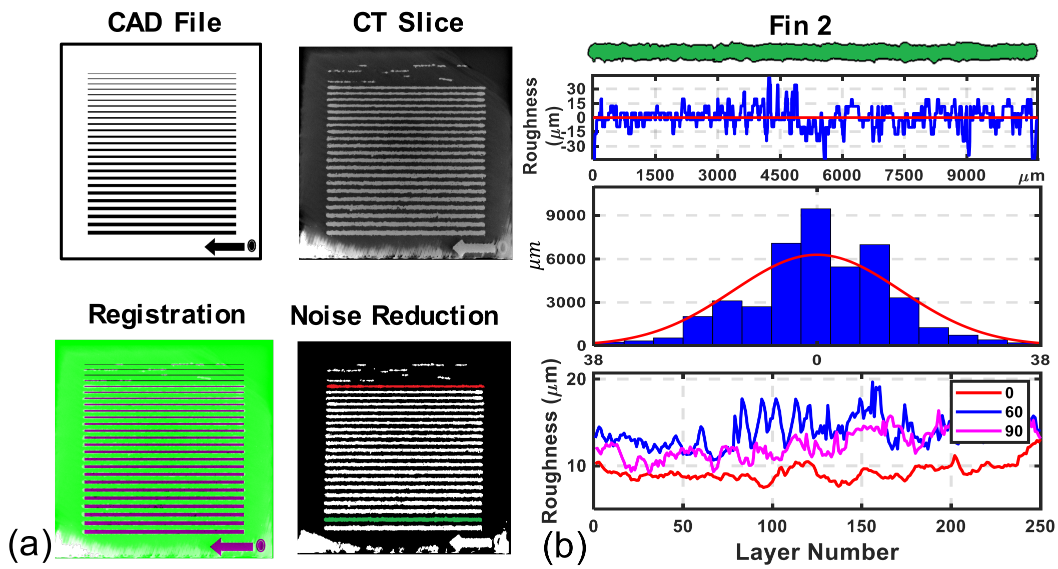

Figure 3.4. (a) Image registration and edge extraction of fin walls; (b) Normality assumption and verification through layer of fin 2. (unit: μm)

3.2.3 Analysis of Variance

Here, we perform the two way analysis of variance (ANOVA) to study the effects of experimental factors, i.e., orientations and fin wall characteristics, on the part quality. Note that the parameters of height, width, and contour spacing are affiliated with the fin wall number in our design of experiments. Therefore, we rearrange four parameters into two factors (i.e., orientation and fin wall characteristics).

		F				
		Fin 1	Fin 2	…	Fin 20	Fin 21
O	0°	$\sigma_1, \sigma_2, \ldots, \sigma_{299}, \sigma_{300}$	$\sigma_1, \sigma_2, \ldots, \sigma_{289}, \sigma_{290}$	…	$\sigma_1, \sigma_2, \ldots, \sigma_{109}, \sigma_{110}$	$\sigma_1, \sigma_2, \ldots, \sigma_{99}, \sigma_{100}$
	60°	$\sigma_1, \sigma_2, \ldots, \sigma_{299}, \sigma_{300}$	$\sigma_1, \sigma_2, \ldots, \sigma_{289}, \sigma_{290}$	…	$\sigma_1, \sigma_2, \ldots, \sigma_{109}, \sigma_{110}$	$\sigma_1, \sigma_2, \ldots, \sigma_{99}, \sigma_{100}$
	90°	$\sigma_1, \sigma_2, \ldots, \sigma_{299}, \sigma_{300}$	$\sigma_1, \sigma_2, \ldots, \sigma_{289}, \sigma_{290}$	…	$\sigma_1, \sigma_2, \ldots, \sigma_{109}, \sigma_{110}$	$\sigma_1, \sigma_2, \ldots, \sigma_{99}, \sigma_{100}$

Figure 3.5. Experimental data structure for the ANOVA analysis: F and O represent two factors, namely fin number and orientation.

As shown in Fig. 3.5, there are 3 levels of orientation with respect to the recoater blade travel direction and 21 levels of thin wall. It is worth mentioning that the last four fin walls were collapsed in the fabrication process, likely due to interference with the recoater blade during recoat operations, and therefore they are not available for ANOVA. Here, fin 1 to fin 21 are taken into account for this ANOVA analysis. The model is expressed as:

$$\sigma_{ij} = \beta_0 + \beta_1 \times O_i + \beta_2 \times F_j + \beta_3 \times O_i \times F_j + \varepsilon_{ij} \tag{3.1}$$

where O and F represent orientation and fin number, respectively. Also, ε_{ij} in Eq. (3.1) denotes the error term in ANOVA model.

3.2.4 Predictive Modeling

In addition, we develop a regression model to quantify the relationship between edge roughness and the orientation, width, height, and contour spacing of each fin wall:

$$\begin{aligned}\sigma = \beta_0 + \beta_1 \times O + \beta_2 \times W + \beta_3 \times H + \beta_4 \times Ha + \beta_5 \times O \times W + \\ \beta_6 \times O \times H + \beta_7 \times O \times Ha + \beta_8 \times W \times H + \beta_9 \times W \times Ha + \\ \beta_{10} \times H \times Ha + \varepsilon\end{aligned} \tag{3.2}$$

where Ha denotes the contour spacing and is a categorical variable with four levels, O stands for the orientation which is also a categorical variable with three levels, and H and W represents the height and width of the corresponding fin wall, respectively. The R-square (R^2) is utilized to statistically measure the performance of the model, and is defined as $R^2 = 1 - \frac{\text{Sum of Square}_{residual}}{\text{Sum of Square}_{total}} = 1 - \frac{\Sigma_i(\sigma_i - \hat{\sigma_i})^2}{\Sigma_i(\sigma_i - \overline{\sigma})^2}$. Where σ_i is the edge roughness, $\hat{\sigma_i}$ is the predicted value of the variance, and $\overline{\sigma}$ is the overall average of the data.

3.3 Experimental Results

3.3.1 Statistical Analysis

3.3.1.1 Analysis of variance to test the hypothesis whether orientations and fin wall characteristics impact the edge roughness

In Table. 3.1, the p-values for orientation, fin wall, and interaction are approximately 0, which shows all three factors have significant impacts on the edge roughness. In this ANOVA table, the **Sum Sq.**, **d.f.**, **mean Sq.**, **F** and **Prob>F** denote sum of squared errors, degrees of freedom, mean of squared errors, the F statistics, and the p-value, respectively. It may be noted that the F test statistically shows whether a specific factor is associated with higher variations than random phenomena. At certain **d.f.** levels of the denominator and the numerator, the higher the F statistics, the smaller the p-value will be. If the p-value is less than 0.05, there are significant effects from a factor.

Table 3.1. ANOVA analysis of variance in two-way layout experiment.

Source	Sum Sq.	d.f.	Mean Sq.	F	Prob>F
fin	200.472	20	10.024	20.412	0
orientation	631.408	2	315.704	642.890	0
fin * orientation	307.300	40	7.683	15.644	0
Error	6156.050	12536	0.491		
Total	7371.040	12598			

3.3.1.2 The impact of orientation on edge characteristics

As shown in Fig. 3.6 (a), the average variation of fin wall edges is not constant for different recoating directions. Note that building the fin part at 0 orientation with respect to recoating direction leads to the smallest edge roughness, while the biggest edge roughness occurs at 60.

3.3.1.3 The impact of fin width on edge characteristics

As illustrated in Fig. 3.6 (b), the mean of edge roughness first increases and then decreases as the fin wall gets wider. The variations of edge roughness is bigger when the fin width is smaller. Fig. 3.6 (b) shows that as the width of fin walls increases, the AM machine can print the thin-wall structure with smaller variations of edge roughness. When the dwidth is as small as 0.10 mm to 0.19 mm, there are more outliers indicating significant variations in surface roughness can occur when building thin wall structures of thin-wall structures.

3.3.2 Predictive Modeling

Next, we develop a regression model to quantify the relationship between edge roughness and design parameters. As shown in Table. 3.2, contour spacing, width,

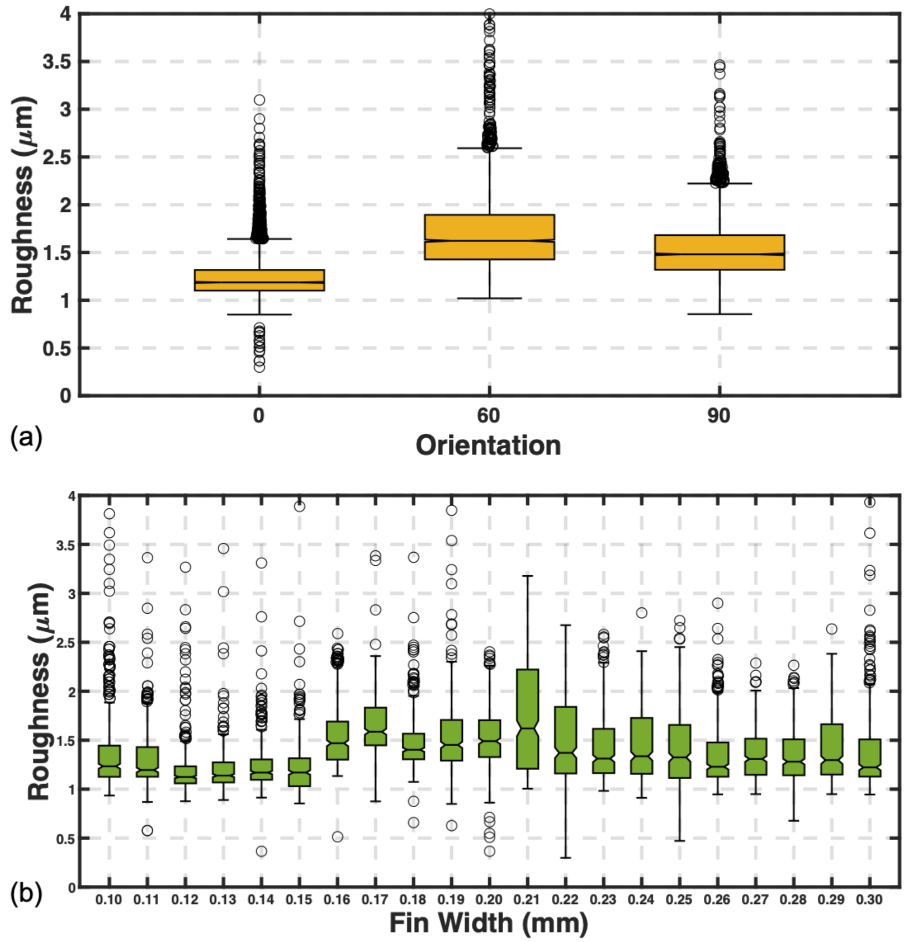

Figure 3.6. (a) Mean and STD of edge roughness under three orientations; (b) Mean and STD of edge roughness when fin width increases.

and two-way interactions of width × orientation, hatching × orientation, and hatching × width are significant at the confidence level of 95%. For further investigation, contour spacing can be adjusted to generate fins with reduced edge roughness, even for thin fins. Besides, the p-value of width is 1.119e-74 which shows that it is an important factor in edge roughness. Also, two-way interaction terms of hatching × orientation and width × orientation are significant which shows that the combination of different design parameters impacts the quality in AM as well. Here, note that we set the 0 orientation as the baseline, and the NA indicates that the variable is correlated with one of the other variables.

The coefficient of determination is utilized to illustrate the percentage of variation in response variable that is explained by the model. The regression model yields the

Table 3.2. Results of Regression Analysis.

Effect	Estimate	Error	t value	P-value
Intercept	1.029	0.0434	23.7	1.223e-120
hatching	15.447	0.7447	20.7	2.480e-93
width	-13.757	0.7452	-18.5	1.119e-74
orientation 60	-0.331	0.0392	-8.4	3.537e-17
orientation 90	-0.246	0.0397	-6.2	5.499e-10
height	0.165	0.0299	5.5	3.583e-8
width * orientation 60	6.350	0.6847	9.3	2.205e-20
width * orientation 90	6.053	0.6946	8.7	3.465e-18
height * orientation 60	-0.034	0.0036	-9.6	1.496e-21
height * orientation 90	-0.078	0.0037	-21.3	1.839e-98
width * height	2.136	0.5119	4.2	3.041e-5
hatching * height	-2.660	0.5168	-5.1	2.699e-7
hatching * orientation 60	-4.764	0.6904	-6.9	5.553e-12
hatching * orientation 90	-4.407	0.7013	-6.3	3.452e-10
hatching * width	-6.564	0.2591	-25.3	1.036e-136

R-squared statistic of 81.36% and adjusted R-squared statistic of 81.33%, showing that variations in response variable are highly dependent on design parameters. Furthermore, we utilize the normal Q-Q plot as descriptive graphical tools for the

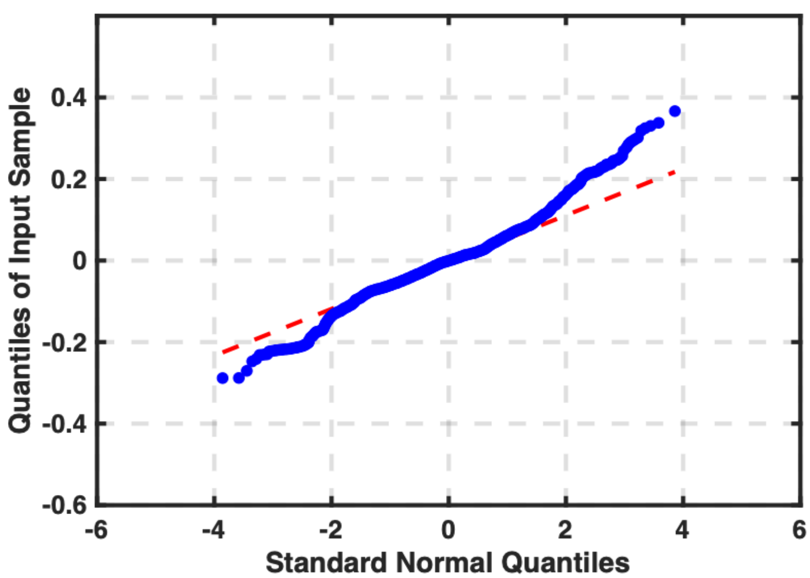

Figure 3.7. Normal Q-Q plot of the regression model.

model diagnosis and checking the normality assumption of residuals. Note that

Fig. 3.7 shows the normal Q-Q plot approximately follows a straight line.

3.4 Limitations and Future Works

AM enables the fabrication of complex structures. Together with the freedom of fabrication, new challenges are introduced for designing for additive manufacturing, including representing and optimizing intricate geometries and functionally graded structures, incorporating design for AM knowledge into the design process, and making design for AM tools and knowledge more accessible to a broad range of expert and novice designers [97]. In this chapter, we focus on investigating the relationship between part quality and AM parameters utilizing the data from a thin-wall part. Specifically, we perform a design of experiment to study the relationship between edge roughness and design parameters. We characterize and the edge roughness from the XCT slices and build a predictive model to quantify the relationship between edge roughness and design parameters. In the proposed regression analysis, only one variable, edge roughness, is considered as the response variable. However, multiple responses are often generated and correlated in many real-world settings. For example, not only the edge roughness is possibly correlated with the design parameters. Other features, the number of pores may also be related to design parameters. In the next chapter, we propose a recurrence network analysis to analyze the AM image data with the network theory, and characterize the part quality with the network quantifiers. We integrate multiple responses into Hotelling's T^2 statistics. Note that Hotelling's T^2 distribution is a multivariate probability distribution related to the F-distribution. In comparison with the univariate hypothesis tests that are associated with t-distribution, Hotelling's T^2 distribution arises in multivariate statistics in undertaking tests of the differences between multiple means from different populations. In addition, a detailed discussion of the resolution and sensitivity regarding the feature extraction from the data is discussed in Chapter 6.

3.5 Conclusions

AM provides the design freedom with complex geometrical structures, which cannot be realized otherwise using conventional manufacturing methods. However, a higher level of design complexity can significantly deteriorate the quality of AM builds. To tackle this challenge, post-build high resolution XCT scans which provides a rich data environment is recently taken into account. There is a dire need to take advantage of this data to decipher the relationship between design parameters and quality of AM builds. In this study, a design of experiments is performed to characterize the impact of design parameters on edge roughness of thin wall structures. First, XCT images of builds are registered to CAD models to characterize and quantify the edge roughness in thin wall structures. Then, we performed the experimental design to study the impact of design parameters on the edge quality of fins. Next, a predictive model is developed to quantify the behavior of edge roughness as a function of these parameters. The regression result shows that the hatching, width, and orientation have significant impacts on the edge roughness at the confidence level of 95%. Further, the adjusted R-squared demonstrates that 92.54% of the edge roughness can be explained by the regression model. This study sheds insights to optimize the engineering design for quality improvement in AM.

Chapter 4
Recurrence Network Analysis of Design-quality Interactions in Additive Manufacturing

Powder bed fusion (PBF) additive manufacturing (AM) provides a great level of flexibility in the design-driven build of metal products. However, the more complex the design, the more difficult it becomes to control the quality of AM builds. The quality challenge persistently hampers the widespread application of AM technology. Advanced imaging (e.g., X-ray computed tomography scans and high-resolution optical images) has been increasingly explored to enhance the visibility of information and improve AM quality control. Realizing the full potential of imaging data depends on the advent of information processing methodologies for the analysis of design-quality interactions. In the previous chapter, we investigate the relationship between design parameters and a single response edge roughness. However, there are often multiple responses in real-world settings. Different models need to develop to handle the multi-response prediction.

This chapter presents a design of AM experiment to investigate how design parameters (e.g., build orientation, thin-wall width, thin-wall height, and hatching distance) interact with multiple quality characteristics in thin-wall builds. Here, the build orientation refers to the position of thin-walls in relation to the recoating direction on the plate. First, we develop a novel generalized recurrence network (GRN) to represent the AM spatial image data. Then, GRN quantifiers, namely degree, betweenness, pagerank, closeness, and eigenvector centralities, are extracted to characterize the quality of layerwise builds. Further, we establish a regression model to predict how the design complexity impacts GRN behaviors in each layer of thin-wall builds. Experimental results show that network features are sensitive to build orientations, width, height, and hatching distance under the significant level $\alpha = 0.05$. Thin-walls with the width bigger than 0.1 mm printed under orientation $0°$ are found to yield better quality compared to $60°$ and $90°$. Also, thin-walls build with orientation $60°$ are more sensitive to the changes in hatching distance compare to the other two orientations. As a result, the orientation $60°$ should be avoided while printing thin-wall structures. The proposed design-quality analysis shows great potential to optimize engineering design and enhance the quality of PBF-AM builds.

4.1 Introduction

Powder bed fusion (PBF) additive manufacturing (AM) provides an unprecedented opportunity to produce metal builds with complex geometries layer by layer directly from digital designs. In contrast with conventional subtractive manufacturing, AM technology offers a higher degree of design freedom and avoids extra tooling costs [98]. Therefore, design constraints in conventional subtractive manufacturing (i.e., design for manufacturing) are lessened by this new technology. In other words, PBF-AM enables a new paradigm of "manufacturing for design" to fabricate the complex design in a layer-by-layer fashion [99]. Consequently, the rapid development of digital manufacturing and material science in recent years fuels the widespread applications of AM in many industries such as aerospace [100] and healthcare [101].

However, a higher level of design complexity tends to degrade the quality of final PBF-AM builds and lower the repeatability of the process [102]. Advanced imaging (e.g., X-ray computed tomography scans and high-resolution optical images) is increasingly utilized to cope with design complexity and enhance the information visibility for quality assessment [103]. However, advanced AM imaging technologies bring complex-structured and high-dimensional spatial data (i.e., a large number of pixels that are spatially correlated in each layerwise image of an AM build). There is a dire need to develop new analytical methodologies that realize the full potential of imaging data for the analysis of design-quality interactions.

Recurrence plot (RP) and recurrence quantification analysis (RQA) are widely used to graphically represent recurrence dynamics and quantify recurrence patterns of nonlinear time series analysis in complex manufacturing systems. However, traditional

RP and RQA tend to be limited in the ability to handle high-dimensional spatial data. To delineate recurrence dynamics in the spatial data, prior efforts have been made to extend the recurrence plot to a four-dimensional hyperspace [104]. However, this conventional method can only visualize the recurrence patterns in the reduced-dimension space and is rather limited in the ability to provide a complete picture of recurrence patterns in AM spatial imaging data. New analytical methodologies are needed to 1) characterize recurrence behaviors and patterns in AM spatial data; 2) measure and quantify the recurrence features; and 3) analyze the relationship between the extracted features and the quality of AM builds.

This study presents our experimental studies on PBF-AM, as well as the analysis of imaging data to investigate the relationship between design parameters and quality characteristics through a recurrence network approach. The proposed methodology, namely the generalized recurrence network (GRN) approach enables 1) effective visualization of complex spatial patterns in AM images that overcomes the "curse of dimensionality" problem in the traditional RP methodologies; 2) the use of network theory to characterize and quantify recurrence properties, thereby reducing high-dimensional image profiles into a lower-dimensionality set of quantifiers; and 3) the design of experiments to select important features, and predict how the design complexity impacts network characteristics in each layer of thin-wall builds.

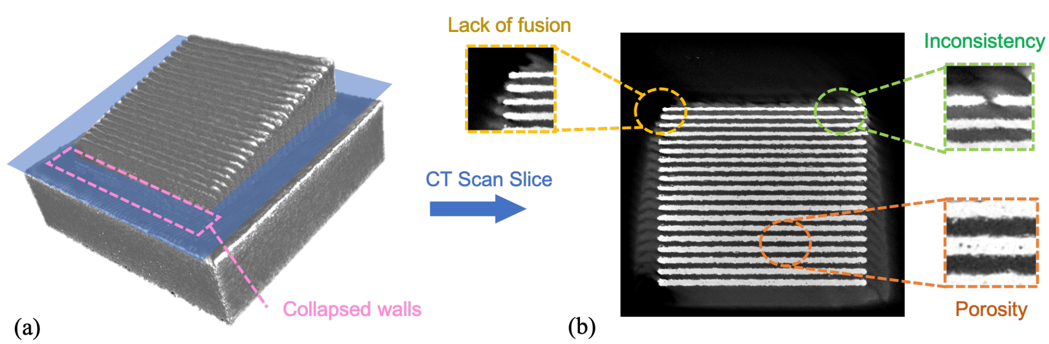

Figure 4.1. (a) XCT scan of the thin-wall build in orientation 0°; (b) a slice of XCT scan from the 103$^{\text{th}}$ layer of 0° build with quality issues such as collapsed walls, lack of fusion, edge inconsistency, and porosity.

The proposed methodology is evaluated and validated with simulation and real-world case studies of thin-wall structures fabricated by the PBF-AM. The simulation study is aimed at evaluating the effectiveness of GRN to characterize layerwise imaging data as well as testing the significance of quantifiers with defect variations. In the real-world case study, we conduct a series of experiments to fabricate thin-wall structures by varying the levels of design parameters such as build orientation (i.e., the planar inclination of thin-walls in the X–Y plane with respect to the recoater blade), thin-wall width, thin-wall height, and hatching distance (see Section 4). Thin-wall structures are commonly utilized in heat exchangers to increase the efficiency of thermal transfer and reduce the material consumption. However, fabricating thin-wall structures is a challenging task for PBF-AM. Therefore, a better understanding the design-quality interaction is urgently needed. As illustrated in Figure 4.1, thin-walls may collapse, contain pores and lack-of-fusion defects, or have structural inconsistency. A total of three thin-wall builds were made using the PBF-AM. A post-build inspection on the parts was conducted with X-ray computed tomography (XCT). Then, we registered the XCT images layer-by-layer with the sliced computer-aided design (CAD) files to delineate the region of interest (ROI) and then measure quality-related features. These network features characterize the defect patterns (i.e., inversely proportional to the quality level) in each layer, which are then used to track the variation of quality across layers so as to detect impending failures in the layers of a thin-wall. Lastly, we performed an analysis of variance (ANOVA) analysis to select important features then constructed a regression model to predict how design complexity impacts network characteristics in each layer of thin-wall structures. Experimental results show that the build quality is sensitive to build orientation, thin-wall width, thin-wall height, and hatching distance.

The rest of the paper is organized as follows: Section 4.2 reviews the related literature on AM design studies and provides the research background in recurrence analysis. Section 4.3 presents the experimental setup and GRN analysis of spatial data. The experimental results are provided in Section 4.4. Section 5.6 concludes this study.

4.2 Research Background

4.2.1 Quality Control and Design Parameters in PBF-AM

The quality of an AM build is impacted by feedstock materials, machine environment, process settings, and design complexity. Our prior studies concentrated on the impact of process and machine settings (e.g., scanning velocity, laser power, and hatch spacing) on the builds quality [12, 90, 105]. Deep learning models are also proposed to study the variant geometry in layerwise imaging profiles for additive manufacturing quality control [106,107]. Furthermore, we developed a Markov decision process model to sequentially optimize the quality of AM builds [95, 108]. This paper specifically focuses on the interactions between design parameters and quality characteristics. Several prior works have been done to study the builds of thin-wall structures when the design parameters are varied. Thomas [109] reported that walls thinner than 0.4 mm are difficult to build based on experimental studies on an MCP Realizer 250 SLM machine. Dunbar et al. [110] tried different process settings (i.e., laser power, velocity, and scan type) to test the limits of thin, metallic components using PBF-AM. They found that thin-walls fabricated with the orientation of 90° are consistently thicker than the thin-wall built with the orientation 45°. Kranz et al. [111] conducted experiments on the EOS 270xt, and showed that it is possible to manufacture thin-wall structures made of TiAl6V4 in all the examined orientations (i.e.,0°, 45°, 90°, 135°, and 180°) at a minimum thickness from 0.4 mm. Thin-walls of 0.3 mm were only successfully printed under orientation 30°; however, the highest deviation is also observed at the orientation of 30°.

Gaikwad et al. [112, 113] extracted statistical features (i.e., thickness, density, edge smoothness, and discontinuity) from imaging data to quantify the build quality, and further leveraged deep learning for real-time flaw detection. Our prior work has also studied the interaction between design complexity and edge roughness [114]. Note that the edge roughness is defined as the geometric deviation of thin-wall boundaries between the sliced CAD file and the registered XCT scan. However, the calculated edge roughness is treated as one-dimensional time series data and does not have a high-dimensional structure with geometric information. Few, if any, previous works have leveraged GRN analysis of imaging data to study interactions between design parameters and the quality of PBF final builds. AM imaging provides spatial data which includes both geographical coordinates and pixel intensity characteristics. Therefore, new analytical methodologies are urgently needed to handle AM spatial data and extract useful information to analyze the design-quality interactions.

4.2.2 Recurrence Analysis and Network Theory

Recurrence is a fundamental property that commonly exists in complex systems. For example, RQA provides an effective tool to analyze acoustic emission signals and extract features to estimate surface roughness of metal cutting [115]. Poincare recurrence theorem shows that the trajectory of a dynamical system will eventually reappear in the ε-neighborhood of former states [116]. Eckmann et al. [117] introduced a graphical tool, namely RP, to visualize recurrence patterns of dynamical systems in 1987. RP characterizes the proximity of two states using the Heaviside function Θ, then obtains the topological relationships in the state spaces as a two-dimensional recurrence plot:

$$\mathbf{R}_{p,q} = \Theta(\varepsilon - \|\mathbf{s}_p - \mathbf{s}_q\|) \quad \mathbf{s}_p, \mathbf{s}_q \in \mathbb{R}^m \tag{4.1}$$

where $\mathbf{R}_{p,q}$ is the recurrence matrix $\mathbf{R}$, $\mathbf{s}_p$ and $\mathbf{s}_q$ are two states, and ε is a threshold. Mutual information and the false nearest neighbor are commonly used to select optimal delay and determine the embedding dimension for state-space reconstruction from time series. Mutual information quantifies both linear and nonlinear interdependence in the time series, and the optimal dimension is determined by varying the dimensionality and comparing the behavior of false nearest neighbors [118]. Zbilut and Webber [119] proposed RQA to extract statistical features from small-structures in the RP to understand the dynamical properties of complex systems. Yang and Chen [120] considered different types of recurrences in the state space and extended the conventional RQA to heterogeneous recurrence quantification analysis (HRQA). The HRQA has been widely applied in the manufacturing domain [121, 122] as well as the healthcare area [123, 124].

However, RP is limited in the ability to handle high-dimensional and geometric spatial data. Marwan et al. [104] extended the one-dimensional RP framework to high-dimensional spatial data:

$$\mathbf{R}(\mathbf{x}_p, \mathbf{x}_q) = \Theta(\varepsilon - \|\mathbf{s}(\mathbf{x}_p) - \mathbf{s}(\mathbf{x}_q)\|) \quad \mathbf{s}(\mathbf{x}_p), \mathbf{s}(\mathbf{x}_q) \in \mathbb{R}^m \tag{4.2}$$

where $\mathbf{s}(\mathbf{x}_p)$ and $\mathbf{s}(\mathbf{x}_q)$ are the states (i.e., pixel intensity), $\mathbf{x}_p$ and $\mathbf{x}_q$ denotes the spatial locations. If the intensity differences between two pixels is less than threshold ε, there exists a recurrence. However, only limited information about the recurrence behaviour can be visualized. Let's denote the spatial reference (i.e., location information) as $\mathbf{x} = (x_1, x_2, ..., x_d)$ with d dimensions, and the attribute set as $\mathbf{a} = (a_1, a_2, ..., a_m)$ with m

dimensions. A pixel p in a two-dimensional image contains the location $\mathbf{x}_p = (x_1^{(p)}, x_2^{(p)})$ and attribute $\mathbf{a}_p = (a_R^{(p)}, a_G^{(p)}, a_B^{(p)})$. Then, a two-dimensional image will generate a four-dimensional RP $\mathbf{R}(\mathbf{x}_p, \mathbf{x}_q) = \mathbf{R}_{x_1^{(p)}, x_2^{(p)}, x_1^{(q)}, x_2^{(q)}}$. However, only three out of four dimensions can be selected for the visualization in the three-dimensional coordinate system. It will be even more challenging to visualize three-dimensional imaging data which generates an RP of six dimensions $\mathbf{R}(\mathbf{x}_p, \mathbf{x}_q) = \mathbf{R}_{x_1^{(p)}, x_2^{(p)}, x_3^{(p)}, x_1^{(q)}, x_2^{(q)}, x_3^{(q)}}$.

Further, Yang et al. [118, 125] introduced a recurrence network for nonlinear time series analysis. Network nodes represent the states and edges denote the recurrence relationship.

$$\mathbf{A}_{p,q} = \Theta(\varepsilon - \|\mathbf{s}(\mathbf{x}_p) - \mathbf{s}(\mathbf{x}_q)\|) - \Delta_{p,q} \quad \mathbf{s}(\mathbf{x}_p), \mathbf{s}(\mathbf{x}_q) \in \mathbb{R}^m \tag{4.3}$$

where ε denotes the recurrence threshold, $\mathbf{A}_{p,q}$ is the adjacency matrix, $\Delta_{p,q}$ is the Kronecker delta, which prevents the self-loop in the recurrence network. However, the proposed recurrence network is designed for time series data, and cannot be utilized for spatial data directly. In this work, we leverage network theory to investigate the recurrence behavior of spatial data, further characterize and quantify spatial characteristics through network statistics.

4.3 Research Methodology

This paper presents the analysis of design-quality interactions in the PBF-AM process. As shown in Figure 5.4 (a), a total of three builds were fabricated, each differing in build direction (i.e., their planar inclination in the X–Y plane with respect to the recoater blade). We performed a post-build inspection through XCT. As shown in Figure 5.4 (b), a shape-to-image registration is conducted between XCT images and layerwise CAD images. Next, we leveraged a GRN analysis to characterize and quantify the layerwise imaging data. Finally, we performed an ANOVA analysis to select important features and established a regression model to predict how the design complexity impacts the network behaviors in each layer of thin-wall builds.

4.3.1 Experimental Setup

In this experiment, thin-wall parts were built from Spherical ASTM B348 Grade 23 Ti-6Al-4V powder with a size distribution of 14-45 μm on an EOS M280 PBF machine.

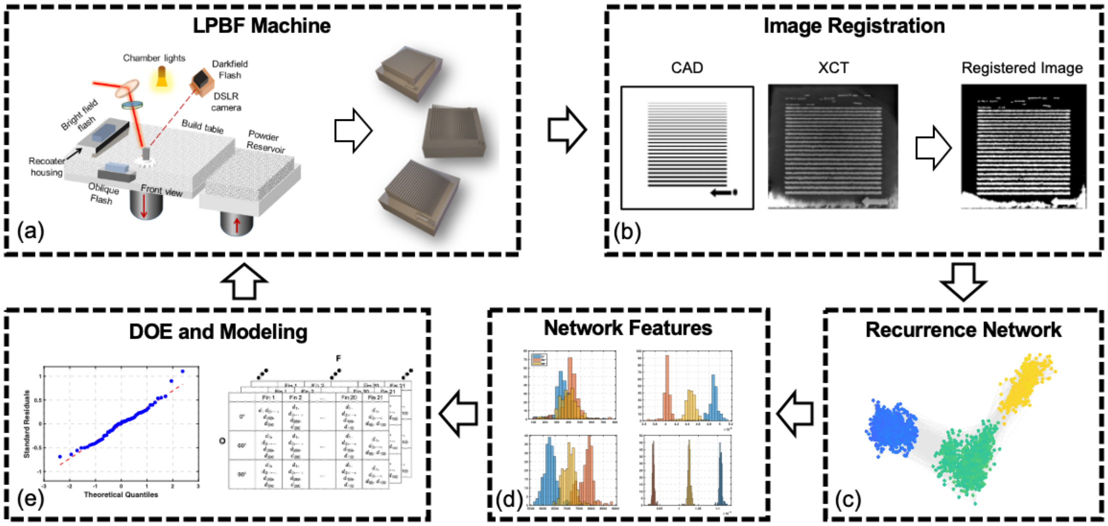

Figure 4.2. The flow chart of research methodology.

The laser power and velocity settings are 340 W and 1250 mm/s, respectively. As shown in Figure 5.5, thin-wall parts are built vertically with a layer thickness of 60 μm in three orientations (i.e., 0°, 60°, and 90°) with respect to the travel direction of recoater blade (i.e., indicated by the arrow on each part). Each thin-wall build consists of 25 thin-walls built on a platform of size 15 mm × 15 mm × 55 mm. The width of thin-walls increases from 0.06 mm, with a step size of 0.01 mm, to 0.3 mm. Also, two thin-walls are separated with a constant distance of 0.3 mm. It is worth mentioning that the height/width ratio of each thin-wall is 10. In other words, if the width of a thin-wall is 0.3 mm, then the height is set to be 3.0 mm. Figure 5.5 (d) shows the hatching pattern for thin-wall 1-24 that includes one outer contour on the blue line, one inner contour with hatches at the same angle inside. However, thin-wall 25 does not have the inner contour as others. Note that there is a 67-degree rotation for the hatching paths on each layer by the default setting of the EOS 280 machine. Table 5.1 shows the variation of hatching distances within the contour from thin-wall 1 to thin-wall 25. The distance between hatches is 0.244 mm for thin wall 1, and decreases from thin-wall 1 to 24 (0.011 mm). Post build XCT data are obtained on General Electric V|tome|X system with a voxel size of 15 μm^3.

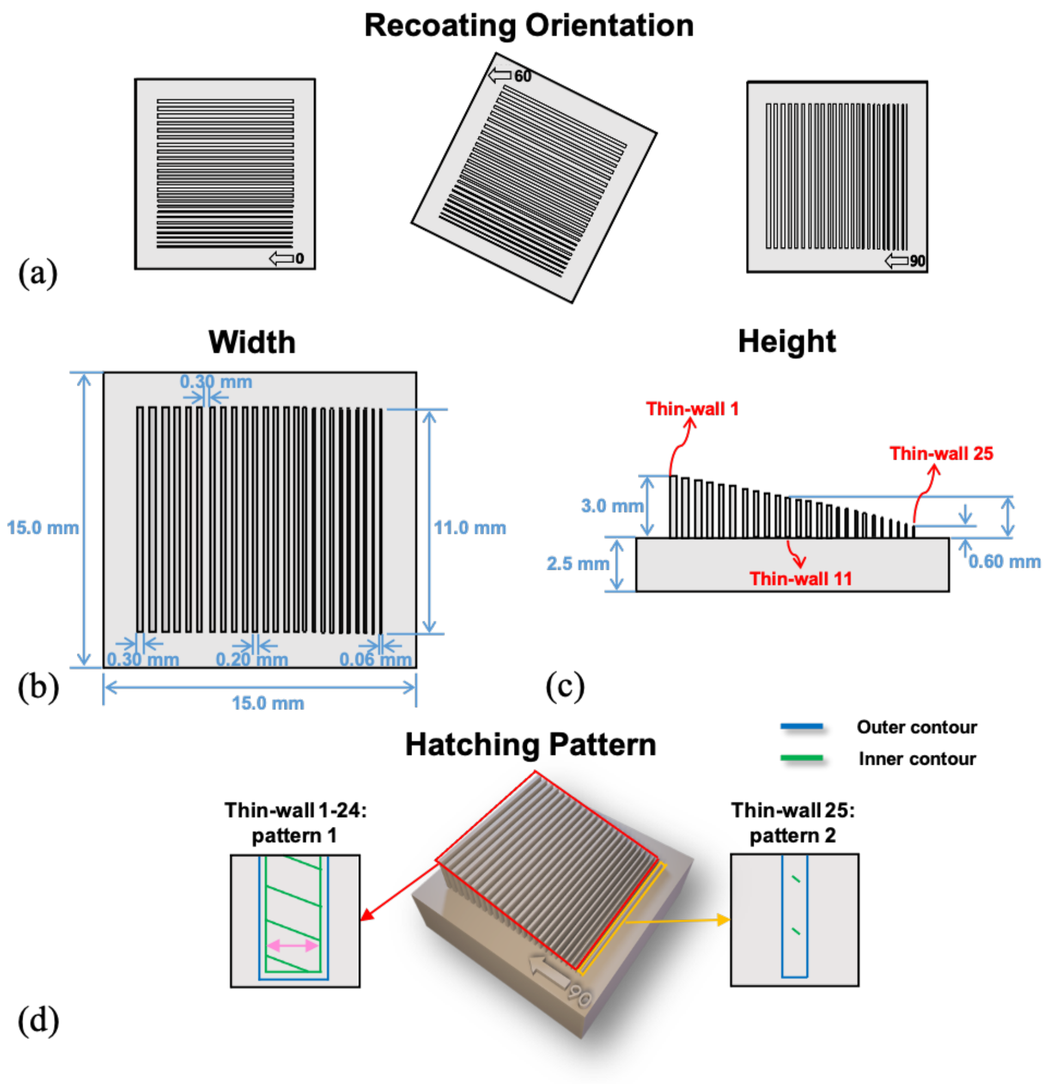

Figure 4.3. (a) The orientation of thin-wall parts, (b) the top view of the CAD model, (c) the side view of the CAD model, and (d) the hatching patterns of the thin-walls. The blue and green solid lines represent outer and inner rectangle paths, respectively.

4.3.2 Image Registration

Image registration helps delineate the correspondence of ROIs between two images (i.e., a moving image and a fixed image) using a common coordinate system. Note that this paper focuses on the analysis of design-quality interactions and does not preclude others to use a different registration approach. We used a standard registration process with four components, namely similarity metric, optimizer, moving transformation,

Table 4.1. The variations of hatching distances within contour from thin-wall 1 to thin-wall 25.

Thin-wall Number	W_h mm	Thin-wall Number	W_h mm	Thin-wall Number	W_h mm	Thin-wall Number	W_h mm	Thin-wall Number	W_h mm
1	0.244	6	0.190	11	0.142	16	0.092	21	0.045
2	0.234	7	0.183	12	0.136	17	0.082	22	0.033
3	0.220	8	0.167	13	0.125	18	0.076	23	0.022
4	0.208	9	0.159	14	0.114	19	0.059	24	0.011
5	0.198	10	0.154	15	0.102	20	0.049	25	N/A

and interpolator. The similarity metric is aimed at evaluating the accuracy of image registration, which takes two images (i.e., the moving image and the fixed image) and returns a scalar value that measures the similarity between two images. Figure 4.4 illustrates this iterative process and flow chart of image registration.

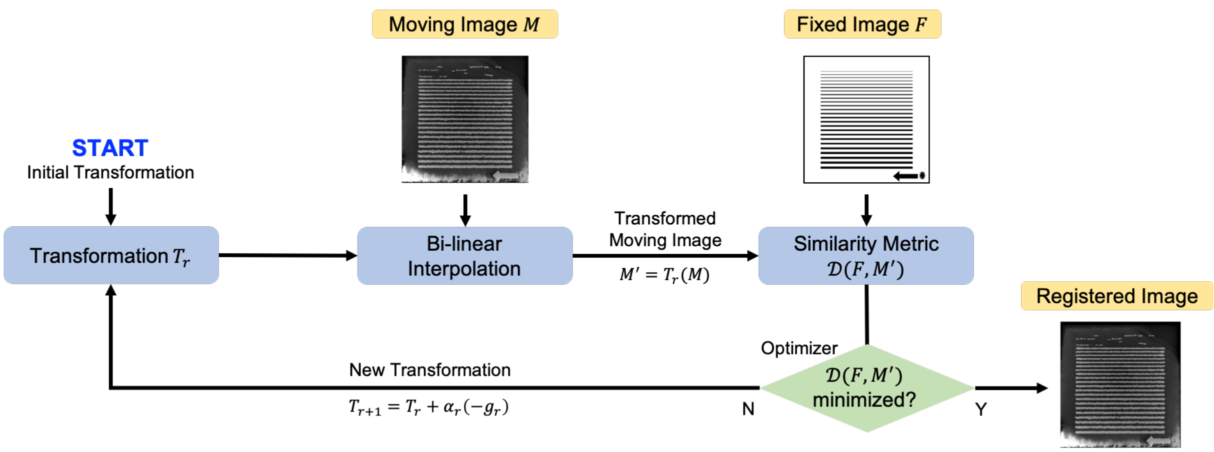

Figure 4.4. The flow chart of image registration.

The mean square differences ($\mathcal{D}$) is used to define the similarity metric between a fixed image F and a transformed image M' as:

$$\mathcal{D}(F, M') = \frac{1}{N}\sum_{p=1}^{N} \|F(p) - M'(p)\|^2 \quad \forall\, p \in F \cap M' \tag{4.4}$$

where N represents the number of pixels in each image, $F(p)$ shows the intensity of pixel p in the fixed image, $M'(p)$ denotes intensity of pixel p in the transformed image.

$$M' = T(M) \tag{4.5}$$

where M is the moving image, and T is the transformation function. The optimization problem is formulated as:

$$\underset{T}{\operatorname{argmin}} \ \mathcal{D}(F, M') \tag{4.6}$$

The gradient descent method is utilized to iteratively update T and search for the minimum value of $\mathcal{D}$:

$$T_{r+1} = T_r + a_r(-g_r) \tag{4.7}$$

where $a_r > 0$ is the step size at iteration r, g_r is the gradient vector of $\mathcal{D}$. Then, we isolate the region of interest (ROI) (i.e., each thin-wall) from the powder area in registered images. The extracted ROIs are used for the GRN analysis in the next session.

4.3.3 Recurrence Network Analysis of Spatial Data

Spatial data contains both spatial locations and intensity values of pixels. The traditional recurrence analysis is limited in the ability to analyze high-dimensional spatial data. Here, we propose a GRN analysis method, which accounts for both spatial closeness and pixel similarity. As discussed in Section 2, let's denote spatial reference as $\mathbf{x} = (x_1, x_2, ..., x_d)$, and attribute information as $\mathbf{a} = (a_1, a_2, ..., a_m)$, where d and m are the dimensions, respectively. For the pixel p in a two-dimensional image, $\mathbf{x}_p = (x_1^{(p)}, x_2^{(p)})$ and $\mathbf{a}_p = (a_R^{(p)}, a_G^{(p)}, a_B^{(p)})$. For a 3D voxel q, $\mathbf{x}_q = (x_1^{(q)}, x_2^{(q)}, x_3^{(q)})$ and $\mathbf{a}_q = (a_R^{(q)}, a_G^{(q)}, a_B^{(q)})$. The edge weight of a recurrence network is formulated as:

$$w_{p,q} = I_{p,q} \times D_{p,q} \tag{4.8}$$

where the intensity similarity $I_{p,q}$ (i.e., the closeness between two pixels) is

$$I_{p,q} = 1 - \frac{\|\mathbf{s}(\mathbf{x}_p) - \mathbf{s}(\mathbf{x}_q)\|}{max\{\|\mathbf{s}(\mathbf{x}_.)\|\} - min\{\|\mathbf{s}(\mathbf{x}_.)\|\}} \quad \mathbf{x}_p, \mathbf{x}_q \in \mathbb{N}^d, \mathbf{s}_p, \mathbf{s}_q \in \mathbb{R}^m \tag{4.9}$$

Spatial closeness $D_{p,q}$ (i.e., the spatial correlation between two pixels) is

$$D_{p,q} = \frac{\phi(\|\mathbf{x}_p - \mathbf{x}_q\|)}{\phi(\|0\|)} \quad \mathbf{x}_p, \mathbf{x}_q \in \mathbb{N}^d \tag{4.10}$$

where $\phi(\cdot)$ denotes the Gaussian function. As shown in Figure 4.5, if two pixels are far away from each other, the spatial correlation between them is low. In other words, $\phi(\|\mathbf{x}_p - \mathbf{x}_q\|) < \phi(\|\mathbf{x}_p - \mathbf{x}_{q'}\|)$ while $D_{p,q} > D_{p,q'}$.

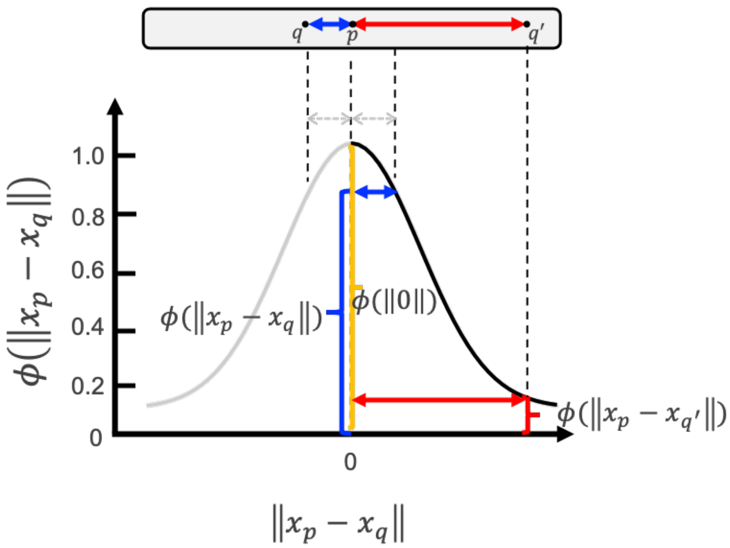

Figure 4.5. The relationship of $\phi(\|\mathbf{x}_p - \mathbf{x}_q\|)$ and spatial distance. If two pixels are far away from each other, the spatial correlation between them is tend to be low. In other words, $\phi(\|\mathbf{x}_p - \mathbf{x}_q\|) < \phi(\|\mathbf{x}_p - \mathbf{x}_{q'}\|)$ while $D_{p,q} > D_{p,q'}$.

The adjacency matrix $\mathbf{A}_{p,q}$ is derived as a binary matrix where $\mathbf{A}_{p,q} = 1$ if there is a link from node p to node q, and otherwise if they are not connected:

$$\mathbf{A}(\mathbf{x}_p, \mathbf{x}_q) = \Theta(\varepsilon - w_{p,q}) - \Delta_{p,q} \tag{4.11}$$

where ε denotes the threshold, Θ is the Heaviside Function, and $\Delta_{p,q}$ is the Kronecker delta which prevents the self-loop in the recurrence network. The threshold ε is often chosen based on the significance level α. Note that the 0.05 significance level is the most commonly used α value in statistics. In this study, we set $\alpha = 0.05$.

4.3.4 Network Characterization and Quantification

Network statistics are established measurements for the characterization of the topology, and provide useful information for statistical inference as well as predictive modeling [126]. Table 4.2 summarizes the network statistics and their corresponding mathematical equations used in this study.

In the proposed GRN framework, degree k_p represents the recurrence frequency relative to the pixel p. The connection between nodes indicates the both the image and spatial similarity. In other words, the distribution of k_p shows the recurrence

Table 4.2. Network measures and the corresponding mathematical expressions.

Quantifiers	Expression	Description
Degree	$k_p = \Sigma_{q=1}^{N} A_{p,q}$	Number of edges connected to node p. N denotes the number of node in the network.
Betweenness Centrality	$BC_p = \sum_{p \neq q \neq r} \frac{\sigma_{qr}p}{\sigma_{qr}}$	σ_{qr} is the total number of paths from node q to node r, $\sigma_{qr}p$ is the number of those paths which pass through node p.
Pagerank Centrality	$PR_p = (1-\alpha)\frac{1}{N} + \alpha \sum_q A_{q,p} \frac{PR_q}{L_q}$	$\alpha \in (0,1)$, L_q is the number of neighbours of node q .
Closeness Centrality	$C_p = \frac{1}{\Sigma_{p \neq q} d_{p,q}}$	$d_{p,q}$ is the distance between node p and node q.
Eigenvector Centrality	$V_p = \frac{1}{\lambda} \Sigma_{q \in M(q)} V_q$	$M(q)$ denotes the set of neighbors of p, λ is a constant.

distribution of spatial data. The centrality measurements reveal recurrence patterns between a node and its neighbors. For example, the betweenness centrality quantifies the number of shortest paths that pass through one node, which indicates how many times a node appears in different patterns. The bigger the betweenness centrality, the more frequent the corresponding recurrence pattern shows in the system. Eigenvector centrality is a measure of the influence of a node in a network, and pagerank centrality is its variant. The bigger the eigenvector centrality, the more a node impacts other nodes in a network. The closeness centrality is calculated as the reciprocal of the sum of the shortest paths between the node and all other nodes in the network. The node with larger closeness centrality is closer to other nodes, and indicates a stronger recurrence pattern.

4.3.5 Hypothesis Testing

We tested the statistical significance of extracted network features using the Mann-Whitney U test [127]. Let X and Y denote two histograms, and contain m and n observations, respectively. The hypothesis of the Mann-Whitney U test is

$$\begin{aligned} &H_0 : \text{Two histograms } X \text{ and } Y \text{ follow the same distribution} \\ &H_1 : \text{Two histograms } X \text{ and } Y \text{ follow different distributions} \end{aligned} \tag{4.12}$$

Mann-Whitney U test begins by arranging the $m + n$ observations in a single sequence from the smallest to the largest. Then, a rank is assigned to each element corresponding to the position. That is, each of the observation is assigned a rank from 1 to $m+n$ in the ordering. If H_0 is true, the observations $X_1, ..., X_m$ (or $Y_1, ...Y_n$) tend to be dispersed throughout the ordering of all $m+n$ observations. Otherwise, the observations are concentrated among the smaller values or among the larger values if H_1 is true. Let S denote the sum of the ranks assigned to m observations from X. Given H_0 is true,

$$E(S) = \frac{m(m+n+1)}{2} \tag{4.13}$$

and

$$Var(S) = \frac{mn(m+n+1)}{12}. \tag{4.14}$$

Note that when the H_0 is true and sample size m and n are large, the distribution of S is approximately normal. The null hypothesis H_0 is rejected if $|S-(1/2)m(m+n+1)| \geq c$, where $c = [Var(S)]^{1/2}\Phi^{-1}(1-\alpha/2)$. The p-value is computed as $2[1-\Phi(z_0)]$, where $z_0 = |S-E(S)|/\sqrt{Var(S)}$. If the p-value is less than the significant level (i.e., $\alpha = 0.05$), H_0 will be rejected and the distributions of X and Y are declared to be different at the significant level of 0.05.

4.3.6 ANOVA and Predictive Modeling

Further, we perform an ANOVA to study the effects of experimental factors (i.e., orientations and other design parameters) on the build quality. Here, the parameters of hatching distance, thin-wall width, and height are associated with the thin-wall number. In total, there are three levels for orientation O and 21 levels for thin-wall characteristics C. The last four thin-walls collapsed during the fabrication process (see Figure 4.1). Therefore, we only take the other 21 thin-walls into account in the ANOVA. We reorganize our design parameters into two groups, i.e., orientation and thin-wall characteristics, with 3 levels and 21 levels, respectively.

Two-way ANOVA is commonly performed when there are two factors (i.e., factor M with m levels and factor N with n levels) in an experiment. Figure 4.6 shows the data structure for ANOVA, which is expressed as:

$$X_{ij} = \mu + O_i + C_j + OC_{ij} + \epsilon_{ij} \tag{4.15}$$

where $i = 1, ..., 3$, $j = 1, ...21$, and ϵ_{ij} represents the error term in the model. In addition, we develop a regression model to predict the effects of design parameters

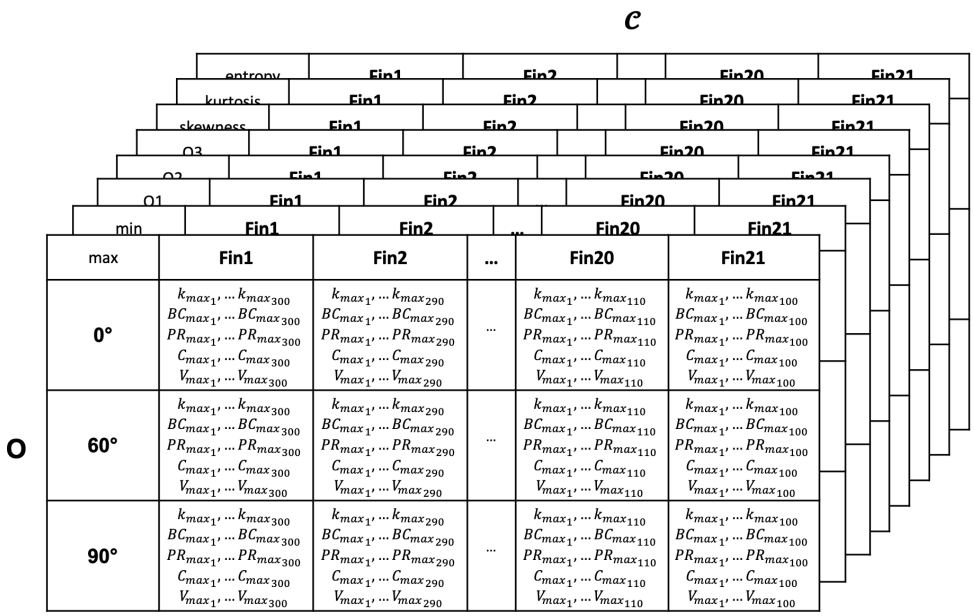

Figure 4.6. Experimental data structure for the ANOVA analysis: C and O represent two factors, namely thin-wall characteristics and orientation.

on network characteristics.

$$\begin{aligned} y = \beta_0 + \beta_1 \times O_1 + \beta_2 \times O_2 + \beta_3 \times W + \beta_4 \times H + \beta_5 \times G + \\ \beta_6 \times O_1 \times W + \beta_7 \times O_2 \times W + \beta_8 * O_1 \times H + \\ \beta_9 \times O_2 \times H + \beta_{10} \times O_1 \times G + \beta_{11} \times O_2 \times G + \\ \beta_{12} \times W \times H + \beta_{13} \times W \times G + \beta_{14} \times H \times G + \varepsilon \end{aligned} \tag{4.16}$$

where the categorical variable O is coded with O_1 and O_2, and stands for the orientation (see Table 4.3). W denotes the width, H represents the height of a thin-wall, and G indicates the hatching distance. Note that in Equation 4.16, the explanatory variables are the design parameters and the response variable y is the Hotelling's T^2 statistic that is computed for the i^{th} observation as $T^2(i) = (\mathbf{x}^{(i)} - \overline{\mathbf{x}})^T \mathbf{S}^{-1} (\mathbf{x}^{(i)} - \overline{\mathbf{x}})$, where $\mathbf{x}^{(i)}$ is the vector of network features, $\overline{\mathbf{x}}$ is the mean vector and $\mathbf{S}$ is the covariance matrix.

4.4 Experimental Results

The proposed methodology is evaluated and validated with both simulation and

Table 4.3. Coding for the Categorical Variable Orientation

	O_1	O_2
orientation 0°	0	0
orientation 60°	1	0
orientation 90°	0	1

real-world case studies. First, we derive the visualization results of GRN and extract corresponding network from simulated images with different types of defects (i.e., edge variations and surface characteristics). Then, we perform pair-wise hypothesis tests on the extracted quantifiers. The simulation study is aimed at testing the significance of quantifiers with defect variations. Next, in the real-world case study, we leverage the proposed GRN to characterize the quality of PBF-AM builds and study the relationships between the design parameters (i.e., build orientation, hatching distance, thin-wall height, and width) and quality characteristics of thin-wall structures. Finally, we develop a regression model to predict how the design complexity impacts the GRN behaviors in each layer of thin-wall builds.

4.4.1 Simulation Study

As shown in Table 4.4, two types of defect patterns (i.e., edge variation and inner surface variation) are simulated to evaluate the visualization and the performance of the proposed GRN methodology. The size and location of porosity defects are varied to simulate three different levels of inner surface variations.

Figure 4.7. Proportional heatmap of the XCT scan from thin-wall 13, layer 100 in the thin-wall part built under orientation 60°, and proportional heatmap of the simulated baseline thin-wall. Note that the blue color represents nodes with smaller pixel values, and the yellow color is corresponding to bigger values in the gray scale.

Figure 4.7 shows the heatmap of the real XCT scan (top) and the simulated XCT scan (bottom). Note that the real-world XCT scan is taken from the layer 100 of thin-wall 13 in the part built under orientation 60°. It may be noted that the

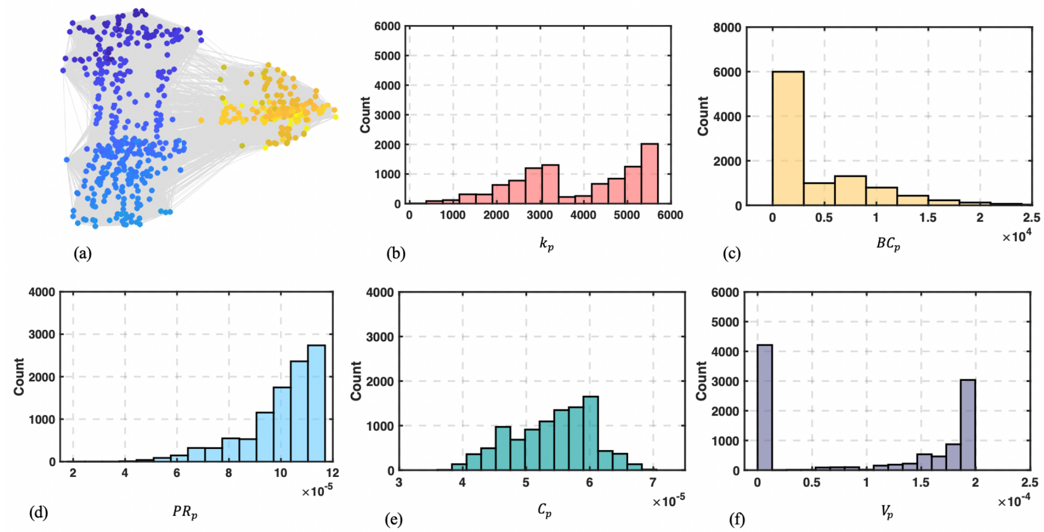

Figure 4.8. (a) Network visualization of the simulated baseline thin-wall in Figure 4.7. (b)-(f) Distributions of k, BC, PR, C, and V.

Table 4.4. Defect variation in the simulation study.

Category	Case	Description
	Baseline	A thin-wall without any flaws
Edge Variation	Case I	Edge roughness with the frequency of 100 Hz
	Case II	Edge roughness with the frequency of 200 Hz
	Case III	Edge roughness with the frequency of 400 Hz
Number of Pores Variation	Case IV	Three pores each with a diameter of 4 pixels
	Case V	Six pores each with a diameter of 4 pixels
	Case VI	Nine pores each with a diameter of 4 pixels
Size of Pores Variation	Case VII	Six pores each with a diameter of 2 pixels
	Case VIII	Six pores each with a diameter of 4 pixels
	Case IX	Six pores each with a diameter of 6 pixels

thin-wall has both edge variation and inner surface issues (i.e., porosity). Therefore, we add variations to edges and surfaces in the baseline to generate different types of defects, see Table 4.4. In addition, it can be seen that the real XCT scan (see Figure 4.7 (a)) shows a transition of pixel values on the edge, i.e., from the yellow region to the blue region. We have also added this transition to the simulated XCT.

Figure 4.8 shows the network visualization and the distribution of network quantifiers (i.e., degree k, betweenness centrality BC, pagerank centrality PR, closeness centrality C, and eigenvector centrality V) for the baseline case (Simulated XCT in Figure 4.7). Note that nodes in the network are clustered into two groups. In the network, yellow nodes (i.e., laser-fused area) are clustered into one group and blue nodes (i.e., powder area) are clustered into another group, and two groups are connected. Peaks shown in Figure 4.8 (b) are corresponding to the degree distribution in two clusters. For example, the smaller peak is related to the cluster of laser-fused surface (i.e., yellow nodes) with less number of nodes in the network, and the bigger peak is relevant to the powder area cluster (i.e., blue nodes). The baseline distributions of network features (Figure 4.8 (b)-(f)) will be benchmarked with the following simulation scenarios.

Figure 4.9. Simulated thin-walls with edge variation of different frequencies. Case I: 100 Hz, case II: 200 Hz, case III: 400 Hz.

First, we explore the relationship between edge variation and network characteristics, as shown in Figure 4.9. In case I, we utilize a sine wave with an amplitude of 15 and a frequency of 100 Hz to generate the edge variation. Then, we increase the frequency to 200 and 400 Hz for case II and case III, respectively.

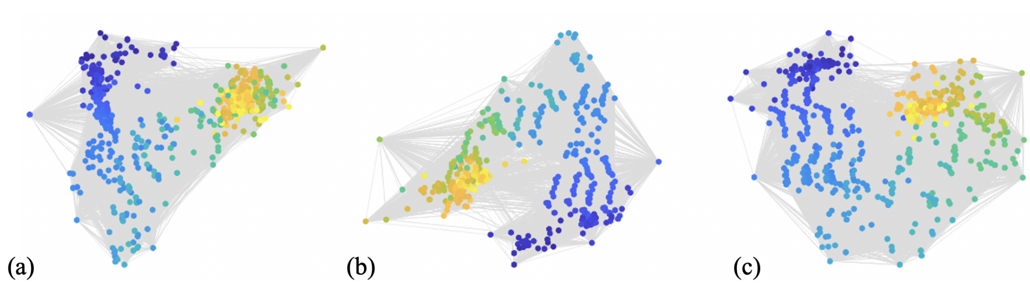

Figure 4.10. Network visualization results of the GRNs in Figure 4.9. (a) case I, (b) case II, and (c) case III.

As shown in Figure 4.10, nodes in background and surface are clustered into three different groups in all networks. The blue cluster represents the powder area, the yellow nodes correspond to the laser-fused layerwise surface, and the green nodes are related to the transitions on the edges, which appear as a “bridge" linking the blue cluster and the yellow cluster. Figure 4.10 (b) and (c) show more variations on

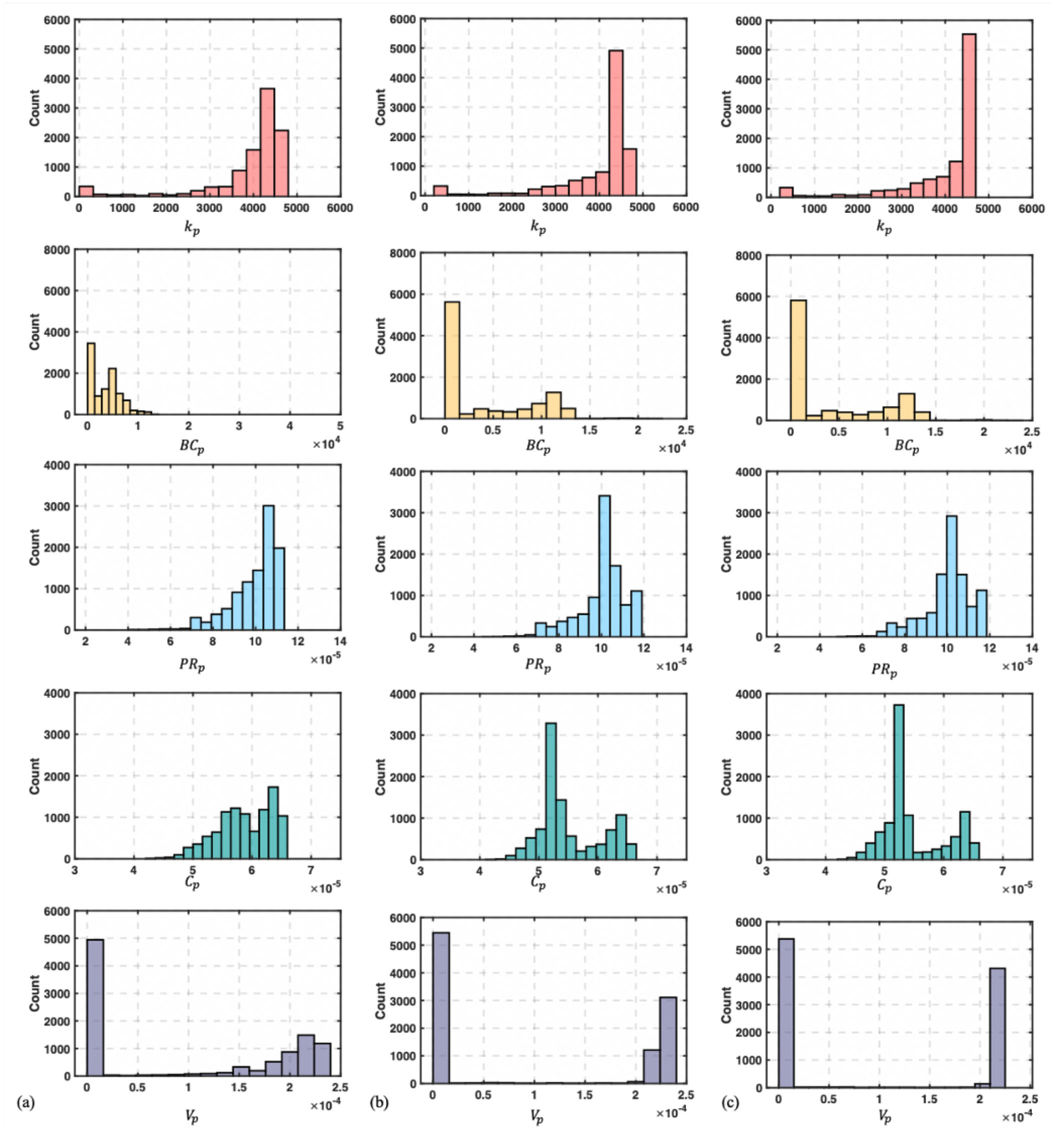

Figure 4.11. The distribution of k, BC, PR, C, and V in GRNs for 3 cases in Figure 4.9. (a) case I, (b) case II, and (c) case III.

the edge (i.e., the frequencies are higher) compared to Figure 4.10 (a). Therefore, the green cluster becomes more dispersed as the variation increases. Distributions of network quantifiers for the case I-III are shown in Figure 4.11. Each degree distribution contains two peaks corresponding to the blue and yellow clusters. In comparison with the baseline case which also has two peaks (see Figure 4.8 (b)), the number of nodes with lower degrees (i.e., 1-500) increases and the number of nodes with the degree around 2000-3000 decreases significantly. The peak between 0-500 is from the edge cluster and is not as high as the others because the edge contains a smaller number of nodes. Also, the number of nodes with a degree around 4500 significantly increases as the edge variation increases. In addition, the increment of edge variation is positively correlated with the number of nodes with closeness centrality of 5.25e-5, and is negatively related to the number of nodes with closeness centrality of 6.25e-5. In summary, the distributions of network quantifiers vary between cases I-III and the baseline.

We perform the Mann-Whitney U test for pairwise comparison between histograms among different simulation cases. The statistically significant results are marked **bold** in Table 4.5. Note that, case I and case II, and case I and case III are significantly different for five quantifiers, but the GRN quantifiers of case II and case III only differ in degree and eigenvector centrality according to the p-values in Table 4.5.

Table 4.5. Two-Sample Mann-Whitney U Testing of Quantifier Distributions among Simulation Cases I-III.

	Case I vs. Case II	Case I vs. Case III	Case II vs. Case III
k	**1.124e-5**	**5.368e-22**	**2.495e-24**
BC	**2.447e-17**	**5.501e-28**	0.395
PR	**3.488e-08**	**1.809e-09**	0.777
C	**0**	**0**	0.2923
V	**8.445e-17**	**2.252e-140**	**0**

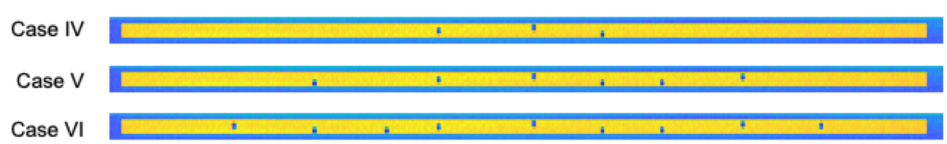

Figure 4.12. Simulated thin-walls with pores of same size (diameter 4 pixels) but different number of pores. Case IV: 3 pores, case V: 6 pores, case VI: 9 pores.

Next, we add porosity defects to the simulated thin-wall (i.e., the baseline case). Each pore has the diameter of 4. Three pores are firstly included to the laser-fused surface area (case IV). Then, we increase the number of pores to six in case V, and nine pores in case VI as shown in Figure 4.12. Similarly, three clusters corresponding to the edge, laser-fused area, and the powder area can be seen among all the networks in Figure 4.13. However, the edge cluster (in green) does not contain as many nodes as in Figure 4.10. This is because (1) there is no edge variations in these cases, and

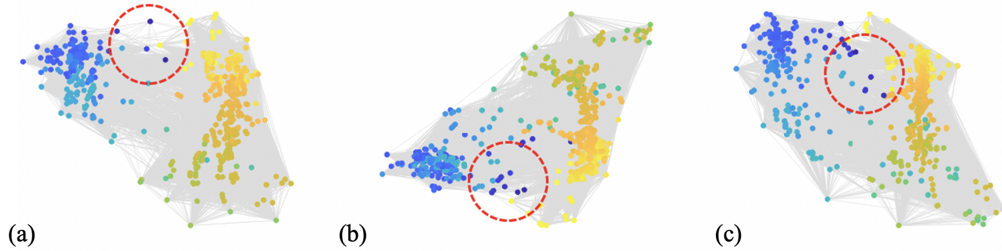

Figure 4.13. Network visualization results of the GRNs in Figure 4.12. (a) case IV, (b) case V, and (c) case VI.

Table 4.6. Two-Sample Mann-Whitney U Testing of Quantifier Distributions among Simulation Cases IV-VI.

	Case IV vs. Case V	Case IV vs. Case VI	Case V vs. Case VI
K	**2.664e-04**	0.497	**3.941e-5**
BC	**0.022**	0.442	0.303
PR	0.839	0.895	0.895
C	0.282	**3.105e-5**	**5.03e-9**
V	**2.738e-18**	**1.984e-20**	**0.0246**

(2) the number of transitional pixels on the edge is limited. Note that the number of nodes in the circled cluster increases as the number of pores increases in (a) and (b). It is challenging to visually find individual groups representing different pores among networks. Here, we keep all parameters the same for further quantification analysis in our simulation study. In Figure 4.14, the first row (i.e., in red) show the distribution of k and the peak around 5000 drops while more pores are added to the laser-fused area. Similarly, the peak of PR at the x-axis with the value of 10e-5 decreases when the number of pores increases. However, as shown in Table 4.6, the hypothesis test does not indicate there exist significant variations in pagerank centrality among pairwise comparisons. The variation is not enough to suggest any differences at the significance level of 0.05. Also, it can be seen from the results that the eigenvector centrality is sensitive to the number of pores in the fin part since the p-values are less than 0.05.

Finally, three more cases are designed with the pore diameters selected as 2, 4, and 6 respectively as shown in Figure 4.15. Figure 4.16 shows that the cluster associated with porosity defect is more noticeable when the size of the pore becomes bigger (see red circles). The number of nodes in the cluster increases as the size of pore increases.

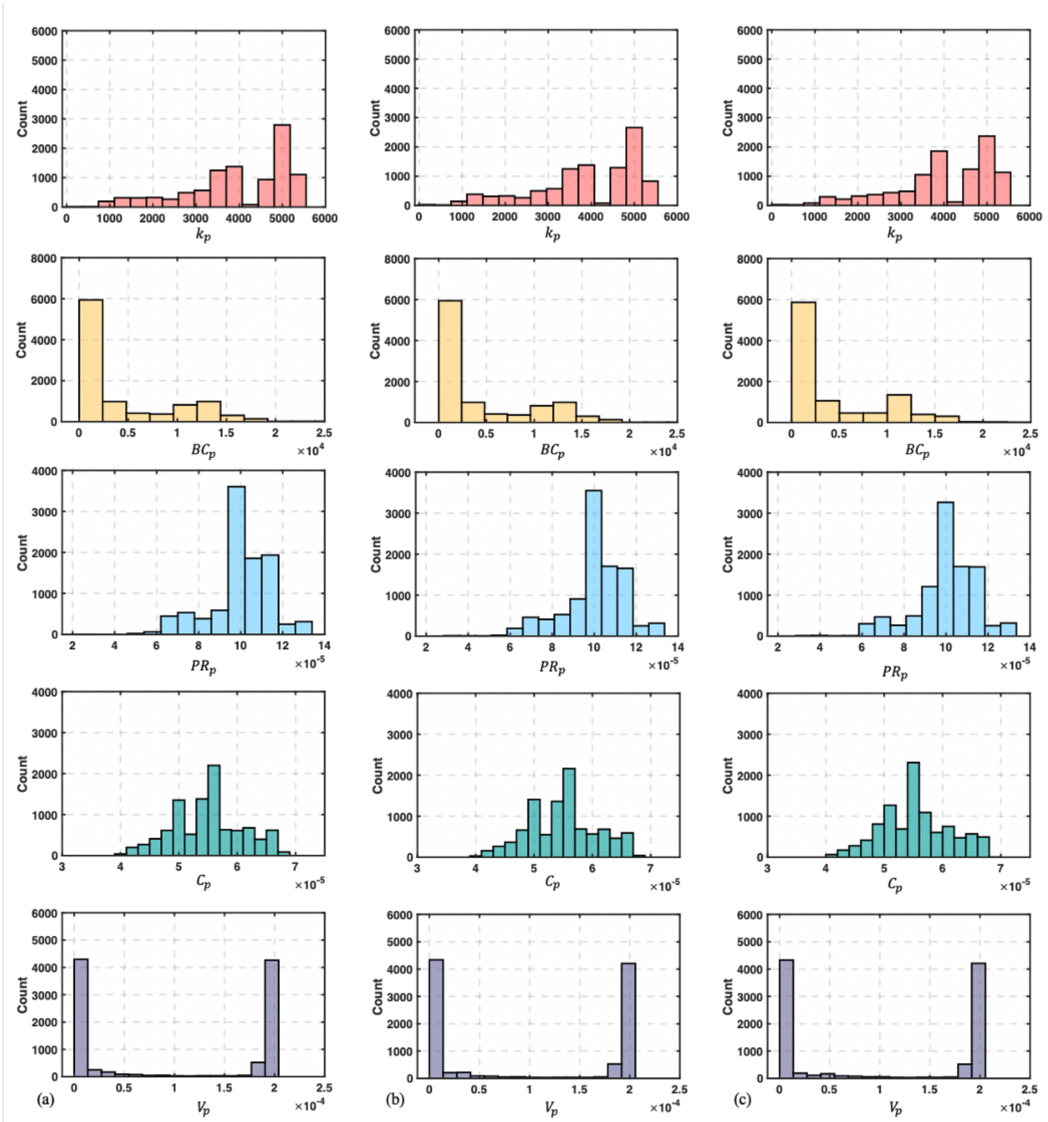

Figure 4.14. The distribution of k, BC, PR, C, and V in GRNs for 3 cases in Figure 4.13. (a) case IV, (b) case V, and (c) case VI.

Figure 4.17 shows the distributions of their quantifiers, and Table 4.7 presents the result of pair-wise hypothesis tests. Degree k, betweenness centrality (BC), closeness centrality (C), and eigenvector (V) centrality track the changes in the size of porosity. Note that pagerank centrality (PR) does not vary significantly in both Table 4.6 and Table 4.7, and is not sensitive to the porosity defect on the surface of thin-wall.

The proposed GRN method provides a complete picture of spatial patterns and recurrence behaviors through the network visualization and hypothesis testing.

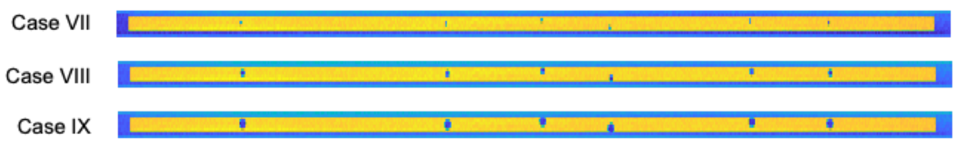

Figure 4.15. Simulated thin-walls with different pore sizes but same number of pores. Case VII: diameter 2 pixels, case VIII: diameter 4 pixels, case VI: diameter 6 pixels.

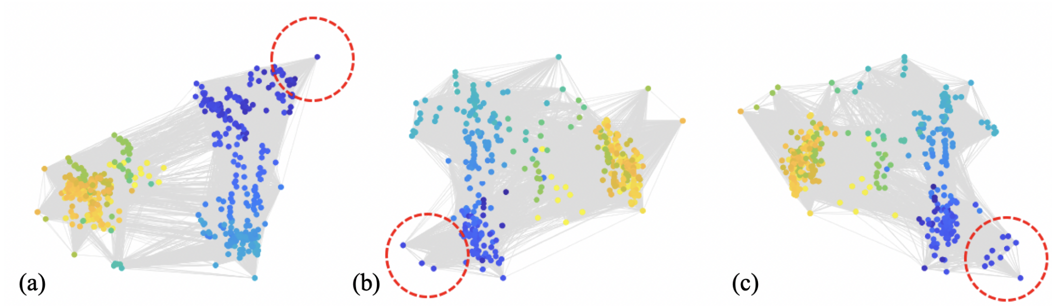

Figure 4.16. Network visualization results of the GRNs in Figure 4.15. (a) case VII, (b) case VIII, and (c) case IX.

Network structures have different patterns with respect to simulated thin-wall images in cases I-IX. From the simulation study, we select the set of five quantifiers (i.e., degree k, betweenness centrality BC, pagerank centrality PR, closeness centrality C, and eigenvector centrality V) that are sensitive to both powder area and laser-fused area in various cases. Note that distributions of quantifiers show different shapes regarding different quality issues. For example, when edge variation increases, there is an increase in the peak among distributions in Figure 4.11. Also, the p-values two sample Mann-Whitney U test indicates the differences between distributions of quantifiers. In the real-world case study, we extract features (i.e., maximum, minimum, quartiles, standard deviation, skewness, kurtosis, and entropy) from these selected quantifiers for further analysis.

4.4.2 Real-world Case Study

We extracted 9 features from each distribution of network quantifiers, i.e., the maximum value, the minimum value, the standard deviation, quartiles (Q1, Q2, Q3), skewness, kurtosis, and entropy. In total, 45 features from 5 quantifiers of each network are extracted where one thin-wall of one layer generates a recurrence network. Figure 4.18 shows distributions of Q1s of degree (k), betweenness centrality

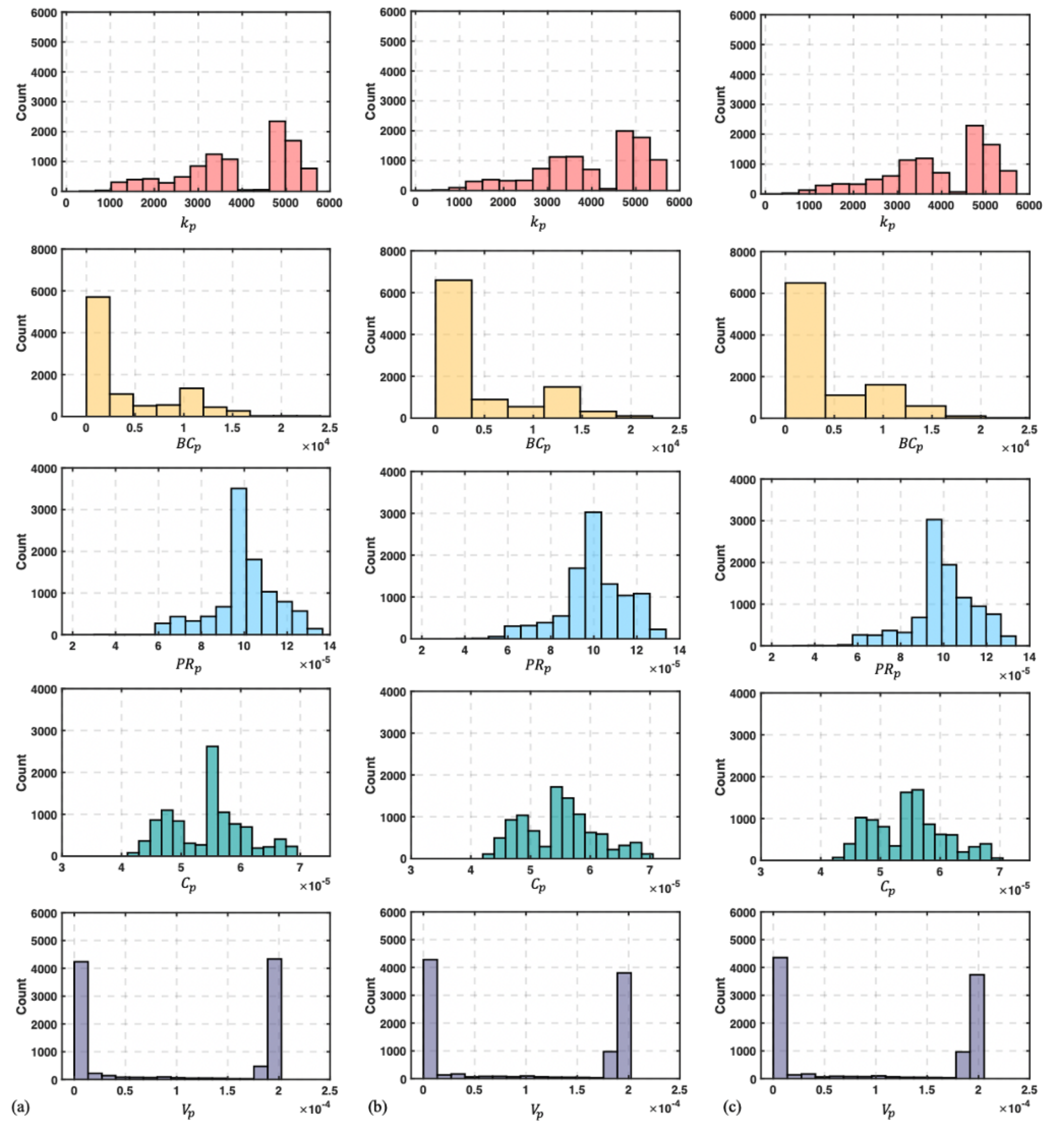

Figure 4.17. The distribution of k, BC, PR, C, and V in GRNs for 3 cases in Figure 4.16. (a) case VII, (b) case VIII, and (c) case IX.

(BC), and pagerank centrality (PR), respectively. Note that the distributions are approximately normal. As shown in Figure 4.18 (a), the Q1 of degree does not vary significantly between parts built under three orientations. However, they are vastly different for the betweenness centrality (Figure 4.18 (b)) and the pagerank centrality (Figure 4.18 (c)).

We perform two-way ANOVA on total of 45 features, and then calculate the Hotelling's T^2 statistic for each thin-wall based on the first seven components (i.e.,

Table 4.7. Two-Sample Mann-Whitney U Testing of Quantifier Distributions among Simulation Cases VII-IX.

	Case VII vs. Case VIII	Case VII vs. Case IX	Case VIII vs. Case IX
k	**0.035**	**4.739e-4**	**1.394e-8**
BC	0.474	**0.004**	0.083
PR	0.965	0.340	0.340
C	**1.804e-8**	**1.787e-4**	0.089
V	**1.234e-6**	**4.078e-47**	**1.998e-27**

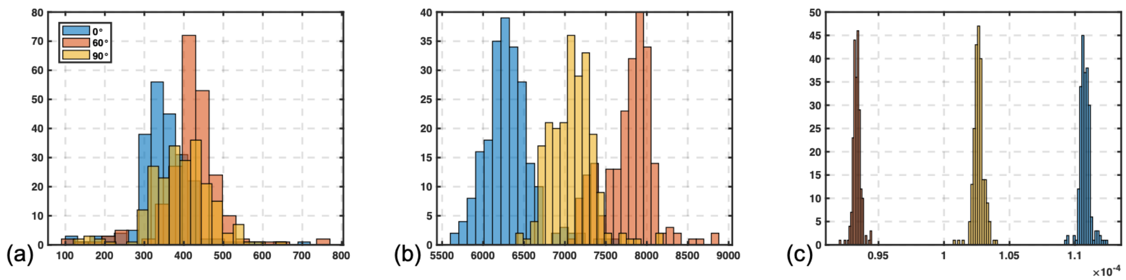

Figure 4.18. The distribution of (a) Q1 (k); (b) Q1 (BC); (c) Q1 (PR) of thin-wall 8 over all layers.

according to the Kaiser rule) to quantify the relationship between design complexity and the network features.

Table 4.8. Example of two-way ANOVA for assessing the significance of C and O on $max(k)$.

Source	Sum Sq.	d.f.	Mean Sq.	F	Prob > F
C	2.686e9	20	1.343e8	676.184	**0**
O	2.621e7	2	1.311e7	65.985	**3.112e-29**
$C * O$	3.010e7	40	7.525e5	3.788	**9.058e-15**
Error	2.491e9	12537	1.987e5		
Total	5.235e9	12599			

We conduct the square root transformation for the response variable to improve the variance stabilization and reduce the heteroscedasticity. Significant variables are summarized in Table 4.9. Orientation O, height H, width W, and hatching distance G are important one-way factors with p-values less than 0.05. It is worth mentioning that the p-value of β_4 is larger than the p-values of other coefficients, this indicates that the parameter height H does not impact the quality of thin-wall builds as much as others. We also observed that most of two-way interactions (e.g., orientation $\times$

width, orientation × hatching distance) are significant, thereby impacting the quality significantly. However, two-way interactions orientation 60° × height ($O_1 \times H$), width × height ($W \times H$), and height × hatching distance ($H \times G$) do not have impact on the quality because p-values of β_8, β_{12}, and β_{14} are greater than 0.05.

Table 4.9. Results of Regression Analysis.

Effect	Variable	Estimate	Error	t value	p-value
β_0	-	2.242	0.331	6.782	1.323e-11
β_1	O_1	2.449	0.294	8.302	1.307e-16
β_2	O_2	1.444	0.295	4.891	1.034e-6
β_3	W	34.885	5.419	6.438	1.327e-10
β_4	H	-0.962	0.310	-3.108	1.985e-3
β_5	G	-104.504	5.173	-20.201	2.699e-87
β_6	$O_1 \times W$	-45.105	5.158	-8.745	3.001e-18
β_7	$O_2 \times W$	-24.270	5.160	-4.704	2.621e-6
β_9	$O_2 \times H$	-0.318	0.039	-8.260	1.853e-16
β_{10}	$O_1 \times G$	50.139	5.241	9.567	1.683e-21
β_{11}	$O_2 \times G$	27.216	5.242	5.192	2.165e-7
β_{13}	$W \times G$	269.259	3.623	74.311	0

The regression model yields the R-squared statistic of 87.12% and the adjusted R-squared statistic of 87.08%, which demonstrates that the variations in response variable (i.e., the Hotelling's T^2 statistic) are highly correlated with the design parameters. Note that the R-squared statistic is defined as $R^2 = 1 - \frac{\text{Sum of Square}_{\text{residual}}}{\text{Sum of Square}_{\text{total}}} = 1 - \frac{\Sigma_i(T(i) - \hat{T(i)})}{\Sigma_i(T(i) - \overline{T})}$, where $T(i)$ is the Hotelling's T^2 statistic, $\hat{T}(i)$ is the predicted value, and $\overline{T}$ is the overall average. The normal Q-Q plot (Figure 4.19) illustrates that the normality assumption is valid because the plot approximately follows a straight line.

In our experiment, quality is inversely proportional to the amount of defects (e.g., lack of fusion, inconsistency, porosity, and edge variation). However, summary statistics tend to be limited in the ability to characterize and quantify complex defect patterns in layerwise images. Therefore, we propose the generalized recurrence network method to effectively represent the spatial imaging data, then leverage network visualization and quantifiers to capture various forms of defect patterns. Experimental results from hypothesis testing showed these network quantifiers are effective and sensitive to different defect patterns. These network quantifiers are then used to interpret and describe the level of quality for each layer of the build, which are further utilized to establish predicative models to investigate how design parameters

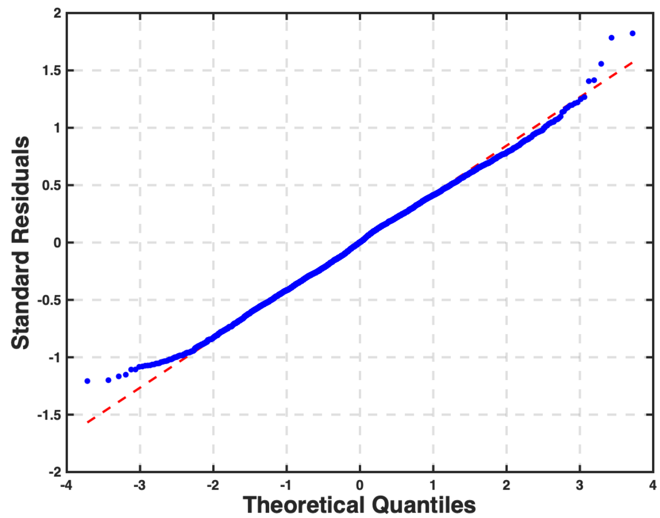

Figure 4.19. Normal Q-Q plot of the regression model.

(e.g., build orientation, thin-wall width, thin-wall height, and hatching distance) impact the quality characteristics in thin-wall builds. In addition, xperimental results show that four thin-walls (width ≤ 0.1 mm) collapsed regardless of what orientation is utilized in the fabrication process. Therefore, only thin-walls with the width greater than 0.1 mm can be printed by the PBF machine are utilized in this study. Thin-walls with the width greater than 0.1 mm printed under orientation 0° generate results with better quality. The result also shows that the quality decreases when the layer number goes up, which may cause by the defect propagation when printing the build layer by layer or by the different thermal conditions between the bottom and the top of each thin wall. We also found that the layer quality varies less in thin-wall builds with orientation 0° in comparison with orientation 60° and orientation 90°. Also, the thin-wall build with orientation 60° is more sensitive to the changes in hatching distance compare to the other two orientations. Therefore, the orientation 60° should be avoided while printing thin-wall structures. Although in our experiment, thin-walls 1-24 and the thin-wall 25 have built with two different hatching patterns, hatching distance within the thin-wall decreases from thin-wall 1 to thin-wall 25. Also, the collapse occurs in both types of hatching patterns. Hatching patterns of the thin-wall are not controllable factors in this study because of the automatic settings by the EOS M280 PBF machine.

4.5 Limitations and Future Works

In this chapter, we propose a generalized recurrence network methodology to visualize the complex spatial patterns in AM images. Similar to Chapter 3, we perform a design of experiment to investigate the relationship between design parameters and network quantifiers in thin-wall builds. While there is only one response variable in Chapter 2, we integrated multiple quantifiers into Hotelling's T^2 statistics in our analysis with the proposed generalized recurrence network. The limitation and the future works are discussed as follows:

- When embedding each AM image into a network, each pixel is treated as a node in the recurrence network. As such, each node contains the location information of the corresponding pixel. Therefore, we can locate the exact coordinate of the pixel in the image from the node in the network. Results in this work show that the embedded networks tend to have clusters. For example, the pores can be clustered by the network representation. Future works can investigate the relationship between the pixel location in an image and the node position in the network visualization.

- The generalized recurrence network analysis is developed based on the traditional homogeneous recurrence analysis. As shown in Equation 4.11, all weights $w_{p,q}$ are treated homogeneously by ε. However, heterogeneous recurrence patterns might exist in complex systems. Previously, we have investigated the heterogeneous recurrence behaviors in medical heart signals [124], where signals are often one-dimensional time series data. In AM, most of the data are high-dimensional image data. New methodologies need to be developed to take the heterogeneous recurrence patterns in AM images into account. Also, sparsity can be considered when embedding the images into a network to cope with the computational complexity.

- In this work, each pixel in the XCT scan is corresponding to 14.43 microns. Image resolution may have a significant impact on the accuracy of feature extraction and the performance of model prediction. For detailed discussion regarding the image resolution and feature extraction, please refer to Chapter 6.

4.6 Discussions and Conclusions

PBF-AM provides the design freedom that cannot be realized by traditional manufacturing techniques such as cutting, milling and casting. PBF-AM provides the design freedom that cannot be realized by traditional manufacturing techniques such as cutting, milling and casting. Engineers may come up with different designs. These designs may have different levels of complexity. A higher level of design complexity tends to degrade the quality of final PBF-AM builds and lower the repeatability of the process. Realizing high quality and repeatability call upon the development of sensor-based monitoring and control of PBF processes. Advanced imaging leads to a rich data environment for AM quality control. However, the structure of spatial data is often high-dimensional with complex geometric patterns. Therefore, there is an urgent need to extract quality characteristics from spatial imaging data and further explore the design-quality relationship for engineering designs.

Machine learning methods are commonly used in the AM community to process image profiles and build predictive models that require minimal feature engineering [128]. For example, contemporary machine algorithms can help to optimize process parameters, and conduct examination of powder spreading and in-process defect monitoring. Recently, there have been increasing interests in using deep learning models for prediction in AM. For example, Zhang et al. [129] investigated the relationship between the mechanisms underlying the layer-by-layer printing process and the resulting product quality through an LSTM network, Mozaffar et al. [130] proposed a recurrent neural network for predicting the high-dimensional thermal history in the AM process. Francis et al. [131] developed a novel Deep Learning approach that accurately predicts distortion within LBAM tolerance limits by considering the local heat transfer. Although deep learning yielded a high predictive power in many studies, they need large amounts of data to study patterns hidden in the AM signals. Also, drawbacks of these deep learning models include high computational cost and black-box approaches lacking physical interpretations.

In this paper, we propose a generalized recurrence network method to visualize the complex spatial patterns in additive manufacturing images, and introduce network quantifiers to characterize recurrence properties across layers. The proposed GRN method can not only extend to high-dimensional data, but also effectively capture the complex defect patterns in spatial imaging data. We leverage high-resolution post-build XCT scan data to analyze the relationship between design parameters and PBF-AM builds through a GRN framework. First, we generate layerwise images from 3D XCT data and register these images to the CAD model layer by layer. Then, the proposed GRN is utilized to extract the quality-related quantifiers from registered images. Next, we perform a design of experiment to investigate the relationship between design parameters and network quantifiers in thin-wall builds. Finally, a regression model is developed to predict the behavior of network features from the design parameters. Experimental results demonstrate that thin-wall build quality is sensitive to build orientation, thin-wall height, thin-wall width, and hatching distance. Thin-walls with the width bigger than 0.1 mm printed under orientation 0° are found to yield better quality compared to 60° and 90°, and the thin-wall build with orientation 60° is more sensitive to the changes in hatching distance compare to the other two orientations.

Network models are flexible and generally applicable to different data forms (e.g., time series [132, 133], two-dimensional image data [125, 134, 135], three-dimensional voxel data [136]). AM provides a higher level of flexibility for the low-volume and high-mix production, even for a one-of-a-kind design. AM fabricates the build directly from a complex CAD design through layer-upon-layer deposition of materials. Each image contains not only metal powders but also many AM parts in the build plate. As such, there is a need to delineate the image for a specific part. In this paper, we register the ROI to the part geometry in each layer, i.e., a rectangle region in each layer of the thin-wall build. However, ROI registration is generalizable to different part geometries, even complex designs with layerwise variations as long as the CAD design files are readily available, as shown in Figure 4. The presented study sheds insights into the optimization of engineering design for quality improvements of PBF-AM builds. Future works may focus on the optimization of design parameters, hatching patterns and process settings to improve the quality of thin walls.

Chapter 5 | Ontology-driven Learning of Bayesian Network for Causal Inference and Quality Assurance in Additive Manufacturing

Additive manufacturing (AM) enables the creation of complex geometries that are difficult to realize using conventional manufacturing techniques. Advanced sensing is increasingly being used to improve AM processes, and installing different sensors onto AM systems has yielded more data-rich environments. In the previous chapters, we considered the inter-relationships between design parameters and quality characteristics in the thin-wall part. For example, we have found that the edge roughness is highly correlated with the hatch spacing, width, and orientation at the confidence level of 95%. The correlation between variables, however, does not necessary indicate that the change in one variable is the cause of the change in the values in other variables. Instead of exploring the correlations between variables and responses, transforming data into useful information and knowledge (i.e., causality detection and process-structure-property (PSP) relationship identification) is important for achieving the necessary quality assurance and quality control (QA/QC) in AM. Causality modeling and PSP relationship establishment in AM are still in early stages of development.

In this chapter, we develop an ontology-based Bayesian network (BN) model to represent causal relationships between AM parameters (i.e., design parameters and process parameters) and QA/QC requirements (e.g., structure properties and mechanical properties). Specifically, a different set of parameters, namely edge roughness, thickness, vertical deviation, discontinuity, number of pores, and density was extracted from the thin-wall part analyzed in Chapter 2. By integrating the AM ontology, we perform a hybrid structure learning to reveal the causal relationships among AM parameters. Then, we perform predictive inference and diagnostic inference to navigate on the constructed BN. Experimental results demonstrate that the proposed ontology-based BN modeling methodology is capable of identifying the causal relationship between variables and can further facilitate AM process monitoring and control. The proposed model enables engineering interpretations and can further advance AM process monitoring and control.

5.1 Introduction

Advanced sensing is increasingly integrated into additive manufacturing (AM) to enhance process understanding and improve process control, thereby leading to data-rich environments. A four-level framework for AM data management and quality improvement is shown in Figure 5.1 [137]. Sensors capture data related to AM processes and an integrated database stores heterogeneous data from multiple sensors. Predictive models and knowledge are extracted from the collected data to further support the process monitoring and quality control. Realizing the full potential of sensing data will lead to an unprecedented opportunity to understand the AM process and offer a new sensor-based solution for quality assurance and quality control (QA/QC). Current practices for QA/QC focus on correlation analysis, which utilizes features (i.e., design parameters, process parameters) to predict the quality of AM builds [94, 114]. A comprehensive review related to QA/QC management of AM is discussed in [138]. However, correlation does not imply causation. New challenges lie in integrating all the information into actionable AM knowledge that captures explicit causal relations, for example, how to select the right parameters to fabricate AM parts that meet QA/QC requirements.

A Bayesian network (BN) contains a graphical structure that represents causal relationships among a large number of variables and allows for probabilistic causal inferences using the observed variables. It moves one step forward to support the inference of causality from observational data and improve interpretability at the same time. Bayesian inferencing is widely used in early expert system development. The conditional probabilities are used to represent complex relationships by the BNs [53]. BNs are widely used to create “expert systems" that capture and model expert knowledge about a complicated domain [139]. However, causal relationships between variables are usually complicated in the AM domain, which can be nonlinear and non-stationary. Despite numerous computational models are developed to represent AM sub-processes. Identifying causal interconnections between variables becomes a challenging task. While there have been some notable contributions to the BN structure from automatically-generated observational data [55, 139, 140], little has been done to integrate BN learning with AM domain knowledge.

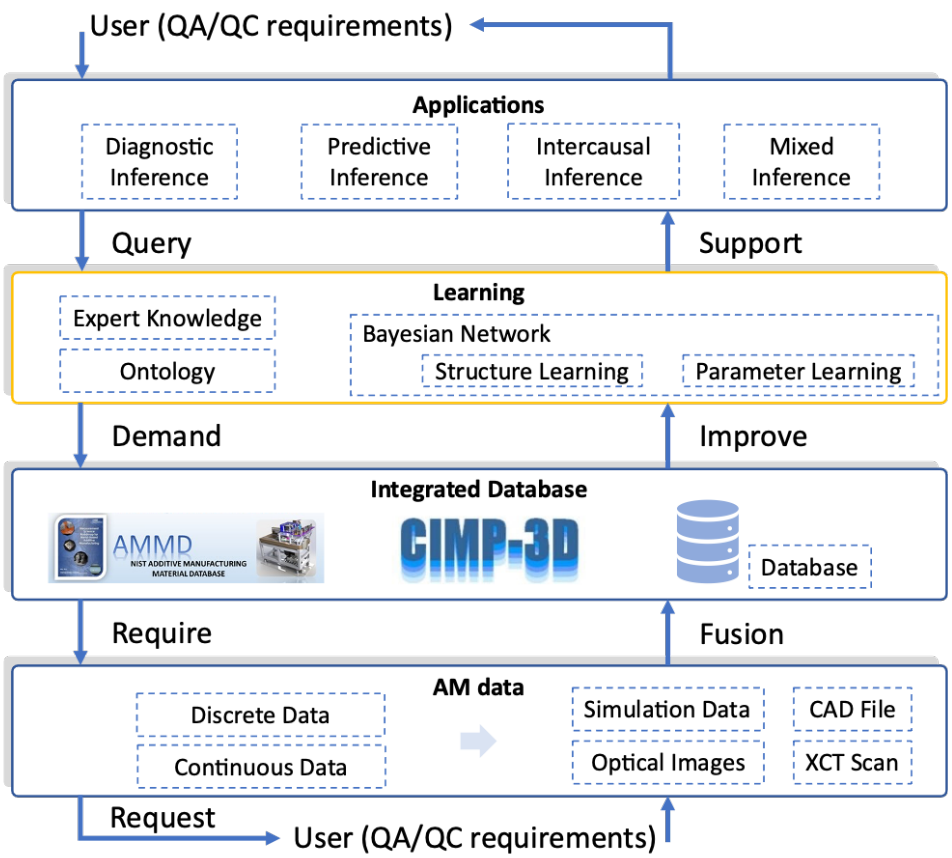

Figure 5.1. A four-level framework for AM data management and QA/QC.

In this paper, we develop an ontology-based Bayesian network (BN) modeling framework for extracting causal relationships among AM parameters, as a key function for the Learning layer in Figure 5.1. BN modeling contains two steps: namely structure learning and parameter learning. The structure of BN represents the qualitative relationships between variables, and parameter values help quantify the interconnections from probability distributions. In this research, we leverage an AM ontology to provide necessary and prior domain knowledge for modeling the causal connections in BN learning. Specifically, we integrate the domain knowledge from our specialized process-based AM ontology with parameter-based data processing and structure learning to create a causal network. Early experimental results demonstrate that our ontology-based BN modeling methodology is capable of demonstrating important causal relationships on which process control can be predicated.

The rest of the chapter is organized as follows: Section 5.2 reviews related literature on BN and ontology. Section 5.3 presents the experimental setup, quantifier extraction, and the proposed ontology-based BN modeling methodology. Experimental results are provided in Section 5.4. Section 5.6 summarizes this study.

5.2 Research Background

5.2.1 Bayesian Network

Bayesian networks, also called Bayesian belief networks or causal probabilistic networks, emerged from artificial intelligence and has been applied to a wide range of problems, ranging from text analysis [141] to medical diagnosis [142]. A Bayesian network is a directed acyclic graph (DAG) $\mathcal{G}$, in which nodes $\mathbf{V} = \{X_1, X_2..., X_n\}$ denote the set of random variables of interests and edges $\mathbf{E}$ represent the independence relationships among the n variables in $\mathbf{V}$. Note that acyclic means that there are no loops or cycles in the system.

In an acyclic graph, the first nodes with no incoming arcs are called the root nodes, and the last nodes without outgoing arcs are named as leaf nodes. In addition, the acyclic nature of the graph defines the topological ordering between nodes based on the direction of arcs. It is defined as follows: if a node X_i precedes X_j, there can be no arc from X_j to X_i. In Figure 5.2, X_2 precedes X_1. No arcs can be from X_1 to X_2 according to the ordering property. If there is a path from X_i to X_j, X_i precedes X_j in the sequence of the ordered nodes, then X_i is defined as an ancestor of X_j, and X_j is defined as the descendant of X_i. In addition, we can define neighbourhood and spouses from the direction of arcs or sequence of ordered nodes. For instance, the

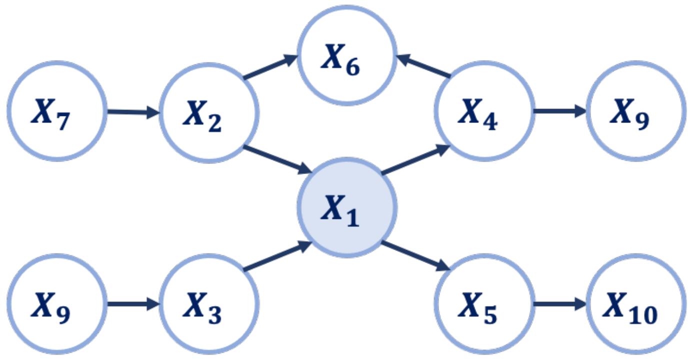

Figure 5.2. An example of parents, children, ancestors, descendants, spouse, and neighborhood of node X_1 in a directed graph.

neighbourhood is defined as the union of its parents (i.e., X_2 and X_3) and its children (i.e., X_4 and X_5) for node X_1. X_6, X_7, X_2 and X_3 are ancestors of node X_1, and X_2, X_4, X_8 and X_9 are descendants of node X_1 Note that parents are ancestors, however, ancestor might not be the parent. In addition, X_5 is the spouse of X_1.

The relationships between nodes in BN can be interpreted as causal relationship because that BNs are based on DAGs. However, it is important to differentiate the probabilistic and causal interpretations in BNs. Three assumptions need to be made before interpreting an edge in a BN as the causal effect.

- Given its direct causes, each variable X_i is conditionally independent of its non-effects both directly and indirectly.
- There must exist a DAG which is faithful to the probability distribution P of $\mathbf{X}$, so that the only dependencies in P are those arising from d-separation in the DAG.
- There must be no latent variables (unobserved variables influencing the variables in the network) acting as confounding factors. Such variables may induce spurious correlations between the observed variables, thus introducing bias in the causal network.

As shown in Figure 5.3, a BN must satisfy the Markov condition where every variable $X_i \in \mathbf{V}$ is independent of any subset of its non-descendant variables conditioned on the set of its parents π_i. Note that the directed edge from Pa_i to X_i indicates a direct causal influence that π_i has on X_i.

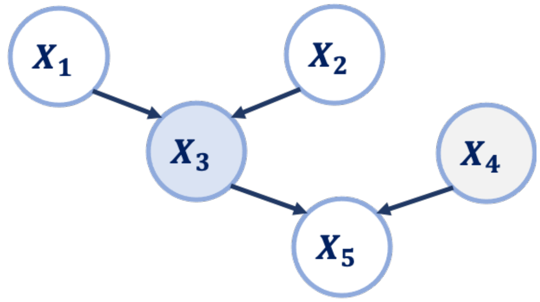

Figure 5.3. An example of the Markov condition: given the parents X_1 and X_2, X_3 is conditionally independent of its non-descendant X_4.

In addition to a DAG, BNs are defined by the global probability distribution of $\mathbf{X}$ with the set of parameter $\mathbf{\Theta}$,

$$P(\mathbf{X}, \mathbf{\Theta}) = \prod_{i=1}^{N} P(X_i | \Pi_{X_i}, \Theta_{X_i}) \tag{5.1}$$

where the global distribution of X (with parameters Θ) decomposes in one local distribution for each X_i (with parameters Θ_{X_i}) conditional on its parents π_{X_i}.

5.2.2 Bayesian Network in Additive Manufacturing

BN gives a structural means to learn and represent causality which helps in capturing causal relationships in a given domain. Ontology, on the other hand, helps to build the conceptual relationships between various entities in a domain of study. At the lowest level of abstraction, it helps to understand measurable (direct or indirect) variables in a system. In principle, both BN and ontology result in the information, navigation, and analysis of networks. However, little has been done to integrate ontology networks with automated Bayesian learning for AM QA/QC. Li and Shi [143] proposed a causal modeling approach to improve the existing causal discovery algorithm by integrating manufacturing domain knowledge (i.e., rolling processes) with the BN learning. Specifically, they combined domain knowledge with variable selection and variable discretization to reduce the search space. Mokhtarian et al. [144] constructed the structure of a BN based on physical relationships between variables. An analytical hierarchy process is utilized to collect preferences from experts. Wang et al. [145] proposed a knowledge management system using BN to model AM knowledge in the presence of uncertainty and fill the knowledge gap between designers and AM technologies. Similarly, the BN structure is generated solely from the domain knowledge. Hertlein et al. [146] proposed a BN model with four process parameters and five quality characteristics for AM, which is a conditional linear Gaussian BN where nodes can be both discrete and continuous. However, parametric assumptions for mixed data (i.e., continuous and discrete) tend to have practical limitations, as they impose constraints on arcs. For example, a continuous node cannot be the parent of a discrete node. Jing and Ma [147] proposed a fuzzy Bayesian Network to study the AM's adaptiveness. Bacha et al. [148] and Verma et al. [149] utilized the BN for fault diagnosis, but network structures are assumed to be known in the prior knowledge. In addition, Tran et al. [150, 151] investigated the inference of sparse networks from noisy and nonstationary processes, studied the latent connectivity in the sparse network, and further leverage the dynamic network for change detection. In the present paper, we instead focus on the integration of manufacturing ontology networks with BN learning and modeling for AM QA/QC.

While BNs are graphical structures for representing the probabilistic relationships among variables and doing probabilistic inference with those variables, ontology describes domain concepts and their semantic relationships that can represent causality. Our previous work developed ontology models to support AM process model development and reuse [62, 152]. The AM process ontology captures a network of variables that can be visualized in a graph, and allows users to navigate complex relationships and understand the connections between different process parameters, microstructural characteristics, and mechanical properties of AM parts. Ontology shows strong potential to support the construction of Bayesian networks [153]. However, most of the existing works focus on utilizing ontology to select variables, identify relationships, and assign conditional probability distributions. Little has been reported on how to integrate ontological representation with automated BN learning algorithms. At the same time, automated BN structure and parameter learning from data are often insufficient in practice due to the limited availability of data. In this study, we utilize AM ontology to extract the causal connections among variables.

5.3 Methodology

This paper presents an ontology-driven Bayesian network modeling for AM design-process-structure-property causal analysis on which future process control analytical methods can be developed. As shown in Figure 5.4, the modeling procedure has four steps. First, we obtain pre-processing computer-aided design (CAD) slices and post-processing X-ray computed tomography (XCT) data. Then, we register the data and extract important features from them. Next, by integrating AM ontology, we perform hybrid structure learning to study the causal relationships between the features. Note that the BN modeling is performed in an inherently Bayesian fashion. Finally, we perform predictive inference and diagnostic inference to navigate on the constructed BN.

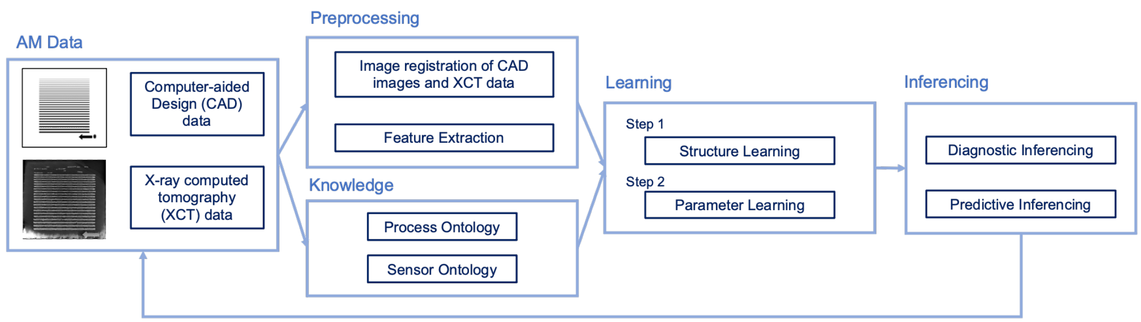

Figure 5.4. The flow chart of the proposed research methodology.

5.3.1 Offline Quantification of Build Quality using Layer-wise XCT scan images

In this experiment, thin-wall parts were built with the powder bed fusion (PBF) technology from Spherical ASTM B348 Grade 23 Ti-6Al-4V powder with a size distribution of 14-45 μm on an EOS M280 machine. PBF refers to a family of AM processes in which thermal energy selectively fuses regions of a powder bed [1]. During the PBF fabrication, a layer of metal powder is first spread across a build plate, then a certain area is selectively melted (fused) with an energy source, such as an electron beam. This procedure continues until the top layer of the build is fused.

As shown in Figure 5.5, thin-wall builds are fabricated in three orientations (i.e., 0°, 60°, and 90°) with respect to the travel direction of the recoater blade (i.e., indicated by the arrow on each part). Standard EOS M280 processing parameters for 60-μm layers were used in the experiments. Each build consists of 25 thin-walls with a height/width ratio of 10. The width of thin-walls increases from 0.06 mm, with a step size of 0.01 mm, to 0.3 mm. Information related to contour space is summarized

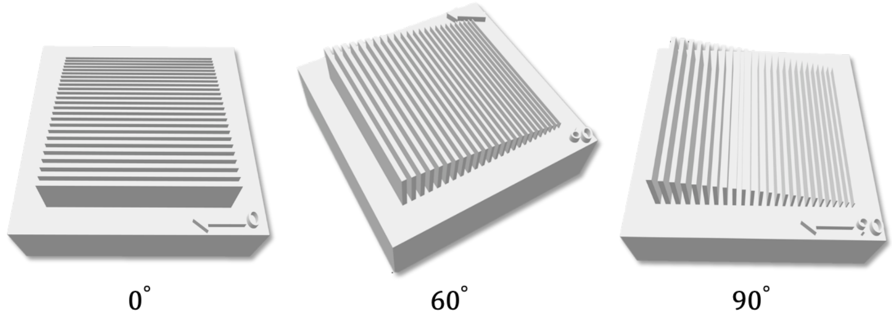

Figure 5.5. Thin-wall parts fabricated with three orientations with respect to the travel direction of recoater blade (i.e., indicated by the arrow on each part).

in Table 5.1. Note that contour space is defined as the width between inner contours in each thin-wall, and there is a 67-degree rotation for the hatching paths on each layer by the default setting of the EOS 280 machine.

Table 5.1. The variations in contour spaces within contour from thin-wall 1 to thin-wall 25.

Thin-wall Number	W_h mm	Thin-wall Number	W_h mm	Thin-wall Number	W_h mm	Thin-wall Number	W_h mm	Thin-wall Number	W_h mm
1	0.244	6	0.190	11	0.142	16	0.092	21	0.045
2	0.234	7	0.183	12	0.136	17	0.082	22	0.033
3	0.220	8	0.167	13	0.125	18	0.076	23	0.022
4	0.208	9	0.159	14	0.114	19	0.059	24	0.011
5	0.198	10	0.154	15	0.102	20	0.049	25	N/A

Post build XCT data are obtained on a General Electric V|tome|X system with a voxel size of 14 μm^3. XCT slices are obtained through the volume graphics viewer myVGL. Several defects can be seen from XCT slices after image registration. For the detailed information related to registration, please refer to our previous work in [154] as well as Chapter 2. As shown in Figure 5.6 (a), we can detect discontinuity, edge variation, and porosity from the top view. In addition, we can observe vertical deviation as well as separation on the top of each thin-wall. Note that larger defects run down the center of thin-walls according to Figure 5.6 (b). The following features are extracted from the XCT scan to quantify the quality of fabricated parts.

- **Edge roughness:** this feature measures how much the printed edge deviates from the CAD design. For example, the edge roughness of the upper edge in

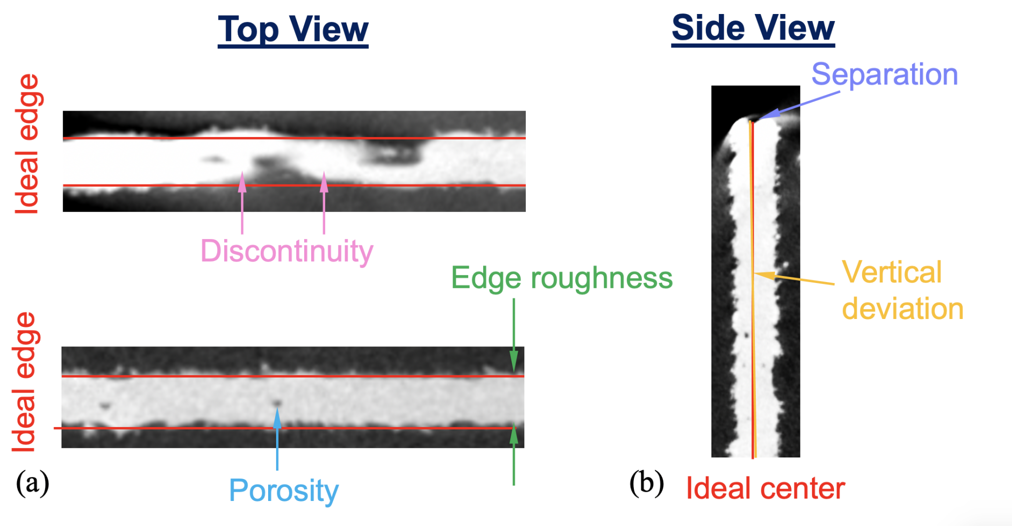

Figure 5.6. (a) Top view of the XCT slice in the thin-wall 5 at layer 70 of 0° build, with quality issues such as edge roughness, discontinuity, and porosity; (b) side view of the XCT slice in the thin-wall 5 at layer 70 of 0° build, with quality issues such as separation and vertical deviation.

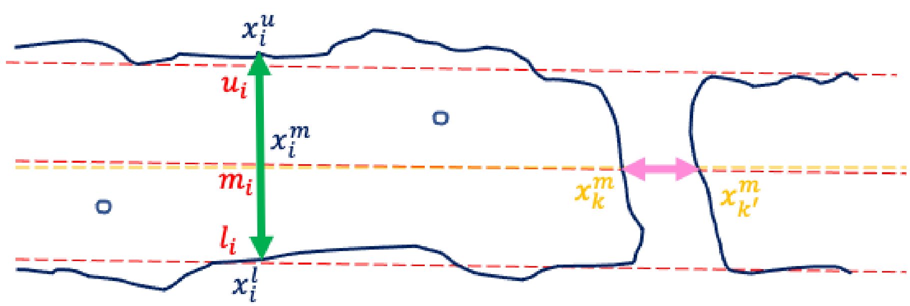

Figure 5.7. Feature extraction from thin-walls from XCT slices.

Figure. 5.7 is calculated as:

$$\sigma_e = \sqrt{\frac{\sum_{i=1}^{N}(x_i^u - u_i)^2}{N}} \tag{5.2}$$

where x_i^u is the i^{th} pixel in the upper printed edge, u_i is the i^{th} pixel in the upper CAD edge, and N is the total length of the thin-wall.

- **Thickness:** the thickness $\bar{t}$ of each thin-wall is calculated as:

$$\bar{t} = \frac{\Sigma_{i=1}^{N}||x_i^u - x_i^l||}{N} \tag{5.3}$$

where x_i^l is the i^{th} pixel in the lower printed edge.

- **Vertical deviation:** this feature quantifies how far the center of each thin-wall deviates from the designed center.

$$\bar{v} = \frac{\Sigma_{i=1}^{N}(x_i^m - m_i)}{N} \tag{5.4}$$

where m_i is the middle point of x_i^u and x_i^l.

- **Discontinuity:** discontinuity is calculated as the length between two pixels on the centerline of the border.

$$d = ||x_k^m - x_k^{m\prime}|| \tag{5.5}$$

where x_k^m and $x_k^{m'}$ are the k^{th} and $k^{'th}$ pixel in m_i, respectively.

- **Number of pores:** this feature counts the number of pores in each layer of the thin-wall. The number of 8-connected binarized XCT pixels over a layer translates to the pore count [12].

- **Density:** this feature is represented by

$$\rho = \frac{\Sigma_{i=1}^{N}\Sigma_{j=1}^{M} I(i,j)}{NM} \tag{5.6}$$

where $I(i,j)$ is the intensity value of the binarized XCT pixel.

5.3.2 Learning a Bayesian Network from Data

As shown in Figure 5.4, BN modeling can be performed with two steps in an inherently Bayesian fashion:

$$\underbrace{P(\mathcal{G},\Theta|\mathcal{D})}_{learning} = \underbrace{P(\mathcal{G}|\mathcal{D})}_{structurelearning} \cdot \underbrace{P(\Theta|\mathcal{G},\mathcal{D})}_{parameterlearning} \tag{5.7}$$

where $\mathcal{G}$ denotes the structure of the DAG, and Θ represents parameters of the BN given the $\mathcal{G}$ obtained from structure learning. $\mathcal{D}$ is the observational data.

Discrete, Gaussian, and conditional linear Gaussian are three most common probability distributions of data for BNs. In real world settings, even if the marginal distributions are normal, not all dependence relationships are linear. Computing partial correlations brings singularities both for large datasets as well as small datasets. In addition, parametric assumptions for mixed data have strong limitations, as they impose constraints on which arcs may be present in the graph. For example, a continuous node cannot be the parent of a discrete node. Therefore, discretization is a common data prepossessing technique for BN learning. Also, after discretization, dependencies are no longer required to be linear.

Further, Using Bayes theorem once more, we can formulate it as:

$$P(\mathcal{G}|\mathcal{D}) \propto P(\mathcal{G})P(\mathcal{D}|\mathcal{G}) \tag{5.8}$$

and following Equation 5.7 we can decompose the marginal likelihood $P(\mathcal{D}|\mathcal{G}$ into one component for each local distribution

$$P(\mathcal{D}|\mathcal{G}) = \int P(\mathcal{D}|\mathcal{G},\Theta)P(\Theta|\mathcal{G})d\Theta = \prod_{i=1}^{N} P(X_i|\Pi_{X_i},\Theta_{X_i})P(\Theta_{X_i}|\Pi_{X_i})d\Theta_{X_i} \tag{5.9}$$

Closed-form expressions for Equation 5.9 are available for both discrete BNs and Gaussian BNs. In addition, in Discrete BN, $P(\mathcal{D}|\mathcal{G})$ is called Bayesian Dirichlet (BD) score [155], and it is constructed using a conjugate Dirichlet prior with imaginary sample size α. Note that α is defined as the the size of an imaginary sample supporting the prior distribution, giving the weight given to the prior compared to the data [156].

$$BD(\mathcal{G},\mathcal{D};\alpha) = \prod_{i=1}^{N} BD(X_i|\Pi_{X_i};\alpha_i) = \prod_{i=1}^{N}\prod_{j=1}^{q_i}\left[\frac{\Gamma(\alpha_{ij})}{\Gamma(\alpha_{ij}+n_{ij})}\prod_{k=1}^{r_i}\frac{\Gamma(\alpha_{ijk}+n_{ijk}}{\alpha_{ijk}}\right] \tag{5.10}$$

5.3.2.1 Structure Learning

Three types of algorithms are commonly utilized to learn the structure of BNs from the observational data: namely constraint-based algorithms, score-based algorithms, and hybrid algorithms. While constraint-based algorithms (e.g., PC [55]) are based on causal graphical models by Verma and Pearl [149], score-based algorithms (e.g., Greedy Equivalent Search [157]) are general-purpose optimisation techniques for structure learning. Specifically, constraint-based methods leverage conditional independence tests to construct the oriented graph, and score-based algorithms maximize the goodness-of-fit scores of the DAG structure. Hybrid algorithms (e.g., Max-Min Hill-

Climbing [140]) first construct the skeleton of a DAG, and then utilize score-based functions to determine the orientation of edges, which combine the advantages from two approaches. In this paper, we integrate the hybrid learning algorithm (i.e., H2PC [61]) with the ontology graph to identify the causal relations between variables in AM. Specifically, the domain knowledge of AM ontology is incorporated into the following steps: (1) discretization of continuous data, and (2) adding constraints between variables from the ontology graph.

Algorithm 2 The Proposed Ontology-based Structure Learning for Bayesian Network

Input: a variable set $\mathbf{V}$, an empty DAG $\mathcal{G}$

1: discretize each continuous variable $X_i \in \mathbf{V}$
2: $\mathcal{G}_o \leftarrow$ ontology graph
3: $\mathbf{PC} \leftarrow HPC(\mathbf{V}, \mathcal{G}_o)$ // identify the parents and children set of each variable through HPC algorithm
4: **For** each pair of $(X_i, X_j) \in \mathbf{PC}$:
5: $\quad \mathcal{G} \leftarrow HC(\mathbf{PC}, \mathcal{G}, \mathcal{G}_o)$ // begins with an empty graph, add, delete, remove edge that leads to the largest increase in score from greedy hill-climbing search

Output: DAG $\mathcal{G}$

The H2PC algorithm learns the BN in two steps. First, it constructs the structure or the skeleton of BN through the constraint-based algorithm. Then, it performs a Bayesian scoring greedy search to add, delete, and change the direction of the edges. In the proposed Algorithm 1, we integrate the ontology information (i.e., $\mathcal{G}_0$) into several steps of HPC and H2PC algorithms. In the first step, the HPC algorithm combines the advantages of incremental and divide-and-conquer methods, targets for the parent-children discovery and contains three sub-algorithms, namely Data-Efficient Parents and Children Superset (DE-PCS), Data-Efficient Spouses Superset (DE-SPS), and Incremental Association Parents and Children with false discovery rate control (FDR-IAPC), respectively. Specifically, DE-PCS and DE-SPS search for supersets of parent, children, and spouses of nodes. In the second step, the H2PC performs a greedy hill-climbing search in the space of BN. The search starts with an empty graph and further adds, deletes, or reverses the edge direction that increase the score. Note that the search only adds the edges that are obtained in the previous step, which is the key difference between the greedy hill-climbing search in the H2PC algorithm and the direct utilization of greedy search to learn a BN structure. As shown in Algorithm 2, we first search the parent-children sets **PC** for every node

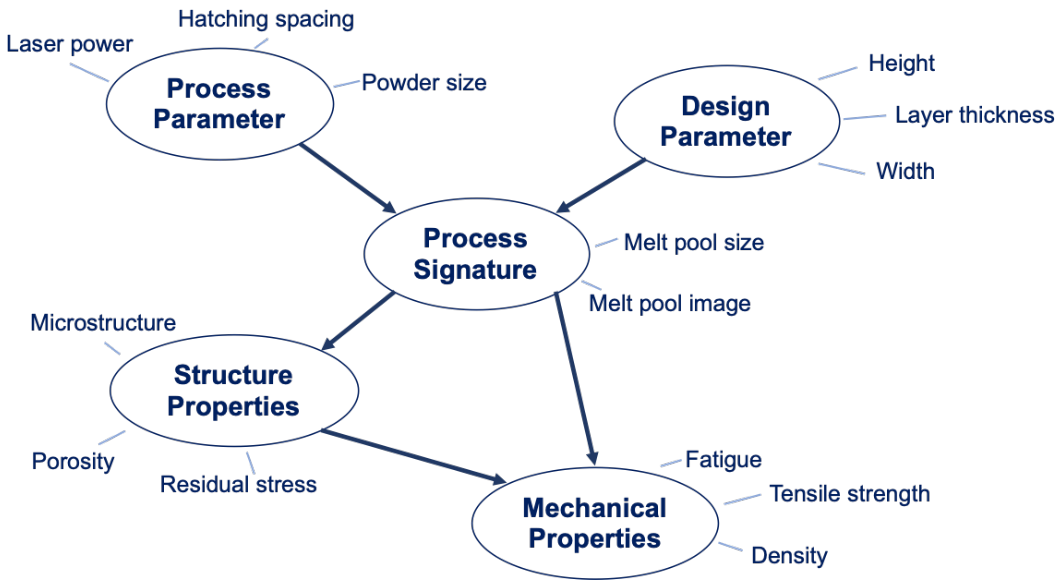

Figure 5.8. The visualization of an AM ontology graph.

in the network through HPC. Then, for all pairs of $(X_i, X_j) \in \mathbf{V}$, add X_i in $\mathbf{PC}_{X_j}$ and add X_j in $\mathbf{PC}_{X_i}$ if $X_i \in HPC(X_j)$ and $X_j \in HPC(X_i)$. Next, starting from an empty graph, we only perform the operator add edge $X_i \rightarrow X_j$ if $X_j \in \mathbf{PC}_{X_i}$.

5.4 Experimental Results

In this section, we evaluate and validate the proposed ontology-based BN modeling methodology with real-world data and then benchmark the performance of obtained BN models with and without AM ontology. As shown in Figure 5.8, data obtained from AM processes can be classified into five categories, namely process parameter, design parameter, process signature, structured properties, and mechanical properties. In the ontology graph, process and parameter can cause variations in structural properties and mechanical properties, process parameter can also lead to changes in process signature. However, BN obtained structural properties and mechanical properties cannot cause either process parameters or process signature. Note that there are important temporal relationships between variables. For example, the shapes of melt pools can be different due to variations in the recoating orientation. Low laser power can cause porosity in the part, and further impact the mechanical properties (e.g., tensile strength) of the final product. Causal connections show that process related parameters influence the mechanical and structural properties.

As mentioned in Section 5.3.1, we extract a total of 12 variables from different parameter groups (see Table 5.2). We discretize features based on domain knowledge as described below. Note that each level of the feature should contain a similar number of observations to avoid bias.

Table 5.2. Process Variables and Quality Variables

Variable	Code	Node	Type
Input variable	1	Contour Space	Process Parameter
	2	Scan Path	Process Parameter
	3	Orientation	Design Parameter
	4	Width	Design Parameter
	5	Height	Design Parameter
QA/QC output	6	Edge Roughness	Structure Proprieties
	7	Thickness	Structure Proprieties
	8	Vertical deviation	Structure Proprieties
	9	Discontinuity	Structure Proprieties
	10	Number of Pores	Structure Proprieties
	11	Fin Separation	Structure Proprieties
	12	Density	Mechanical Proprieties

- **Contour space:** is the measured width between the hatches of the inner rectangle for each thin-wall. We discretize the contour space into three groups based on the melt pool diameter (i.e. 110 μm) and laser diameter (i.e. 80 μm).

- **Scan path:** there is a 67-degree rotation for the hatching paths on each layer by the default setting of the EOS 280 machine. Therefore, the scan path is batched into three groups.

- **Orientation:** orientation has three levels because three parts are built under three directions (i.e., 0°, 60°, 90°).

- **Width:** width is divided into four balanced groups.

- **Height:** height is grouped into four levels according to the height/width ratio of each layer. For example, if the height/width ratio of a layer is 10, and the width of the thin-wall is 0.3 mm, then the height is 3.0 mm.

- **Edge roughness:** edge roughness has three levels according to warning limits of the distribution.
- **Thickness:** thickness is partitioned into three groups, i.e., within 10% tolerance, above 10% tolerance, and below 10% tolerance.
- **Vertical deviation:** binary variable which indicates the direction of deviation, i.e., deviates towards left or right.
- **Discontinuity:** discontinuity is divided into three groups where each group consists of a similar number of data.
- **Number of pores:** this feature counts the number of pore with a diameter greater than 100 μm [158].
- **Separation:** binary variable where $X_{11} = L1$ stands for there is a separation of the top of the fin, and $X_{11} = L2$ denotes there is no separation.
- **Density:** in our experiment, we set $X_{12} = L1$ when the density of the thin-wall is greater than or equal to 95%, and $X_{12} = L2$ when is less than 95% [159].

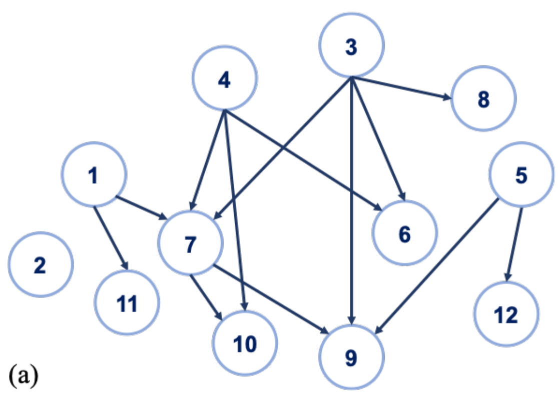

Figure 5.9. (a) The constructed BN with knowledge from AM ontology; (b) the constructed BN without knowledge from AM ontology. Dashed arrows in pink shows edges that are not learned, solid yellow arrows indicate the edges that are not supposed to be learned, solid green arrows denote edges learned in the wrong direction.

Figure. 5.9 compares two BN structures learned with and without AM ontology. Note that the dashed arrows in pink show edges that are not learned, solid yellow arrows indicate the edges that are not supposed to be learned, solid green arrows denote edges learned in the wrong direction. In Figure. 5.9 (b), the contour space is linked to width, showing that there is a causal relationship between the two nodes. However, design parameters cannot be causal factors of process parameters according to the ontology knowledge, and vice versa. In addition, the structure indicates that thickness is the causal factor of width, structure properties if not the causal factor of design parameters based on the temporal relationships between nodes in the ontology graph. In addition, some of the edges (i.e., two arcs in pink) cannot be learned without domain knowledge.

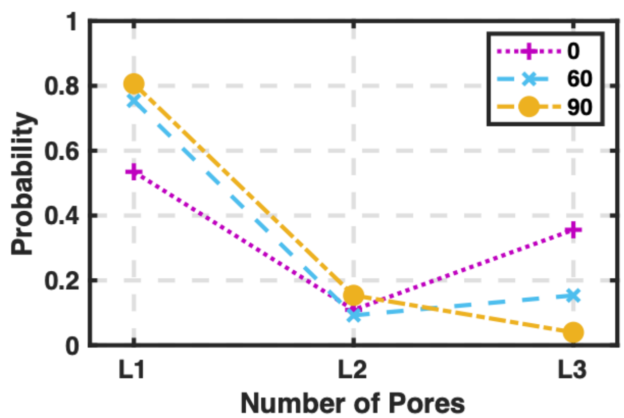

Figure 5.10. The conditional distribution plot of number of pores at different levels given orientation at different levels.

Once the BN is learnt, the causal relationships among variables can be identified qualitatively through the learned structure, and quantitatively through predictive inference and diagnostic inference. Figure 5.10 shows the conditional distribution plot of number of pores at different levels given orientation at different levels (i.e., $P(\text{number of pores}|\text{orientation})$). Orientation orientation (node 1) has three levels and number of pores (node 10) has three levels in our experiment. For example, when we target at number of pores at level 1, the orientation of 90° is more likely to generate the desirable result in comparison with the orientation of 60° and 30°.

As shown in Figure. 5.9 (a), $P(\sigma_e|\text{orientation, width})$ can be obtained by conditional distribution plots in Figure 5.11. Note that orientation (node 1) has three levels, width (node 4) has four levels, and the edge roughness (i.e., σ_e) has three levels. Based on the results of predictive inference, it is more likely to have a higher probability of severe edge roughness (i.e., $\sigma_e = L3$ when thin-walls have a width of $L2$ (i.e., $(0.16\text{mm}, 0.21\text{mm}]$) and orientation $L1$ (i.e., 0°).

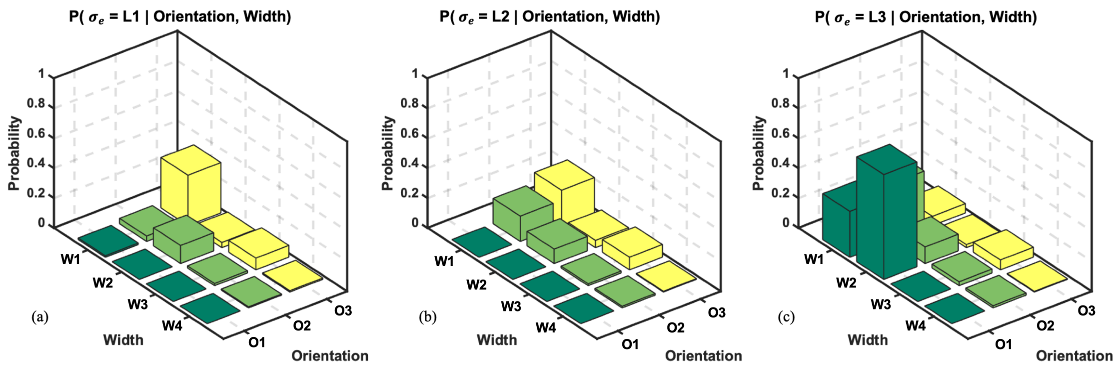

Figure 5.11. (a) Conditional distribution plots of $\sigma_e = L1$ given orientation and width at different levels, (b) conditional distribution plots of $\sigma_e = L2$ given orientation and width at different levels, and (c) conditional distribution plots of $\sigma_e = L3$ given orientation and width at different levels.

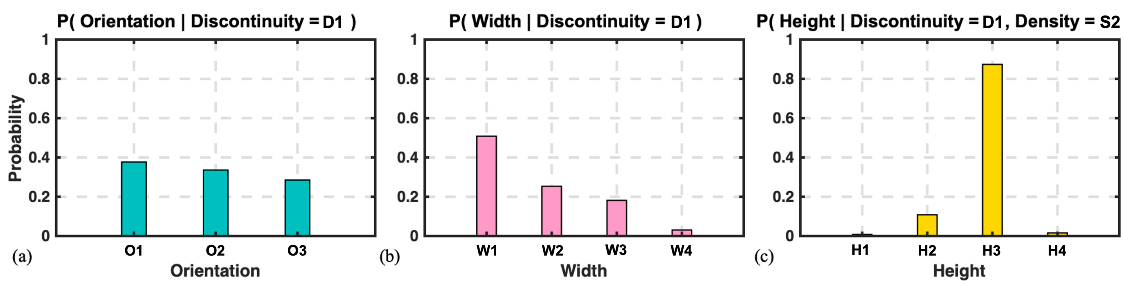

Figure 5.12. (a) Conditional distribution plots of orientation at different levels given discontinuity $= D1$, (b) conditional distribution plots of width at different levels given discontinuity $= D1$, and (c) conditional distribution plots of height at different levels given discontinuity $= D1$ and density $= S2$.

The example of diagnostic inference is shown in Figure 5.12. Figure. 5.9 (a) shows that contour space, width, orientation, and height are causal factors of the discontinuity. Therefore, we can determine which state of these causal factors has the least probability to cause the discontinuity issue in the thin-wall builds. For example, when discontinuity is $D1$ (i.e., no discontinuity), we should build the part under orientation $O1$ with width in the range of $W2$ according to Figure 5.12 (a) and (b), respectively. In addition, height is the causal factor of both density and discontinuity, so we can perform the diagnostic inference for $P(\text{height}|\text{discontinuity, density})$. In Figure 5.12 (c), when the height of the thin-wall is at $H3$ (i.e., height/width ratio is in (5, 7.5]), the part has better quality because the discontinuity is at $D1$ (i.e., no discontinuity) and density is at $S2$ (i.e., density is greater than 95%).

Finally, we perform the prediction through the learned BN model.Note that we

Output	Edge Roughness	Thickness	Vertical Deviation	Discontinuity
Accuracy	78.70% ± 0.012	87.77% ± 0.011	58.01% ± 0.008	96.79% ± 0.005
Output	Number of Pores	Fin Separation	Density	
Accuracy	59.80% ±0.013	76.93% ±0.021	1.00% ±0.000	

Table 5.3. Prediction results for QA/QC output from the learned BN.

separate 80% of our data for training and 20% for testing in our analysis. For the construction of BN, we performed the model averaging for the structure learning. Note that structures were slightly different among each of the 50 runs. Therefore, we kept arcs that are learned for more than 80% of the time. As shown in Table 5.3, the prediction accuracy varies from 47.71% to 100%. In this study, we discretize our continuous data into different levels based on either physical information or statistical property. Although the less group we discretize, the more accuracy we will reach by the proposed model. The goal to construct a ontology-based BN is to integrate the knowledge and discover the causal relationships between variables in a specific domain. This is the reason why that the accuracy varies significantly in different variables.

5.5 Limitations and Future Directions

In this chapter, we propose a hybrid structure learning to reveal the causal relationships among AM parameters. Specifically, we integrated the knowledge graph into the automated learning of the BN structure. Experimental results show that the proposed ontology-driven BN modeling methodology is capable of identifying the causal relationships between the AM parameters and extracted features.

The proposed ontology-driven model has the following limitations:

- The limitation in the dataset: the experimental design is based on the thin-wall part analyzed throughout the whole dissertation. For the generalization of the proposed methodology, more parts need to be normalized and analyzed to generate a bigger BN network. Also, the thin-wall part is fabricated with Ti-

6Al-4V by BPF technology. Future works can consider extra nodes representing material and fabrication technology. Different materials and processes can be set as levels of the node. In addition, sparse learning needs to be considered when dealing with BN in large size.

- The validation of the proposed model: In our experiment, we split our data into a training dataset (i.e., contains 80% data) for model development and a testing dataset (i.e., contains 20% data) for model validation. Future works can validate the proposed model with real-world experiments. Regarding the high costs in metal AM experiments, synthetic data can also contribute to the BN construction and validation.

5.6 Conclusions

With the rapid development of sensing capabilities, a variety of sensors are being installed on different AM systems to collect data, increase performing visibility, as well as to improve the QA/QC of AM builds. The challenge now lies in integrating all the data and information into useful AM knowledge, and making this process more repeatable and reliable.

In this paper, we propose an ontology-based BN model for the representation of causal relationships between AM parameters (i.e., design parameters and process parameters) and QA/QC requirements (e.g., structure properties and mechanical properties). We leverage the real-world data from thin-walls to demonstrate the prediction inference and diagnostic inference from the constructed BN model. The proposed methodology facilitates both forward prediction and backward diagnosis. We illustrated two quantitative results for predicting the quality as well as root cause diagnosis with two examples, respectively. In addition, we compared experimental results between BN learning methods with and without AM ontology. The proposed methodology enables engineering interpretations of causality interrelations in AM and can further facilitate AM process monitoring and control. Although BN learned is aimed at the PBF AM process in this work, the proposed ontology-based BN modeling methodology can be further extended and generalized to other AM processes. However, because there are variations in process parameters and materials in different AM processes, it is necessary to incorporate newly added domain knowledge (i.e., ontology networks) and introduce more nodes (e.g., material, design variables, process parameters, sensors) in the model generalization. The proposed algorithm may also need slight modifications for different data types, but the structure and parameter learning process is generally applicable. Future work will continue to investigate the dynamics between empirical observations and their physical counterparts, with the goal of a methodology that does not "ground" one with the other but instead supports reciprocated learning in the identification of key variables and causal relationships.

Chapter 6
Conclusions and Future Works

Recent development in sensing technology provides unprecedented opportunities to synchronize physical world to the cyberspace. Cyber-physical systems are systems of collaborating computational entities which are in intensive connection with the surrounding physical world and its on-going processes, providing and using, at the same time, data-accessing and data-processing services available on the Internet [15]. In additive manufacturing (AM) cyber-physical systems, the physical world (i.e., AM machines) is reflected in cyberspace through data-driven information processing, modeling, and simulation. AM is a set of fabrication processes that produce parts layer-by-layer from 3D computer-aided design (CAD) models. AM enables the creation of complex, freeform geometries that are difficult, if not impossible, to realize using conventional subtractive and formative manufacturing processes. The novel AM technology not only enables the creation of builds with complex features, innovative shapes, and lightweight structures, but also enables opportunities for individuals in acquiring, providing, and sharing access to goods and services. AM can provide manufacturers a competitive advantage by offering the flexibility of on-demand manufacturing and mass customization. However, the decentralization among manufacturers introduces new challenges in the service optimization of on-demand services and AM supply chain. Also, the ability to produce complex shapes in low volumes, combined with rapid advancements in AM technology, is challenging our current paradigms for process quality management.

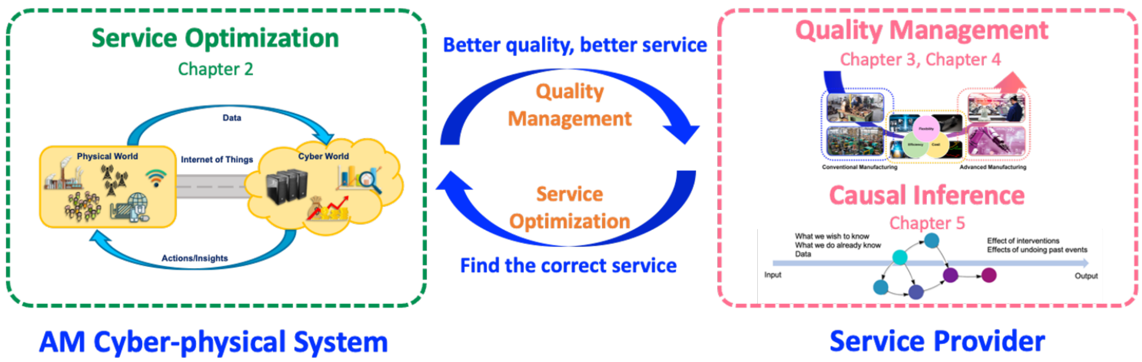

Figure 6.1. Summary of the dissertation.

6.1 Research Summary

Figure 6.1 shows the summary of my research. My research goal is to develop new machine learning methodologies to improve operations management in AM cyber-physical systems, including enhancing understanding of design-quality interactions, facilitate causality discovery. Contributions of this dissertation are summarized as follows:

- In Chapter 2, we designed a bipartite matching framework to model and optimize resource allocation among customers and service providers through a stable matching algorithm in cyber-physical systems. Recently, sharing economy paves a new way for people to "share" assets and services with others that disrupts traditional business models across the world. In the cyber-physical AM systems, the rapid development of AM technology enables individuals and small manufacturers to own machines and share under-utilized resources with others. Such a decentralized market calls upon the development of new analytical methods and tools to help customers and manufacturers find each other and further shorten the AM supply chain. The proposed framework was implemented in customer-manufacturing allocation in cyber-physical platforms. The proposed sharing economy framework showed strong potential to realize a smart and decentralized AM sharing economy.

- In Chapter 3, we designed an experiment to investigate how design parameters (e.g., build orientation, thin-wall width, thin-wall height, and hatch spacing) interact with edge roughness in thin-wall builds. Specifically, we performed the experimental design to study the impact of design parameters on the edge quality of thin-walls. This research shed insights on the optimization of engineering design to improve the quality of AM builds.

- In Chapter 4, the second design of experiments was proposed to investigate how design parameters (e.g., build orientation, thin-wall width, thin-wall height, and hatch spacing) interact with different quality characteristics in thin-wall builds. A generalized recurrence network analysis was proposed to not only capture recurrence dynamics in complex systems but also take the computational complexity into account. Here, we studied the relationship between network quantifiers and design parameters. The proposed design-quality analysis showed great potential to optimize engineering design and enhance the quality of AM builds.

- In Chapter 5, we developed an ontology-based Bayesian network (BN) model to represent causal relationships between AM parameters (i.e., design parameters and process parameters) and QA/QC requirements (e.g., structure properties and mechanical properties). Here, we integrated the information from the first principal (i.e., ontology) to the automated BN learning model to obtain an AM causality network. Note that the ontology introduces constraints for the learning algorithm, and therefore the learning outcome showed a better causal learning result. With the network representation, causal relationships among variables can be identified and then be used to facilitate prediction, diagnosis, and support decision making in manufacturing production.

6.2 Discussions

The service management and improvement in AM cyber-physical systems are studied with the top-down approach in this dissertation. We discussed the bigger picture - the overall service allocation optimization of the system in Chapter 2, and then narrow it down to investigate the quality management of each agent in the cyber-physical system from Chapter 3. In real-world experiments, data resolution plays an important role in image processing. Higher resolution means that there exist more pixels in each image, resulting in more pixel information and creating a high-quality image.

In Chapters 3, 4, and 5, we utilized data from three thin-wall parts for correlation and causal analysis. First, we obtain the XCT slices from the XCT scan of each part, then register each slice with the corresponding CAD file. Note that for the image registration, we obtain one transformation matrix for each part. Therefore, there is no deviation in the z-direction from image registration. For example, the vertical deviation calculated in this chapter (see Equation. 5.4) only collects the deviation from each thin wall. Otherwise, the deviation in the z-direction will impact the vertical deviation if we calculate the optimal transfer matrix for each layer.

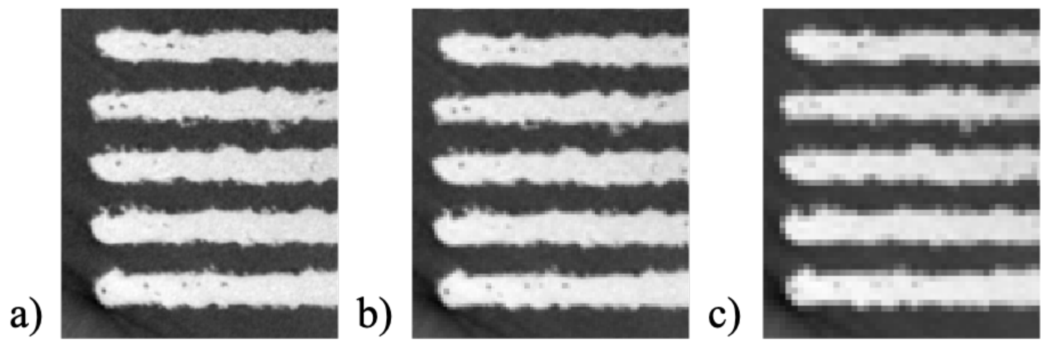

Figure 6.2. An XCT slice when image resolution is different. a) each pixel represents 14.43 microns, b) each pixel represents 28.86 microns, and c) each pixel represents 43.29 microns.

In our analysis, different features (i.e., edge roughness, thickness) are extracted from the XCT slices. This is because XCT scans have higher resolution compared to optical images. However, the resolution of XCT slices (size of the slice) can also impact the feature extraction significantly. For example, Figure 6.2 shows an example XCT slice from high resolution to low resolutions.

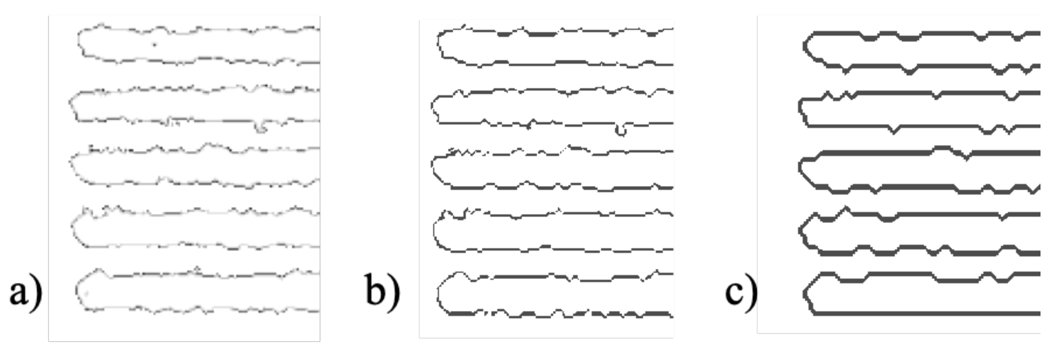

Figure 6.3. Contoured XCT slice when image resolution is different. a) each pixel represents 14.43 microns, b) each pixel represents 28.86 microns, and c) each pixel represents 43.29 microns.

As shown in Figure 6.3, different resolutions might impact the edge roughness significantly. For example, when the resolution is higher, we can extract more variation within each edge. When the resolution is low, the edge of each thin-wall tends to be a line. Also, the binarized edges in the low-resolution image are thicker than edges from high-resolution images. Note that the region of interest (ROI) of each XCT slice is 762-by-762, which indicates that each pixel is around 14.43 microns. For different analyses proposed in this dissertation, the resolution of the AM images will have more impact on the generalized recurrence analysis methodology more compared to the other analysis because we directly embed the images to the network and each pixel is related to a node in the graph. The more the resolution, the more the pixels we need to embed into the network, thereby leading to higher computational complexity. For the BN analysis, we discretize each variable into different levels based on its physical or statistical properties. Therefore, the impact of image resolution on the proposed model should be less than the impact on GRN analysis. Future works can explore the trade-off between resolution of AM images and model performance. Low-resolution images cannot provide enough detailed information, but process a low computation complexity. Increase the image resolution will most likely increase the model accuracy, however, will slow down the speed of the algorithm. Also, it is also possible that high resolution will have a negative impact on the model prediction as small variation will introduce noise to the system. Therefore, the optimization between data resolution and the performance of the model is an interesting area to explore for the next step. In addition, sparse methods can be incorporated into the model to help reduce the computational complexity in learning procedures.

6.3 Future Directions

My future research plans include:

- *Dynamic Bayesian Learning of Causal Relationships with Domain Structures in Complex Systems:*
  The increasing capability for bidirectional inferences and the development of probabilistic models lead to the rapid emergence of Bayesian networks as the method of choice for reasoning and causality discovery. Bayesian networks have been widely used to discover the causal structures in raw statistical datasets

in various domains. However, this learning process for the causal structure often requires a significant amount of data, and such a large dataset is often not available in practice due to cost constraints. This research study is aimed at transferring the historical structure learned from similar processes to help to build the Bayesian network of the new process with limited data. Specifically, this research will extend the Bayesian network developed in Chapter 4 and further 1) construct the informative prior structure using historical information; and 2) integrate the heterogeneous data into the structure through dynamic Bayesian networks. The proposed research will lead to the knowledge transfer between network structures and boost the performance of the graph learning process.

- *Statistical Learning in Non-stationary Environments with Cybersecurity Applications:*
  Beyond classification, nonstationarity is an important part of many other practical engineering problems. For example, nonstationarity in the system can be unexpected changes in the system due to the cybersecurity attacks, aging effects that sensors or actuators bring to the human-computer interactive environments, the long-term behavior changes among customers over years, or genetic mutations in genomics emerging. Currently, most of the existing statistical learning techniques rely on the stationarity assumption of environments. For example, we need to assume that the dataset follows the stationary assumption before running ARIMA or ARMA models for the time series analysis. In addition, many problems in this domain are sensitive, as they often deal with living organs, and many factors need to be taken into account during the decision making process. Therefore, conventional learning algorithms in a batch off-line setting fail whenever dynamic changes of the process appear due to non-stationary environments and external influences. The objective of this work is to develop new statistical learning methods (e.g., classification and reinforcement learning) for non-stationary environments and enable risk-based decision making by incorporating various sources of uncertainty. Specifically, my objective is to 1) develop a Bayesian learning of drifts and risk-based classification to capture drifts in class conditional distributions for any arbitrary types of data (e.g., discrete, continuous, and combinatorial); 2) introduce dimensionality reduction Bayesian optimization frameworks that map the original space to a

lower-dimensional space; and 3) design online Bayesian learning frameworks capable of learning and decision making through online/real-time data.

- *Distributed Learning in Privacy-preserving Dynamic Matching Mechanism for Cyber-physical Systems:*
  With the rapid advances of cyber-physical systems, sharing economy becomes a new way for people to "share" assets and services with others. By utilizing the Internet of Things (IoT), we now can facilitate the sharing of our existing devices through embedded sensors and network connectivity to collect and exchange data. Information privacy is a rising concern for the design, development, and deployment of sharing economy. The cyber-physical platform supports the exchange of sensitive data such as personal information from the customer's side, as well as operation information from service providers. Therefore, privacy-preserving analytics is urgently needed for the development of sharing economy platforms. My research objective is to develop new privacy-preserving matching frameworks for cyber-physical platforms in a distributed manner. Specifically, I plan to 1) develop novel sharing economy paradigms and privacy-preserved dynamic matching models for cyber-physical systems; and 2) design new service optimization models with distributed learning for large-scale IoT. This proposed research will facilitate: 1) the design of state-of-the-art privacy-preserving matching framework for sharing economy; and 2) handling of massive, complex data from IoT sensing systems in a distributed manner.

Bibliography

[1] ASTM (2012) *Standard terminology for additive manufacturing technologies*, ASTM International, West Conshohocken, PA, Standard No. ASTM 52900-15.

[2] Bukkapatnam, S. T., K. Afrin, D. Dave, and S. R. Kumara (2019) "Machine learning and AI for long-term fault prognosis in complex manufacturing systems," *Cirp Annals*, **68**(1), pp. 459–462.

[3] Simpson, T. W. (2020) "Book Review: Additive Manufacturing for the Aerospace Industry," *AIAA Journal*, **58**(4), pp. 1901–1902.

[4] Liu, R., Z. Wang, T. Sparks, F. Liou, and J. Newkirk (2017) "Aerospace applications of laser additive manufacturing," in *Laser additive manufacturing*, Elsevier, pp. 351–371.

[5] Singh, S. and S. Ramakrishna (2017) "Biomedical applications of additive manufacturing: present and future," *Current opinion in biomedical engineering*, **2**, pp. 105–115.

[6] Bourell, D. L. (2016) "Perspectives on additive manufacturing," *Annual Review of Materials Research*, **46**, pp. 1–18.

[7] Zhang, B., Y. Li, and Q. Bai (2017) "Defect formation mechanisms in selective laser melting: a review," *Chinese Journal of Mechanical Engineering*, **30**(3), pp. 515–527.

[8] Mukherjee, T., W. Zhang, and T. DebRoy (2017) "An improved prediction of residual stresses and distortion in additive manufacturing," *Computational Materials Science*, **126**, pp. 360–372.

[9] Abdelrahman, M., E. W. Reutzel, A. R. Nassar, and T. L. Starr (2017) "Flaw detection in powder bed fusion using optical imaging," *Additive Manufacturing*, **15**, pp. 1–11.

[10] Tang, H., M. Qian, N. Liu, X. Zhang, G. Yang, and J. Wang (2015) "Effect of powder reuse times on additive manufacturing of Ti-6Al-4V by selective electron beam melting," *Jom*, **67**(3), pp. 555–563.

[11] Achillas, C., D. Aidonis, E. Iakovou, M. Thymianidis, and D. Tzetzis (2015) "A methodological framework for the inclusion of modern additive manufacturing into the production portfolio of a focused factory," *Journal of manufacturing Systems*, **37**, pp. 328–339.

[12] Imani, F., A. Gaikwad, M. Montazeri, P. Rao, H. Yang, and E. Reutzel (2018) "Process mapping and in-process monitoring of porosity in laser powder bed fusion using layerwise optical imaging," *Journal of Manufacturing Science and Engineering*, **140**(10).

[13] Khanzadeh, M., R. J. Marandi, M. S. Tootooni, L. Bian, B. Smith, and P. Rao (2016) "Profiling and optimizing the geometric accuracy of additively manufactured components via self-organizing map," *SFF*, pp. 1303–1313.

[14] Lee, Y.-H., S. R. Kumara, and K. Chatterjee (2003) "Multiagent based dynamic resource scheduling for distributed multiple projects using a market mechanism," *Journal of Intelligent Manufacturing*, **14**(5), pp. 471–484.

[15] Monostori, L., B. Kádár, T. Bauernhansl, S. Kondoh, S. Kumara, G. Reinhart, O. Sauer, G. Schuh, W. Sihn, and K. Ueda (2016) "Cyber-physical systems in manufacturing," *Cirp Annals*, **65**(2), pp. 621–641.

[16] Allaire, G., C. Dapogny, R. Estevez, A. Faure, and G. Michailidis (2017) "Structural optimization under overhang constraints imposed by additive manufacturing technologies," *Journal of Computational Physics*, **351**, pp. 295–328.

[17] Qin, J., Y. Liu, and R. Grosvenor (2017) "A framework of energy consumption modelling for additive manufacturing using internet of things," *Procedia CIRP*, **63**, pp. 307–312.

[18] Shi, X., S. Ma, C. Liu, and Q. Wu (2017) "Parameter optimization for Ti-47Al-2Cr-2Nb in selective laser melting based on geometric characteristics of single scan tracks," *Optics & Laser Technology*, **90**, pp. 71–79.

[19] Smith, R. W., D. J. Corbin, J. Petrich, and E. W. Reutzel (2019) "Acoustic signals associated with laser-substrate interaction in powder bed fusion additive manufacturing process," *The Journal of the Acoustical Society of America*, **146**(4), pp. 2758–2758.

[20] Elkaseer, A., S. Dimov, D. Pham, K. Popov, L. Olejnik, and A. Rosochowski (2018) "Material microstructure effects in micro-endmilling of Cu99. 9E," *Proceedings of the Institution of Mechanical Engineers, Part B: Journal of Engineering Manufacture*, **232**(7), pp. 1143–1155.

[21] Snow, Z., A. Nassar, and E. W. Reutzel (2020) "Review of the Formation and Impact of Flaws in Powder Bed Fusion Additive Manufacturing," *Additive Manufacturing*, p. 101457.

[22] Codagnone, C. and B. Martens (2016) "Scoping the sharing economy: Origins, definitions, impact and regulatory issues," *Cristiano Codagnone and Bertin Martens (2016). Scoping the Sharing Economy: Origins, Definitions, Impact and Regulatory Issues. Institute for Prospective Technological Studies Digital Economy Working Paper*, **1**.

[23] Yang, H., S. Kumara, S. T. Bukkapatnam, and F. Tsung (2019) "The internet of things for smart manufacturing: A review," *IISE Transactions*, pp. 1–27.

[24] Zanetti, V., S. Cavalieri, M. Kalchschmidt, and R. Pinto (2015) "The role of additive manufacturing in the B2C value chain: challenges, opportunities and models," in *IFIP International Conference on Advances in Production Management Systems*, Springer, pp. 137–145.

[25] Wohlers, T. (2014) "Wohlers report," *Wohlers Associates Inc.*

[26] Yaraghi, N. and S. Ravi (2017) "The current and future state of the sharing economy," *Available at SSRN 3041207*.

[27] Rosen, D. W., C. C. Seepersad, T. W. Simpson, and C. B. Williams (2015) "Design for additive manufacturing: A paradigm shift in design, fabrication, and qualification," *Journal of Mechanical Design*, **137**(11).

[28] Thompson, M. K., G. Moroni, T. Vaneker, G. Fadel, R. I. Campbell, I. Gibson, A. Bernard, J. Schulz, P. Graf, B. Ahuja, et al. (2016) "Design for Additive Manufacturing: Trends, opportunities, considerations, and constraints," *CIRP annals*, **65**(2), pp. 737–760.

[29] Gibson, I., D. Rosen, B. Stucker, and M. Khorasani (2021) "Design for additive manufacturing," in *Additive manufacturing technologies*, Springer, pp. 555–607.

[30] Ponche, R., O. Kerbrat, P. Mognol, and J.-Y. Hascoët (2014) "A novel methodology of design for Additive Manufacturing applied to Additive Laser Manufacturing process," *Robotics and Computer-Integrated Manufacturing*, **30**(4), pp. 389–398.

[31] Doubrovski, Z., J. C. Verlinden, and J. M. Geraedts (2011) "Optimal design for additive manufacturing: opportunities and challenges," in *International Design Engineering Technical Conferences and Computers and Information in Engineering Conference*, vol. 54860, pp. 635–646.

[32] Rosen, D. (2014) "Design for additive manufacturing: past, present, and future directions," *Journal of Mechanical Design*, **136**(9).

[33] Boothroyd, G. (2005) *Assembly automation and product design*, crc press.

[34] Kuo, T.-C., S. H. Huang, and H.-C. Zhang (2001) "Design for manufacture and design for 'X': concepts, applications, and perspectives," *Computers & industrial engineering*, **41**(3), pp. 241–260.

[35] Molloy, E., H. Yang, J. Browne, and B. Davies (1991) "Design for assembly within concurrent engineering," *CIRP annals*, **40**(1), pp. 107–110.

[36] Nagarajan, H. P., H. Mokhtarian, H. Jafarian, S. Dimassi, S. Bakrani-Balani, A. Hamedi, E. Coatanéa, G. Gary Wang, and K. R. Haapala (2019) "Knowledge-based design of artificial neural network topology for additive manufacturing process modeling: a new approach and case study for fused deposition modeling," *Journal of Mechanical Design*, **141**(2).

[37] Dinar, M. and D. W. Rosen (2017) "A design for additive manufacturing ontology," *Journal of Computing and Information Science in Engineering*, **17**(2).

[38] Eddy, D., S. Krishnamurty, I. Grosse, M. Perham, J. Wileden, and F. Ameri (2015) "Knowledge management with an intelligent tool for additive manufacturing," in *International Design Engineering Technical Conferences and Computers and Information in Engineering Conference*, vol. 57045, American Society of Mechanical Engineers, p. V01AT02A023.

[39] Nagarajan, H. P., S. Panicker, H. Mokhtarian, E. Coatanéa, and K. R. Haapala (2020) "Improving worker health and safety in wire arc additive manufacturing: A graph-based approach," *Procedia CIRP*, **90**, pp. 461–466.

[40] Guo, S., W. uo, and L. Bain (2020) "Hierarchical spatial-temporal modeling and monitoring of melt pool evolution in laser-based additive manufacturing," *IISE Transactions*, **52**(9), pp. 977–997.

[41] Guo, S. and W. Guo (2020) "Process Monitoring and Fault Prediction in Multivariate Time Series Using Bag-of-Words," *IEEE Transactions on Automation Science and Engineering*.

[42] Imani, F., R. Chen, C. Tucker, and H. Yang (2019) "Random Forest Modeling for Survival Analysis of Cancer Recurrences," in *2019 IEEE 15th International Conference on Automation Science and Engineering (CASE)*, IEEE, pp. 399–404.

[43] Imani, F., C. Cheng, R. Chen, and H. Yang (2019) "Nested Gaussian process modeling and imputation of high-dimensional incomplete data under uncertainty," *IISE Transactions on Healthcare Systems Engineering*, pp. 1–12.

[44] Imani, F., C. Cheng, R. Chen, and H. Yang (2018) "Nested gaussian process modeling for high-dimensional data imputation in healthcare systems," in *IISE 2018 Conference & Expo, Orlando, FL, May*, pp. 19–22.

[45] Tian, Q., S. Guo, Y. Guo, et al. (2020) "A physics-driven deep learning model for process-porosity causal relationship and porosity prediction with interpretability in laser metal deposition," *CIRP Annals*, **69**(1), pp. 205–208.

[46] Heckerman, D., J. S. Breese, and K. Rommelse (1995) "Decision-theoretic troubleshooting," *Communications of the ACM*, **38**(3), pp. 49–57.

[47] De Campos, L. M. and N. Friedman (2006) "A scoring function for learning Bayesian networks based on mutual information and conditional independence tests." *Journal of Machine Learning Research*, **7**(10).

[48] De Campos, L. M. and J. F. Huete (2000) "A new approach for learning belief networks using independence criteria," *International Journal of Approximate Reasoning*, **24**(1), pp. 11–37.

[49] Friedman, N. and D. Koller (2003) "Being Bayesian about network structure. A Bayesian approach to structure discovery in Bayesian networks," *Machine learning*, **50**(1), pp. 95–125.

[50] Spirtes, P., C. Glymour, R. Scheines, S. Kauffman, V. Aimale, and F. Wimberly (2000) "Constructing Bayesian network models of gene expression networks from microarray data," .

[51] Craeghs, T., S. Clijsters, E. Yasa, F. Bechmann, S. Berumen, and J.-P. Kruth (2011) "Determination of geometrical factors in Layerwise Laser Melting using optical process monitoring," *Optics and Lasers in Engineering*, **49**(12), pp. 1440–1446.

[52] Bernard, A. and A. J. Hartemink (2005) "Informative structure priors: joint learning of dynamic regulatory networks from multiple types of data," in *Biocomputing 2005*, World Scientific, pp. 459–470.

[53] Pearl, J. (1998) "Graphical models for probabilistic and causal reasoning," *Quantified representation of uncertainty and imprecision*, pp. 367–389.

[54] Scutari, M. (2009) "Learning Bayesian networks with the bnlearn R package," *arXiv preprint arXiv:0908.3817*.

[55] Colombo, D. and M. H. Maathuis (2014) “Order-independent constraint-based causal structure learning,” *The Journal of Machine Learning Research*, **15**(1), pp. 3741–3782.

[56] Margaritis, D. (2003) *Learning Bayesian network model structure from data*, *Tech. rep.*, Carnegie-Mellon Univ Pittsburgh Pa School of Computer Science.

[57] Tsamardinos, I., C. F. Aliferis, A. R. Statnikov, and E. Statnikov (2003) “Algorithms for large scale Markov blanket discovery.” in *FLAIRS conference*, vol. 2, pp. 376–380.

[58] Meidani, H. and R. Ghanem (2015) “Random Markov decision processes for sustainable infrastructure systems,” *Structure and Infrastructure Engineering*, **11**(5), pp. 655–667.

[59] Yaramakala, S. and D. Margaritis (2005) “Speculative Markov blanket discovery for optimal feature selection,” in *Fifth IEEE International Conference on Data Mining (ICDM’05)*, IEEE, pp. 4–pp.

[60] Pena, J. M. (2008) “Learning gaussian graphical models of gene networks with false discovery rate control,” in *European conference on evolutionary computation, machine learning and data mining in bioinformatics*, Springer, pp. 165–176.

[61] Gasse, M., A. Aussem, and H. Elghazel (2014) “A hybrid algorithm for Bayesian network structure learning with application to multi-label learning,” *Expert Systems with Applications*, **41**(15), pp. 6755–6772.

[62] Roh, B.-M., S. R. Kumara, T. W. Simpson, P. Michaleris, P. Witherell, and I. Assouroko (2016) “Ontology-based laser and thermal metamodels for metal-based additive manufacturing,” in *International Design Engineering Technical Conferences and Computers and Information in Engineering Conference*, vol. 50077, American Society of Mechanical Engineers, p. V01AT02A043.

[63] Wallsten, S. (2015) “The competitive effects of the sharing economy: how is Uber changing taxis,” *Technology Policy Institute*, **22**, pp. 1–21.

[64] Cheng, M. (2016) “Sharing economy: A review and agenda for future research,” *International Journal of Hospitality Management*, **57**, pp. 60–70.

[65] Schor, J. B. and C. J. Fitzmaurice (2015) “Collaborating and connecting: the emergence of the sharing economy,” *Handbook of research on sustainable consumption*, **410**.

[66] Botsman, R. and R. Rogers (2010) “Beyond zipcar: Collaborative consumption,” *Harvard business review*, **88**(10), p. 30.

[67] Belk, R. (2014) “You are what you can access: Sharing and collaborative consumption online,” *Journal of business research*, **67**(8), pp. 1595–1600.

[68] Wohlers, T. (2019) “Wohlers report 2019: 3D printing and additive manufacturing state of the industry,” *Wohlers Associates Inc.*

[69] Einav, L., C. Farronato, and J. Levin (2016) “Peer-to-peer markets,” *Annual Review of Economics*, **8**, pp. 615–635.

[70] Botsman, R. and R. Rogers (2011) *What’s mine is yours: how collaborative consumption is changing the way we live*, vol. 5, Collins London.

[71] Economist, T. (2013) “All eyes on the sharing economy,” *The Economist*, **406**(8826), pp. 13–S.15.

[72] Wang, X., N. Agatz, and A. Erera (2017) “Stable matching for dynamic ride-sharing systems,” *Transportation Science*, **52**(4), pp. 850–867.

[73] Boysen, N., D. Briskorn, and S. Schwerdfeger (2019) “Matching supply and demand in a sharing economy: Classification, computational complexity, and application,” *European Journal of Operational Research*, **278**(2), pp. 578–595.

[74] Gale, D. and L. S. Shapley (1962) “College admissions and the stability of marriage,” *The American Mathematical Monthly*, **69**(1), pp. 9–15.

[75] Abraham, D. J., R. W. Irving, and D. F. Manlove (2003) “The student-project allocation problem,” in *International Symposium on Algorithms and Computation*, Springer, pp. 474–484.

[76] Knuth, D. E. (1976) “Mariages stabiles,” *English translation:(1997) Stable Marriage and Its Relation to Other Combinatorial Problems: An Introduction to the Mathematical Analysis of Algorithms (American Mathematical Society, Providence, RI)*.

[77] Gu, Y., W. Saad, M. Bennis, M. Debbah, and Z. Han (2015) “Matching theory for future wireless networks: fundamentals and applications,” *IEEE Communications Magazine*, **53**(5), pp. 52–59.

[78] Li, F., L. Zhang, Y. Liu, and Y. Laili (2018) “QoS-Aware service composition in cloud manufacturing: a gale-shapley algorithm-based approach,” *IEEE Transactions on Systems, Man, and Cybernetics: Systems*, (99), pp. 1–12.

[79] Liu, Y., L. Zhang, F. Tao, and L. Wang (2017) “Resource service sharing in cloud manufacturing based on the Gale–Shapley algorithm: advantages and challenge,” *International Journal of Computer Integrated Manufacturing*, **30**(4-5), pp. 420–432.

[80] Argoneto, P. and P. Renna (2013) "Capacity sharing in a network of enterprises using the Gale–Shapley model," *The International Journal of Advanced Manufacturing Technology*, **69**(5-8), pp. 1907–1916.

[81] Renna, P. and P. Argoneto (2011) "Capacity sharing in a network of independent factories: A cooperative game theory approach," *Robotics and Computer-Integrated Manufacturing*, **27**(2), pp. 405–417.

[82] Argoneto, P. and P. Renna (2016) "Supporting capacity sharing in the cloud manufacturing environment based on game theory and fuzzy logic," *Enterprise Information Systems*, **10**(2), pp. 193–210.

[83] McGinley, M. J. (2010) *The Development of Digi-net at the Pennsylvania State University to Support Interdisciplinary Innovation*, Ph.D. thesis, Pennsylvania State University.

[84] Nakamoto, S. (2008) "Bitcoin: A peer-to-peer electronic cash system," *Decentralized Business Review*, p. 21260.

[85] Chen, R., M. Chen, and H. Yang (2020) "Dynamic Physician-patient Matching in the Healthcare System," in *2020 42nd Annual International Conference of the IEEE Engineering in Medicine & Biology Society (EMBC)*, IEEE, pp. 5868–5871.

[86] Hu, Q., R. Chen, H. Yang, and S. Kumara (2020) "Privacy-Preserving Data Mining for Smart Manufacturing," .

[87] Boyer, J., C. Seepersad, T. W. Simpson, C. B. Williams, and P. Witherell (2017) "Special Section: Designing for additive manufacturing recent advances in design for additive manufacturing," *Journal of Mechanical Design, Transactions of the ASME*, **139**(10).

[88] Reutzel, E. W. and A. R. Nassar (2015) "A survey of sensing and control systems for machine and process monitoring of directed-energy, metal-based additive manufacturing," *Rapid Prototyping Journal*, **21**(2), pp. 159–167.

[89] Shamsaei, N., A. Yadollahi, L. Bian, and S. M. Thompson (2015) "An overview of Direct Laser Deposition for additive manufacturing; Part II: Mechanical behavior, process parameter optimization and control," *Additive Manufacturing*, **8**, pp. 12–35.

[90] Imani, F., A. Gaikwad, M. Montazeri, P. Rao, H. Yang, and E. Reutzel (2018) "Layerwise in-process quality monitoring in laser powder bed fusion," in *ASME 2018 13th International Manufacturing Science and Engineering Conference*, American Society of Mechanical Engineers Digital Collection, p. V001T01A038.

[91] Imani, F., R. Chen, E. Diewald, E. Reutzel, and H. Yang (2019) "Deep Learning of Variant Geometry in Layerwise Imaging Profiles for Additive Manufacturing Quality Control," *Journal of Manufacturing Science and Engineering*, **141**(11).

[92] Yazdi, R. M., F. Imani, and H. Yang (2020) "A hybrid deep learning model of process-build interactions in additive manufacturing," *Journal of Manufacturing Systems*, **57**, pp. 460–468.

[93] Imani, F., B. Yao, R. Chen, P. Rao, and H. Yang (2019) "Joint Multifractal and Lacunarity Analysis of Image Profiles for Manufacturing Quality Control," *Journal of Manufacturing Science and Engineering*, **141**(4), p. 044501.

[94] Yao, B., F. Imani, A. S. Sakpal, E. Reutzel, and H. Yang (2018) "Multifractal analysis of image profiles for the characterization and detection of defects in additive manufacturing," *Journal of Manufacturing Science and Engineering*, **140**(3).

[95] Yao, B., F. Imani, and H. Yang (2018) "Markov decision process for image-guided additive manufacturing," *IEEE Robotics and Automation Letters*, **3**(4), pp. 2792–2798.

[96] Imani, F., Z. Qiu, and H. Yang (2020) "Markov Decision Process Modeling for Multi-stage Optimization of Intervention and Treatment Strategies in Breast Cancer," in *2020 42nd Annual International Conference of the IEEE Engineering in Medicine & Biology Society (EMBC)*, IEEE, pp. 5394–5397.

[97] Seepersad, C. C. (2014) "Challenges and opportunities in design for additive manufacturing," *3D Printing and Additive Manufacturing*, **1**(1), pp. 10–13.

[98] Conner, B. P., G. P. Manogharan, A. N. Martof, L. M. Rodomsky, C. M. Rodomsky, D. C. Jordan, and J. W. Limperos (2014) "Making sense of 3-D printing: Creating a map of additive manufacturing products and services," *Additive Manufacturing*, **1**, pp. 64–76.

[99] Liu, J., C. Liu, Y. Bai, P. Rao, C. B. Williams, and Z. Kong (2019) "Layer-wise spatial modeling of porosity in additive manufacturing," *IISE Transactions*, **51**(2), pp. 109–123.

[100] Huang, S. H., P. Liu, A. Mokasdar, and L. Hou (2013) "Additive manufacturing and its societal impact: a literature review," *The International Journal of Advanced Manufacturing Technology*, **67**(5-8), pp. 1191–1203.

[101] Lyons, B. (2014) "Additive manufacturing in aerospace: Examples and research outlook," *The Bridge*, **44**(3), pp. 13–19.

[102] Jin, Y., S. J. Qin, and Q. Huang (2020) "Modeling inter-layer interactions for out-of-plane shape deviation reduction in additive manufacturing," *IISE Transactions*, **52**(7), pp. 721–731.

[103] Bastani, K., P. K. Rao, and Z. Kong (2016) "An online sparse estimation-based classification approach for real-time monitoring in advanced manufacturing processes from heterogeneous sensor data," *IIE Transactions*, **48**(7), pp. 579–598.

[104] Marwan, N., J. Kurths, and P. Saparin (2007) "Generalised recurrence plot analysis for spatial data," *Physics Letters A*, **360**(4-5), pp. 545–551.

[105] Imani, F., B. Yao, R. Chen, P. Rao, and H. Yang (2018) "Fractal pattern recognition of image profiles for manufacturing process monitoring and control," in *ASME 2018 13th International Manufacturing Science and Engineering Conference*, American Society of Mechanical Engineers, pp. V003T02A003–V003T02A003.

[106] Imani, F., R. Chen, E. Diewald, E. Reutzel, and H. Yang (2019) "Image-Guided Variant Geometry Analysis of Layerwise Build Quality in Additive Manufacturing," in *International Manufacturing Science and Engineering Conference*, vol. 58745, American Society of Mechanical Engineers, p. V001T02A041.

[107] Imani, F. (2020) "Sensor-based Modeling and Analysis of Advanced Manufacturing Systems for Quality Improvements," .

[108] Yao, B. and H. Yang (2018) "Constrained Markov Decision Process Modeling for Sequential Optimization of Additive Manufacturing Build Quality," *IEEE Access*, **6**, pp. 54786–54794.

[109] Thomas, D. (2009) *The development of design rules for selective laser melting*, Ph.D. thesis, University of Wales.

[110] Dunbar, A., G. Gunderman, M. Mader, and E. Reutzel (2017) "Fabrication and Quality Assessment of Thin Fins Built Using Metal Powder Bed Fusion Additive Manufacturing," in *28th Annual International Solid Freeform Fabrication Symposium – An Additve Manufacturing Conference*, Austin, TX: University of Texas at Austin, pp. 2650–2663.

[111] Kranz, J., D. Herzog, and C. Emmelmann (2015) "Design guidelines for laser additive manufacturing of lightweight structures in TiAl6V4," *Journal of Laser Applications*, **27**(S1), p. S14001.

[112] Gaikwad, A., F. Imani, H. Yang, E. Reutzel, and P. Rao (2019) "In-situ monitoring of thin-wall build quality in laser powder bed fusion using deep

learning," *ASTM International journal Smart and Sustainable Manufacturing Systems (SSMS)*, **3**(1), pp. 98–121.

[113] Gaikwad, A., F. Imani, P. Rao, H. Yang, and E. Reutzel (2019) "Design Rules and In-Situ Quality Monitoring of Thin-Wall Features Made Using Laser Powder Bed Fusion," in *International Manufacturing Science and Engineering Conference*, vol. 58745, American Society of Mechanical Engineers, p. V001T01A039.

[114] Chen, R., F. Imani, E. Reutzel, and H. Yang (2018) "From Design Complexity to Build Quality in Additive Manufacturing—A Sensor-Based Perspective," *IEEE sensors letters*, **3**(1), pp. 1–4.

[115] Kamarthi, S., S. Sultornsanee, and A. Zeid (2016) "Recurrence quantification analysis to estimating surface roughness in finish turning processes," *The International Journal of Advanced Manufacturing Technology*, **87**(1-4), pp. 451–460.

[116] Marwan, N., M. C. Romano, M. Thiel, and J. Kurths (2007) "Recurrence plots for the analysis of complex systems," *Physics reports*, **438**(5-6), pp. 237–329.

[117] Eckmann, J., S. O. Kamphorst, D. Ruelle, et al. (1995) "Recurrence plots of dynamical systems," *World Scientific Series on Nonlinear Science Series A*, **16**, pp. 441–446.

[118] Yang, H. and G. Liu (2013) "Self-organized topology of recurrence-based complex networks," *Chaos: An Interdisciplinary Journal of Nonlinear Science*, **23**(4), p. 043116.

[119] Zbilut, J. P. and C. L. Webber Jr (2007) "Recurrence quantification analysis: Introduction and historical context," *International Journal of Bifurcation and Chaos*, **17**(10), pp. 3477–3481.

[120] Yang, H. and Y. Chen (2014) "Heterogeneous recurrence monitoring and control of nonlinear stochastic processes," *Chaos: An Interdisciplinary Journal of Nonlinear Science*, **24**(1), p. 013138.

[121] Chen, Y. and H. Yang (2016) "Heterogeneous recurrence representation and quantification of dynamic transitions in continuous nonlinear processes," *The European Physical Journal B*, **89**(6), p. 155.

[122] Kan, C., C. Cheng, and H. Yang (2016) "Heterogeneous recurrence monitoring of dynamic transients in ultraprecision machining processes," *Journal of Manufacturing Systems*, **41**, pp. 178–187.

[123] Cheng, C., C. Kan, and H. Yang (2016) "Heterogeneous recurrence analysis of heartbeat dynamics for the identification of sleep apnea events," *Computers in biology and medicine*, **75**, pp. 10–18.

[124] Chen, R., F. Imani, and H. Yang (2019) "Heterogeneous Recurrence Analysis of Disease-altered Spatiotemporal Patterns in Multi-Channel Cardiac Signals." *IEEE journal of biomedical and health informatics*.

[125] Yang, H., C.-B. Chen, and S. Kumara (2020) "Heterogeneous recurrence analysis of spatial data," *Chaos: An Interdisciplinary Journal of Nonlinear Science*, **30**(1), p. 013119.

[126] Cui, L., S. Kumara, and R. Albert (2010) "Complex networks: An engineering view," *IEEE Circuits and Systems Magazine*, **10**(3), pp. 10–25.

[127] Mann, H. B. and D. R. Whitney (1947) "On a test of whether one of two random variables is stochastically larger than the other," *The annals of mathematical statistics*, pp. 50–60.

[128] Wang, C., X. Tan, S. Tor, and C. Lim (2020) "Machine learning in additive manufacturing: State-of-the-art and perspectives," *Additive Manufacturing*, p. 101538.

[129] Zhang, J., P. Wang, and R. X. Gao (2020) "Attention Mechanism-Incorporated Deep Learning for AM Part Quality Prediction," *Procedia CIRP*, **93**, pp. 96–101.

[130] Mozaffar, M., A. Paul, R. Al-Bahrani, S. Wolff, A. Choudhary, A. Agrawal, K. Ehmann, and J. Cao (2018) "Data-driven prediction of the high-dimensional thermal history in directed energy deposition processes via recurrent neural networks," *Manufacturing letters*, **18**, pp. 35–39.

[131] Francis, J. and L. Bian (2019) "Deep learning for distortion prediction in laser-based additive manufacturing using big data," *Manufacturing Letters*, **20**, pp. 10–14.

[132] Kan, C. and H. Yang (2017) "Internet of hearts-large-scale stochastic network modeling and analysis of cardiac electrical signals," in *Stochastic Modeling and Analytics in Healthcare Delivery Systems*, World Scientific, pp. 211–251.

[133] Liu, G. and H. Yang (2018) "Self-organizing network for variable clustering," *Annals of Operations Research*, **263**(1-2), pp. 119–140.

[134] Kan, C. and H. Yang (2015) "Network models for monitoring high-dimensional image profiles," in *2015 IEEE International Conference on Automation Science and Engineering (CASE)*, IEEE, pp. 1078–1083.

[135] Chen, C.-B., H. Yang, and S. Kumara (2018) "Recurrence network modeling and analysis of spatial data," *Chaos: An Interdisciplinary Journal of Nonlinear Science*, **28**(8), p. 085714.

[136] Yang, H., R. Liu, and S. Kumara (2020) "Self-organizing network modelling of 3D objects," *CIRP Annals*.

[137] Lu, Y., Z. Yang, D. Eddy, and S. Krishnamurty (2018) "Self-improving additive manufacturing knowledge management," in *International Design Engineering Technical Conferences and Computers and Information in Engineering Conference*, vol. 51739, American Society of Mechanical Engineers, p. V01BT02A016.

[138] Yang, H., P. Rao, T. Simpson, Y. Lu, P. Witherell, A. R. Nassar, E. Reutzel, and S. Kumara (2020) "Six-Sigma Quality Management of Additive Manufacturing," *Proceedings of the IEEE*.

[139] Scutari, M., C. E. Graafland, and J. M. Gutiérrez (2019) "Who learns better Bayesian network structures: Accuracy and speed of structure learning algorithms," *International Journal of Approximate Reasoning*, **115**, pp. 235–253.

[140] Tsamardinos, I., L. E. Brown, and C. F. Aliferis (2006) "The max-min hill-climbing Bayesian network structure learning algorithm," *Machine learning*, **65**(1), pp. 31–78.

[141] Dong, A. and A. M. Agogino (1997) "Text analysis for constructing design representations," *Artificial Intelligence in Engineering*, **11**(2), pp. 65–75.

[142] Sesen, M. B., A. E. Nicholson, R. Banares-Alcantara, T. Kadir, and M. Brady (2013) "Bayesian networks for clinical decision support in lung cancer care," *PloS one*, **8**(12), p. e82349.

[143] Li, J. and J. Shi (2007) "Knowledge discovery from observational data for process control using causal Bayesian networks," *IIE transactions*, **39**(6), pp. 681–690.

[144] Mokhtarian, H., A. Hamedi, H. P. Nagarajan, S. Panicker, E. Coatanéa, and K. Haapala (2019) "Probabilistic modelling of defects in additive manufacturing: A case study in powder bed fusion technology," *Procedia CIRP*, **81**, pp. 956–961.

[145] Wang, Y., R. Blache, P. Zheng, and X. Xu (2018) "A knowledge management system to support design for additive manufacturing using Bayesian networks," *Journal of Mechanical Design*, **140**(5).

[146] Hertlein, N., S. Deshpande, V. Venugopal, M. Kumar, and S. Anand (2020) "Prediction of selective laser melting part quality using hybrid Bayesian network," *Additive Manufacturing*, **32**, p. 101089.

[147] Jing, L. and J. Ma (2020) "Additive Manufacturing Adaptiveness Analysis Using Fuzzy Bayesian Network," in *International Design Engineering Technical Conferences and Computers and Information in Engineering Conference*, vol. 83952, American Society of Mechanical Engineers, p. V006T06A004.

[148] Bacha, A., A. H. Sabry, and J. Benhra (2019) "Fault Diagnosis in the Field of Additive Manufacturing (3D Printing) Using Bayesian Networks." *International Journal of Online & Biomedical Engineering*, **15**(3).

[149] Verma, T. and J. Pearl (1991) *Equivalence and synthesis of causal models*, UCLA, Computer Science Department.

[150] Tran, H. M. and S. T. Bukkapatnam (2016) "Inferring sparse networks for noisy transient processes," *Scientific reports*, **6**(1), pp. 1–13.

[151] Tran, H. M., S. T. Bukkapatnam, and M. Garg (2019) "Detecting changes in transient complex systems via dynamic network inference," *IISE Transactions*, **51**(3), pp. 337–353.

[152] Witherell, P., S. Feng, T. W. Simpson, D. B. Saint John, P. Michaleris, Z.-K. Liu, L.-Q. Chen, and R. Martukanitz (2014) "Toward metamodels for composable and reusable additive manufacturing process models," *Journal of Manufacturing Science and Engineering*, **136**(6).

[153] Fenz, S. (2012) "An ontology-based approach for constructing Bayesian networks," *Data & Knowledge Engineering*, **73**, pp. 73–88.

[154] Chen, R., P. Rao, Y. Lu, E. Reutzel, and H. Yang (2021) "Recurrence Network Analysis of Design-quality Interactions in Additive Manufacturing," *Additive Manufacturing*, p. 101861.

[155] Heckerman, D. and M. P. Wellman (1995) "Bayesian networks," *Communications of the ACM*, **38**(3), pp. 27–31.

[156] Scutari, M. (2018) "Dirichlet Bayesian network scores and the maximum relative entropy principle," *Behaviormetrika*, **45**(2), pp. 337–362.

[157] Chickering, D. M. (2002) "Optimal structure identification with greedy search," *Journal of machine learning research*, **3**(Nov), pp. 507–554.

[158] Snell, R., S. Tammas-Williams, L. Chechik, A. Lyle, E. Hernández-Nava, C. Boig, G. Panoutsos, and I. Todd (2020) "Methods for rapid pore classification in metal additive manufacturing," *JOM*, **72**(1), pp. 101–109.

[159] Dunbar, A. J., G. J. Gunderman, M. C. Mader, and E. W. Reutzel (2020) "Fabrication and quality assessment of thin fins built using metal powder bed fusion additive manufacturing," in *28th Annual International Solid Freeform Fabrication Symposium-An Additive Manufacturing Conference, SFF 2017*.

Vita

Ruimin Chen

Education

Ph.D. August 2021	**Industrial Engineering** The Pennsylvania State University
M.S. May 2018	**Dual-title in Industrial Engineering & Operations Research** The Pennsylvania State University
Exchange 2014-2015	**Industrial & Systems Engineering** San José State University
B.S. July 2016	**Industrial Engineering** Southeast University

Honors & Awards

- **2020, 3rd Place, Doctoral Student Colloquium Awardee,** Institute of Industrial and System Engineering (IISE) Annual Conference & Expo, 2020
- **2019, NSF Student Travel Award,** IEEE CASE 2019, Vancouver, Canada
- **2019, Best Poster Award,** Northeastern Regional Conference on Complex Systems, Binghamton, NY
- **2019, Best Poster Award,** Poster Competition in Industrial Advisory Board Meetings, NSF Center for Health Organization Transformation (CHOT), Seattle, WA
- **2019, CoE Graduate Student Travel Support,** Penn State
- **2018, NSF INTERN Scholarship,** IBM Thomas J. Watson Research Center, Yorktown Heights, NY

Selected Publications

Journal Articles

1. **R. Chen**, Y. Lu, P. Witherell, T. Simpson, S. Kumara, and H. Yang, "Ontology-driven Bayesian Network for Causal Inference and Quality Assurance in Additive Manufacturing," *IEEE Robotics and Automation Letters*, 2021. DOI: https://doi.org/10.1109/LRA.2021.3090020
2. **R. Chen**, P. Rao, Y. Lu, E. W. Reutzel, and H. Yang, "Recurrence Network Analysis of Design-quality Interactions in Additive Manufacturing," *Additive Manufacturing*, Vol. 39, p101861, 2021. DOI: https://doi.org/10.1016/j.addma.2021.101861
3. **R. Chen**, F. Imani, and H. Yang, "Heterogeneous Recurrence Analysis of Disease-altered Spatiotemporal Patterns in Multi-channel Cardiac Signals," *IEEE Journal of Biomedical and Health Informatics*, Vol. 24, No. 6, p1619-1631, 2019. DOI: http://dx.doi.org/10.1109/JBHI.2019.2952285 *(Best poster award in the 2019 Northeastern Regional Conference on Complex Systems)*
4. **R. Chen**, F. Imani, E. Reutzel, and H. Yang, "From Design Complexity to Build Quality in Additive Manufacturing - A Sensor-based Perspective," *IEEE Sensor Letters*, Vol. 3, No. 4, p1-4, 2018. DOI: http://dx.doi.org/10.1109/LSENS.2018.2880747
5. **R. Chen**, M. Chen, and H. Yang, "Dynamic Physician-patient Matching in the Healthcare System," *42nd Annual International Conference of the IEEE Engineering in Medicine and Biology Society*, 2020. DOI: http://dx.doi.org/10.1109/EMBC44109.2020.9176324